

**Conceptual Design of a  
Crew Escape Module  
for a Single Stage To Orbit Vehicle**

by

**Jason Scott Bacon**

**B.S.M.E. May 1992, Oklahoma State University**

**A Thesis Submitted to**

**The Faculty of**

**The School of Engineering and Applied Science  
of The George Washington University in partial satisfaction  
of the requirements for the degree of Master of Science**

**July 1994**

**This research was conducted at the NASA Langley Research Center**

## I. Abstract

The objective of this study was to produce a conceptual design for a crew escape module that provides the highest crew safety attainable at a minimum expense of weight, volume, and complexity on the parent vehicle design. In this study, the parent vehicle is a single stage vehicle, with a crew of six, which uses liquid hydrogen and liquid oxygen as propellants. The crew escape module has pyrotechnics to separate it from the single stage vehicle and two solid rockets to propel it to a safe distance. The crew escape module then glides until parachutes are deployed and an ocean landing takes place.

Initially, the crew module geometry and subsystems were defined and the aerodynamics and heating environment were estimated. Abort trajectories were determined using initial conditions throughout a nominal ascent trajectory of the single stage vehicle. The trajectory analysis verified the abort solid rocket design and determined the most severe aerodynamic heating environment experienced by the crew escape module. The results of this study show that a jettisonable crew escape module carries with it a weight penalty of approximately 6,100 lb compared to a non-jettisonable crew cabin. This penalty translates into a 24,500 lb (10.5%) increase in the dry weight and a 216,300 lb (9%) increase in the gross lift-off weight of the single stage vehicle.

In the end, the choice to develop and use a crew escape module is one of economics. This paper does not delve into the economics of the design, but instead gives an accounting of the system weights and definitions. In the future, these system weights and definitions can be used to project the cost of developing a crew escape module.

## II. Acknowledgments

Completion of this thesis was possible only as a result of the help given to me by many of the members of the Vehicle Analysis Branch at NASA Langley. I am especially thankful to Chris Naftel for not only serving as my NASA advisor but also for his generous assistance with the trajectory analysis portion of this thesis. Thanks also goes to Walt Engelund for his assistance with aerodynamics, Kay Wurster for her help with the heating analysis, Garry Qualls for his help on the geometry modeling, Roger Lepsch for his time and effort in weights and sizing, and Anne Costa for her most generous help in preparing the figures. I would also like to thank Dr. Robert Tolson who has served as my GWU advisor for the past two years.

Special thanks goes to my grandmother, my parents, my brother, and my nephew who was born during the writing of this paper. I regret that I was unable to be with them these last two years, at a time when they needed me most. Their support and strength have inspired me and pushed me to be where I am today. Thanks.

### III. Table of Contents

I. Abstract .....	i
II. Acknowledgments .....	ii
III. Table of Contents .....	iii
IV. Lists of Tables and Figures .....	v
V. Nomenclature .....	viii
1. Introduction .....	1
Background .....	3
Objectives and Approach .....	6
2. SSV Mission Summary .....	9
3. CEM Configuration and Mass Summary .....	10
Design and Packaging .....	10
Mass Summary .....	12
Center of Gravity .....	13
4. CEM Elements and Subsystems .....	15
Airframe .....	15
Avionics .....	17
Crew and Gear .....	17
Environmental Control and Life Support .....	18
Personnel Provisions .....	18
Power Supply .....	18
Propulsion Subsystem .....	19
Pyrotechnic Separation Subsystem .....	23
Reaction Control Subsystem .....	25
Recovery Subsystem .....	25
Thermal Protection Subsystem .....	31

5. Aerodynamics .....	34
Subsonic/Transonic .....	34
Supersonic .....	35
Hypersonic .....	35
6. Trajectory Analysis .....	36
Abort On-the-Pad .....	36
Abort at Maximum Dynamic Pressure .....	37
Abort at Maximum Heat Rate .....	38
7. Conclusions .....	39
8. Recommendations for Future Work .....	41
9. References .....	42
10. Tables .....	45
11. Figures .....	47
12. Appendix .....	83
A. Subsystem Weight Breakdown for Previously Defined Systems .....	83
B. Aerodynamic Preliminary Analysis System (APAS) .....	85
C. Mini-Version of JA70 Aerodynamic Heating Program (MINIVER) .....	87
D. Program to Optimize Simulated Trajectories (POST) .....	90

#### IV. List of Tables and Figures

Table 3.1:	Summary of SSV Dry Weight Increase .....	45
Table 3.2:	Summary of SSV Propellant Increase .....	45
Table 4.1:	Power Requirements for CEM After Abort .....	46
Figure 4.1:	Two View of Crew Escape Module .....	47
Figure 4.2:	Crew Escape Module Mated with the SSV .....	48
Figure 4.3:	Overpressure Boundaries .....	49
Figure 4.4:	Human Tolerance Limits to Acceleration .....	49
Figure 4.5:	Explosive Cord Schematic .....	50
Figure 4.6:	Explosive Nut/Bolt Schematic .....	50
Figure 4.7:	Cable Disconnection Plate Schematic .....	51
Figure 4.8:	Airlock Shape Charge Schematic .....	51
Figure 4.9:	Explosive Transfer Line Schematic .....	52
Figure 4.10:	Stable, Unaccelerated Parachute Descent .....	52
Figure 4.11:	Thermal Protection System Lay-up .....	53
Figure 5.1:	Longitudinal Aerodynamic Coefficients at Mach 0.3 .....	54
Figure 5.2:	Longitudinal Aerodynamic Coefficients at Mach 0.6 .....	55
Figure 5.3:	Longitudinal Aerodynamic Coefficients at Mach 0.9 .....	56
Figure 5.4:	Longitudinal Aerodynamic Coefficients at Mach 1.2 .....	57
Figure 5.5:	Longitudinal Aerodynamic Coefficients at Mach 1.6 .....	58
Figure 5.6:	Longitudinal Aerodynamic Coefficients at Mach 2.0 .....	59
Figure 5.7:	Longitudinal Aerodynamic Coefficients at Mach 4.0 .....	60
Figure 5.8:	Longitudinal Aerodynamic Coefficients at Mach 6.0 .....	61
Figure 5.9:	Longitudinal Aerodynamic Coefficients at Mach 9.0 .....	62

Figure 5.10: Longitudinal Aerodynamic Coefficients at Mach 12.0 .....	63
Figure 5.11: Longitudinal Aerodynamic Coefficients at Mach 15.0 .....	64
Figure 5.12: Longitudinal Aerodynamic Coefficients at Mach 20.0 .....	65
Figure 5.13: Longitudinal Aerodynamic Coefficients at Mach 25.0 .....	66
Figure 6.1: SSV Nominal Ascent — Altitude vs. Time .....	67
Figure 6.2: SSV Nominal Ascent — Altitude vs. Downrange .....	67
Figure 6.3: SSV Nominal Ascent — Velocity vs. Time .....	68
Figure 6.4: SSV Nominal Ascent — Mach Number vs. Time .....	68
Figure 6.5: SSV Nominal Ascent — Angle of Attack vs. Time .....	69
Figure 6.6: SSV Nominal Ascent — Flight Path Angle vs. Time .....	69
Figure 6.7: SSV Nominal Ascent — Dynamic Pressure vs. Time .....	70
Figure 6.8: SSV Nominal Ascent — Total Acceleration vs. Time .....	70
Figure 6.9: CEM Abort at T=0s — Altitude vs. Time .....	71
Figure 6.10: CEM Abort at T=0s — Altitude vs. Downrange .....	71
Figure 6.11: CEM Abort at T=0s — Velocity vs. Time .....	72
Figure 6.12: CEM Abort at T=0s — Mach Number vs. Time .....	72
Figure 6.13: CEM Abort at T=0s — Angle of Attack vs. Time .....	73
Figure 6.14: CEM Abort at T=0s — Dynamic Pressure vs. Time .....	73
Figure 6.15: CEM Abort at T=0s — Total Acceleration vs. Time .....	74
Figure 6.16: CEM Abort at T+55s — Altitude vs. Time .....	75
Figure 6.17: CEM Abort at T+55s — Altitude vs. Downrange .....	75
Figure 6.18: CEM Abort at T+55s — Velocity vs. Time .....	76
Figure 6.19: CEM Abort at T+55s — Mach Number vs. Time .....	76
Figure 6.20: CEM Abort at T+55s — Angle of Attack vs. Time .....	77
Figure 6.21: CEM Abort at T+55s — Dynamic Pressure vs. Time .....	77
Figure 6.22: CEM Abort at T+55s — Total Acceleration vs. Time .....	78

Figure 6.23: CEM Abort at T+320s — Altitude vs. Time .....79  
Figure 6.24: CEM Abort at T+320s — Altitude vs. Downrange .....79  
Figure 6.25: CEM Abort at T+320s — Velocity vs. Time .....80  
Figure 6.26: CEM Abort at T+320s — Mach Number vs. Time .....80  
Figure 6.27: CEM Abort at T+320s — Angle of Attack vs. Time.....81  
Figure 6.28: CEM Abort at T+320s — Dynamic Pressure vs. Time .....81  
Figure 6.29: CEM Abort at T+320s — Total Acceleration vs. Time .....82

## V. Nomenclature

### Abbreviations

ACRV	Assured Crew Return Vehicle
Al-Li	Aluminum-Lithium
AMLS	Advanced Manned Launch System
APAS	Aerodynamic Preliminary Analysis System
CEM	Crew Escape Module
CERV	Crew Emergency Return Vehicle
CG	Center of Gravity
CPU	Central Processing Unit
ECLS	Environmental Control and Life Support
EVA	Extra-Vehicular Activity
GPS	Global Positioning System
IAS	Impact Attenuation System
IMU	Inertial Measurement Unit
IVA	Inter-Vehicular Activity
LaRC	Langley Research Center
LH <sub>2</sub>	Liquid Hydrogen
LO <sub>2</sub>	Liquid Oxygen
MDM	Multiplexer/Demultiplexer
MINIVER	Mini-Version of JA70 Aerodynamic Heating Program
MOSES	Manned Orbital Space Escape System
NASA	National Aeronautics and Space Administration
POST	Program to Optimize Simulated Trajectories
RCS	Reaction Control System
SARSAT	Search and Rescue Satellite
SCRAM	Station Crew Return Alternate Module
SMART	Solid Modeling Aerospace Research Tool
SSV	Single Stage Vehicle
STS	Space Transportation System
TNT	Tetranitromethane
TPS	Thermal Protection System
UHF	Ultra-High Frequency
VAB	Vehicle Analysis Branch

## Symbols

$\alpha$	Angle of Attack (deg)
$C_L$	Lift Coefficient
$C_D$	Drag Coefficient
$C_M$	Pitching Moment Coefficient
$dm$	Change in Mass (lb)
$dt$	Change in Time (s)
$dV$	Change in Velocity (ft/s)
$D$	Drag (lb)
$D_l$	Drag of Load (lb)
$D_p$	Drag of Parachute (lb)
$F$	Force (lb)
$\gamma$	Flight Path Angle (deg)
$g$	Gravitational Constant at Altitude
$g_0$	Gravitational Constant at Sea Level (32.2 ft/s <sup>2</sup> )
$I_{sp}$	Specific Impulse (s)
$m$	mass (lb)
$m_i$	Initial Mass (lb)
$m_f$	Final Mass (lb)
$n$	Number of Parachutes
$p$	Overpressure (psi)
$P_x$	Atmospheric Pressure (psi)
$q$	Dynamic Pressure (lb/ft <sup>2</sup> )
$\rho$	Density of Atmosphere (slugs/ft <sup>3</sup> )
$S$	Parachute Area (ft <sup>2</sup> )
$t$	Time (s)
$t_1$	Initial Time (s)
$t_2$	Final Time (s)
$T$	Thrust (lb)
$u$	Exhaust Velocity (ft/s)
$V$	Velocity (ft/s)
$\Delta V$	Velocity Change (ft/s)
$V_e$	Descent Velocity (ft/s)
$V_R$	Relative Velocity (ft/s)
$W$	Weight (lb)
$W_l$	Weight of Load (lb)
$W_p$	Weight of Parachute (lb)
$W_T$	Weight of TNT (tons)

## 1. Introduction

On January 28, 1986, the Space Shuttle Challenger began its tenth and final mission. Approximately 73 seconds after launch, the Challenger fell prey to a catastrophic failure which destroyed the orbiter. Seven astronauts survived the subsequent fireball and breakup of the orbiter but perished either due to decompression of the crew cabin shortly thereafter or upon impact with the ocean nearly three minutes after the incident.<sup>1</sup>

Much discussion followed the accident about whether any escape system would have been able to save the crew. Common opinion was that there was no time to respond because the failure happened instantaneously, however, telemetry and photographic data show otherwise. Even at launch, cameras captured a puff of smoke emanating from the now infamous O-ring, while at T+59.82 seconds a still camera photographed an intensifying glow coming from the same area. Twelve seconds later, the flame cut through the half inch thick steel solid rocket booster and then perforated the external tank which resulted in the fireball.<sup>1</sup> Though these pictures provided visual proof of the impending disaster, it is unlikely that anyone on the ground could have analyzed the images and determined the need to initiate an abort before the failure occurred. Also, it is unreasonable for someone to have responsibility for pushing the eject button of the multi-billion dollar Shuttle based on visual evidence alone. However, more convincing than pictures was the detailed telemetry data which confirms that a serious accident was about to take place.

"At 60.16 seconds after launch, telemetry registered a drop in right booster chamber pressure compared with that in the left booster. At 62.4

seconds, the right elevon moved and the engines gimbled apparently compensating for the drop in right booster thrust. At 66.48 seconds a pressure drop was registered in the liquid hydrogen fuel compartment of the external tank. At 67.68 seconds, telemetry registered a decrease in liquid oxygen inlet (tank to engine) pressure. At 72.14 to 72.28 seconds, telemetry showed divergent pitch and yaw rates by the right and left boosters and lateral acceleration by the right booster. Hydrogen and oxygen inlet pressure was falling at 72.8 seconds, indicating escape of propellant from the tank. At 73 seconds, chamber pressure in the right booster fell 24 psi lower than that in the left booster, indicating escape of exhaust gas from a hole in the side of the booster. Detailed analysis of telemetry tapes at the Johnson Space Center revealed that 1.25 seconds before data were lost, the right-hand booster's rate gyroscope indicated that the nose of the rocket was swinging toward the external tank, while the aft part of the booster was swinging away. The aft attachment between tank and booster had burned through. The nose of the booster crashed into the tank and ruptured it at the bulkhead between the liquid hydrogen and liquid oxygen containers. The fireball then erupted."<sup>1</sup>

This evidence makes it apparent that not only was the problem detected soon enough to give the crew time to respond but also sensors were in place to record the events. Unfortunately hardware was not in place to allow something to be done about the developing hazard. "In the shuttle design, the crew was committed to flight during the first two minutes of the ascent to orbit, when the boosters were firing. Only after that first stage did escape become possible through the flight abort and contingency landing system. During its first two minutes of flight, the orbiter was a death trap for the crew if a booster failed. That fact had not been publicized."<sup>1</sup>

## Background

In recent years, NASA has been examining options for a next generation manned space transportation system known as the Advanced Manned Launch System (AMLS). Toward this end, the Vehicle Analysis Branch (VAB) at the NASA Langley Research Center (LaRC) is currently performing a systems analysis of a rocket powered single stage vehicle (SSV) whose mission it would be to replace the Space Shuttle. One of the abort options being considered for the SSV is a jettisonable crew escape module (CEM) capable of surviving a catastrophic failure of the SSV and returning the astronauts safely to Earth.

The concept of an ejectable module is not new. "Historically the parachute, used first during World War I, was the first of the escape systems. As speed and altitude of aircraft increased however, it became virtually impossible to abandon the aircraft without serious risk of damage. This led first to the development of the open ejection seat and later to the development of more sophisticated escape systems, such as the encapsulated ejection seat and the ejectable nose capsule."<sup>2</sup>

In 1954, the X-15 program began. This marked one of the first efforts to push the aeronautical system into the realm of space flight. At speeds exceeding Mach 6 and altitudes over 300,000 feet, extensive studies showed that the vehicle itself provided the best protection from an accident and that an escape system useful during the entire flight regime was prohibitively expensive. However, at lower speeds and altitudes (below Mach 4 and 120,000 feet), a combination open ejection seat and pressure suit proved to be the escape system of choice.

In 1957, the XB-70 program utilized individual encapsulated ejection seats for its escape system. Clamshell doors over and under the seat closed in an emergency while still allowing the pilot to control the aircraft until the final decision to eject was made. This design proved successful in 1966 when an XB-70 collided with a chase plane and the crew ejected safely. The XB-70 program also demonstrated the need for an on-board automatic emergency detection system when on flight 12 a wing apex failed and was ingested by the engines causing a rapid degradation of the propulsion system. The response of the crew was determined to be too slow and sometimes inappropriate as the emergency information displayed was inadequate for a proper diagnosis of the situation. Fortunately, the plane was landed successfully.

Manned space flight began with the Mercury Project initiated in 1958. The Mercury capsule rode atop a Redstone or Atlas booster which had calculated reliabilities of less than 0.8, too little for manned space flight. To increase the reliability to over 0.99 it was shown that an escape system was needed for the launch phase. Due to the design, the capsule itself served as the escape system. In the event of an emergency, an escape rocket mounted on an escape tower above the capsule was fired and pulled the Mercury capsule away from the booster. This system was supplemented by an abort sensing and implementation system which was capable of sensing an emergency and automatically initiating the abort.

The Gemini Program, established in 1962, used ejection seats for aborts below 70,000 feet. Above this altitude, the retrorockets could be fired to separate the capsule from the booster. The use of ejection seats eliminated the need for the large escape rocket and tower.

During the mid 1960's the Apollo program had begun and was facing the escape issue with the added complexity that the spacecraft would be headed for the moon. An escape system similar to Mercury was used for aborts on-the-pad. An escape rocket and tower were mounted atop the capsule and were jettisoned later if not used during the launch phase. Once the tower was jettisoned, escape could be accomplished by igniting the service propulsion reaction control motors or the main service propulsion system engine. After either abort scenario, parachutes would be deployed to allow the command module to safely land in the ocean. During the trip to the moon, abort could be accomplished by firing the service propulsion engine and returning to Earth on a predetermined abort trajectory or by completing a circumlunar trajectory to obtain a free Earth return. This abort procedure was used on Apollo 13 when the main power supply failed and the lunar module descent engine was fired to put the vehicle on a circumlunar trajectory. This was the first case in which occurrence of an on-board emergency led to use of another spacecraft to effect the safe return of the crew.<sup>3</sup>

The current Space Transportation System (STS), which includes four Shuttle Orbiters, provides no sure means of survival in the event of a major failure. Several times during the development of the Shuttle, a first-stage abort option was considered. However, no system was ever implemented due to the limited utility, technical infeasibility, or program cost and schedule.<sup>4</sup>

As a result of the Challenger accident, a Presidential Commission recommended that NASA "make all efforts to provide a crew escape system for use during gliding flight."<sup>5</sup> Although some changes have been implemented, the abort capabilities of the Shuttle remain limited. The escape

equipment provided is for gliding flight only and consists of an eight foot telescoping pole which deploys through a jettisoned escape hatch on the middeck. The pole allows crew members to bail out and pass under the wing of the orbiter. A crew of seven can escape in 1.5 minutes.<sup>6</sup> Therefore, crew members have no chance of escape from a catastrophic event like the Challenger accident.

Recent studies into the development of escape systems for manned space vehicles have led to the design and analysis of several escape module concepts. The concepts which NASA has investigated are generally lumped together and referred to as the ACRV (Assured Crew Return Vehicle)<sup>7</sup>. This category of escape modules includes at least four basic configurations. These are a hemisphere type module, an Apollo type module, MOSES (Manned Orbital Space Escape System)<sup>8</sup>, and SCRAM (Station Crew Return Alternate Module). Other studies have led to the development of more complicated escape systems such as the CERV (Crew Emergency Return Vehicle)<sup>9</sup> and the Hermes Crew Escape Module.<sup>10,11,12</sup> The ACRV configurations are primarily designed to provide a means of escape from the Space Station, while the CERV and the Hermes CEM are designed to provide abort capability from a launch vehicle.

### Objectives and Approach

The objective of this study was to produce a conceptual design for a crew escape module that provides the highest crew safety attainable for the six crew members at a minimum expense of weight, volume, and complexity on the SSV design. In particular, the CEM was to be capable of surviving a catastrophic failure of the SSV, similar to the Challenger accident.

Toward this end, an assessment of the required subsystems had to be performed. Once all of the required elements and subsystems pertinent to the operation of the CEM and the crew within the CEM were identified, masses had to be defined for each component.

Next, a geometry for the hull of the CEM was designed based on the space available inside the SSV. After the hull design was completed, most of the elements and subsystems identified above were packaged within the CEM. These components were then assigned their predicted masses and the CG of the CEM was calculated. Some subsystems could not be assigned a mass for CG location purposes, because the subsystems themselves did not have a preferred size, shape, or location. For example, the environmental control and life support (ECLS) subsystem is composed of several components. The size, shape, and location of each are at best arbitrary. For this study, it was assumed that the ECLS system could be designed in such a way as to have little effect on the CG.

The aerodynamic characteristics of the CEM were then estimated based on the geometry and CG. Lift, drag, and pitching moment coefficients were obtained over a wide range of speeds from subsonic to hypersonic.

Trajectories of the CEM were developed based on the vehicle's aerodynamics, center of gravity, mass, and time of separation from the SSV. Using these trajectories, it was possible to determine the maximum aerodynamic and aeroheating loads on the CEM as well as determine if sufficient altitude and range could be obtained to deploy parachutes and land in the ocean.

A detailed heating analysis was then performed to define the thermal protection system design for the CEM. Also, a body flap had to be designed

which would not only be able to trim the vehicle but also remain intact when confronted by the temperatures and heat loads imposed on the CEM during aborts initiated at high Mach numbers.

## 2. SSV Mission Summary

The SSV mission guidelines call for a vehicle capable of delivering a 25,000 lb payload to a 220 nmi circular orbit with a  $51.6^\circ$  inclination (this is the Space Station orbit). The vehicle will also be capable of delivering 40,000 lb to a 50x100 nmi orbit with a  $28.5^\circ$  inclination. The SSV will carry a flight crew of 2, and 4 passengers for rotation to and from the Space Station. Therefore, the total number of crew on an SSV mission is 6. The mission duration guideline is 7 days.

During a nominal ascent, the SSV will initially achieve a 50x100 nmi orbit. At apogee, the SSV performs a burn to circularize the orbit at 100 nmi. From the 100 nmi, circular orbit, the SSV orbit is phased to its final 220 nmi, circular orbit.

After lift-off at 0 seconds, the SSV passes through its maximum dynamic pressure of 590 psf at 75 seconds. At 170 seconds, the SSV has reached the axial acceleration limit of 3 g's which is maintained until main engine cutoff at 369 seconds. At this time, the SSV is at an altitude of 303,800 ft and an inertial velocity of 25,844 ft/s.

### 3. CEM Configuration and Mass Summary

The following sections detail the CEM design, layout, subsystem masses, and center of gravity location. The weight penalty associated with having a CEM, rather than a crew cabin, is also defined.

#### Design and Packaging

Current and previous studies conducted in the Vehicle Analysis Branch of NASA LaRC have focused on the development of a single stage vehicle along with its various subsystems. This paper makes use of certain previously defined subsystems (e.g. avionics, ECLS, personnel provisions) as well as defining new subsystems (e.g. pyrotechnics, recovery, TPS) for use on the crew escape module. The CEM design investigated in this paper is for a manned, vertical takeoff/horizontal landing SSV with rocket engines that use liquid oxygen/liquid hydrogen propellants. The VAB is also investigating the possibility of other SSV configurations and propulsion options.

As a result of the SSV configuration used in this study, the CEM will be self-contained. This means that the avionics required for the crew to operate the SSV as well as the crew's gear will be carried within the CEM during an abort. In contrast, the Space Shuttle has a middeck where any equipment can be stored which is not essential for the survival of the crew after abort (although the Shuttle does not have an escape module). This allows for the possibility of ejecting only the crew and a minimal amount of equipment necessary for the safe recovery of the astronauts. The SSV configuration used in this study, however, possesses no mid-deck, and the only inhabitable area

is the crew escape module. This means that during an abort the CEM will contain many items which are not essential to the escape process or to the safe recovery of the crew. These items include among other things, cameras, sleep stations, the galley, and the toilet.

The subsystems required for the CEM are summarized in the next section and further defined in Chapter 4. Once the hull of the CEM was designed for integration within the SSV, the subsystems were laid out inside the CEM. The main components to be placed within the CEM were the avionics, crew seats, galley, toilet, parachute containers, and power supply. The avionics (displays, computer, etc.) are located in the front of the CEM. The commander and pilot will sit immediately behind the avionics. The four remaining crew members will sit behind the commander and pilot forming three rows and two columns of seats. The galley and toilet are located in the rear of the CEM. The parachutes are located in the rear center of the module. The parachute canisters are just above the airlock hatch, which is on the rear face of the CEM in the center of the vehicle (between the galley and toilet). The power supply, which consists of two batteries, is located in the front of the CEM, below the avionics equipment.

As mentioned before, other subsystems (specifically ECLS, water management, and fire detection subsystems) were not assigned a specific location because their size and shape are not easily defined. These subsystems weigh 3,730 lb, or 21.8% of the total CEM weight, and will therefore affect the CG and in turn the aerodynamics of the CEM. The final location of all subsystems should be subjected to optimization to improve both the aerodynamic performance as well as the human factors of the CEM.

### Mass Summary

This section contains a mass summary of all the subsystems which comprise the CEM. It should be noted that the total weight of the CEM, as reported at the end of this mass summary, is the total of all the masses with the exception of the pyrotechnics. This is because the pyrotechnics serve only to disconnect the CEM from the SSV and will not be carried with the CEM after the module is jettisoned. Thus, the pyrotechnics weight will add to the weight of the SSV but not to the weight of the CEM. This fact has been indicated by showing the pyrotechnics weight in parentheses.

Avionics	1,645
Crew and Gear	2,782
Environmental Control and Life Support	3,441
Personnel Provisions (7 days)	1,198
Power Supply	15
Airframe (Al-Li 2095)	4,600
Propulsion Subsystem	1,820
Pyrotechnic Separation Subsystem	(269)
Reaction Control Subsystem	300
Recovery Subsystem	500
Thermal Protection Subsystem	750
	=====
Total Mass of CEM	17,051 lb

The weight penalty imposed on the SSV by having a jettisonable crew escape module is 6,106 lb. This penalty is composed of the weights of the propulsion subsystem (1,820 lb), pyrotechnic separation subsystem (269 lb), reaction control subsystem (300 lb), recovery subsystem (500 lb), TPS (750 lb), and additional structural weight (2,467 lb). The additional structural weight is defined to be the difference in the weight of the jettisonable CEM (4,600 lb) and the non-jettisonable crew cabin (2,133 lb) identified in Reference 13.

This weight penalty corresponds to a weight increase of the SSV. Through personal communication with Roger Lepsch of the VAB at NASA LaRC, a 6,100 lb weight penalty imposed by the CEM translates into an increase in the dry weight of the SSV of nearly 24,500 lb (10.5%) and an increase in the gross lift-off weight of nearly 216,300 lb (9%). These weight increases are detailed in Tables 3.1 and 3.2, and were calculated by Mr. Lepsch using CONSIZ (Configuration Sizing Program). The dry weight increase is due to the fact that the SSV must carry more propellant to accommodate the CEM than it would need to carry for a crew cabin configuration. This increase in propellant requires that the tanks be made larger and therefore heavier. Larger tanks, in turn, require that the SSV be made larger and therefore heavier. A larger, heavier SSV requires that many systems be made larger and heavier to withstand the loads. These systems include such things as the nose gear, main gear, wings, and engines.

#### Center of Gravity

The software tool SMART was used to design and package the CEM. This tool not only allows for the size and shape of each component to be defined, but also allows the weight and location of each component to be defined for the purpose of finding the CG of the vehicle. Once the CEM shape was defined, it was assigned its weight of 4,600 lb which is distributed evenly around the hull of the CEM. Next, the components which were able to be given a specific shape and size were assigned their weights. These components are those described in the design and packaging section above. They include the avionics, crew and gear, seats, power supply, propulsion subsystem, and recovery subsystem. For the purposes of this analysis, it was

assumed that the remaining elements and subsystems which could not be defined by a specific shape, size, or location (such as the ECLS, TPS, and most of the personnel provisions) could be sized and located in such a way as to affect the location of the CG only minimally.

The CEM is 19.5 ft long, 13.3 ft wide, and 7.9 ft high. The CG is located at  $x=11.53$  ft,  $y=0$  ft, and  $z=-2.76$  ft, as measured from an axis system located at the nose of the CEM with the  $+x$  axis pointing back along the length of the module, the  $+y$  axis pointing out the right side of the CEM, and the  $+z$  axis pointing up, forming a right handed system. For this study, the moment reference center was assumed to be the CG.

#### 4. CEM Elements and Subsystems

This chapter describes the weight of each subsystem and how (or where) the weight estimate was obtained. The subsystems are listed alphabetically and possess varying degrees of detail. For the subsystems common to both a crew cabin and the CEM (e.g. Avionics, Crew and Gear, ECLS, Personnel Provisions, and Power Supply) the mass summary source is referenced in this chapter and a detailed list of the masses is presented in Appendix A. For the subsystems which are unique to the CEM (e.g. Airframe, Propulsion Subsystem, Pyrotechnic Separation Subsystem, Reaction Control Subsystem, Recovery Subsystem, and Thermal Protection Subsystem), the design and mass estimate are detailed in this chapter.

##### Airframe

The basic shape of the CEM, shown in Figure 4.1, was dictated by the space available inside the SSV. The radius of curvature of the top of both vehicles is identical. This allows the CEM to mate with the SSV in such a way as to use the pre-existing structure of the SSV to serve as the top skin of the CEM as well. The bottom of the CEM is flat to allow for the proper mating of the body flap. The sides of the CEM are rounded to provide more interior room as well as to eliminate sharp corners where the sides meet the top and bottom of the CEM causing an increase in thermal loads in those areas. The length of the crew module allows for enough room to incorporate all the necessary subsystems and crew into the CEM while also allowing for an airlock between the back of the CEM and the front of the LH<sub>2</sub> tank.

During ejection, the module will be propelled away from the SSV at an angle of  $45^\circ$  relative to the body axis of the SSV. This value was determined by the need to achieve maximum altitude for parachute deployment while not interfering with the SSV during ejection. It can be seen in Figure 4.2 that the CEM must eject at an angle of no more than about  $45^\circ$  ( $0^\circ$  being horizontal and  $90^\circ$  being straight up) to avoid possible collision with the LO<sub>2</sub> tank immediately in front of the CEM. This interference also necessitated that the nose of the CEM be rounded to avoid contact with the tank.

The airframe is made of aluminum-lithium (Al-Li) 2095. This material was chosen primarily because it is 15% lighter than aluminum 2219 for the same application. In addition, the baseline material for the SSV is Al-Li 2095. The weight of an aluminum hull structure was determined to be 3.7 times the pressurized volume of the CEM, based on the HL-20 design (which is a vehicle of similar configuration to the CEM, and takes into account a 10 psi overpressure). In this case the volume of the CEM is found to be 1,420 ft<sup>3</sup> and therefore the weight is 5,250 lb for aluminum. Factoring in a 15% weight savings for using aluminum-lithium rather than aluminum, the weight is approximately 4,500 lb.

The body flap will be the only control surface on the crew escape module. It is located on the bottom rear of the CEM and is also made of aluminum-lithium. The flap is 9 ft wide and 6 ft long, for a total surface area of 54 ft<sup>2</sup>. Regression analysis indicates that typical Al-Li body flaps have a weight per unit area of approximately 2 lb/ft<sup>2</sup>, therefore the CEM body flap will weigh approximately 100 lb. This establishes a total airframe weight of 4,600 lb.

## Avionics

The avionics subsystems and weights used in this paper are those identified in Reference 13 for the orbiter of a two-stage Advanced Manned Launch System (AMLS). These weights are detailed in Appendix A. The entire avionics subsystem will weigh 1,645 lb. For this design, this system will be contained within the CEM such that, in an abort situation, the avionics required to perform the flight control and other vital abort functions will be on-board the CEM. This arrangement allows one set of avionics equipment to perform its duty for both the SSV and CEM rather than maintaining the full avionics subsystem for the SSV, and adding a second smaller avionics subsystem to be used on the CEM in case of abort.

A disadvantage of using one set of avionics equipment is that during an abort, the CEM will be carrying several hundred pounds of electronics which will be unnecessary for the proper functioning of the CEM during abort. This corresponds to an increase in weight of the parachutes as well as the solid rocket ejection motors. It may be difficult to avoid this weight penalty due to the necessary integration of the avionics equipment and displays into the cockpit.

## Crew and Gear

Crew weight is based on an average size of 165 lb/person. Therefore, the crew of six has been allocated a total weight of 990 lb. The gear associated with the crew is detailed in Appendix A. This gear is representative of the gear used on-board the Space Shuttle and includes, among other things, clothes, hygiene and medical equipment, tool kits, and personal effects. The total weight of the gear is 1,792 lb (304 lb/person).

### Environmental Control and Life Support

The environmental control and life support (ECLS) subsystems and weights used in this paper are those identified in Reference 13 for the orbiter of a two-stage AMLS. This subsystem includes heat transport and rejection systems as well as equipment cooling and a personnel system for the crew. The total weight of the ECLS subsystem is 3,441 lb. A detailed weight breakdown of the ECLS subsystem is shown in Appendix A.

### Personnel Provisions

Food, waste and water management systems along with crashworthy seats and a fire detection system make up the personnel provisions weight of 1,198 lb. A detailed breakdown of these weights is in Appendix A and was obtained from the Orbiter Detail Weight Statement (Reference 14).

### Power Supply

The CEM's electrical power subsystem consists of two lithium thynol-chloride (Li-SClO<sub>2</sub>) batteries capable of providing 270Vdc power.<sup>15</sup> These batteries will provide the necessary power to run the avionics, ECLS, and body flap actuator after separation from the SSV. The power requirements and duty cycles of each component were obtained from References 16 and 17, as well as through personal communication with Howard Stone of NASA LaRC. These requirements and duty cycles are shown in Table 4.1. The total energy requirement for the CEM after abort is calculated to be less than 4.1 kWh. The Li-SClO<sub>2</sub> batteries have an energy density of 650 W-hr/kg (or about 300 W-hr/lb)<sup>18</sup>, corresponding to a battery weight of nearly 15 lb.

### Propulsion Subsystem

Once detached from the SSV, the CEM is propelled away from the SSV by two solid rocket motors attached to the hull of the CEM. These motors have been sized to provide the CEM with sufficient energy to escape a catastrophic explosion of the SSV, specifically on the pad where the greatest amount of thrust is needed to clear the maximum tolerable overpressure zone. The exact sizing of these motors is detailed in this section.

The SSV will carry on-board 2,200,000 lb (1,100 tons) of propellant. After the SSV lifts off, it will burn fuel at the rate of 7,550 lb/s and therefore the explosive potential will decrease as the mission continues. However, on the pad the explosive potential is at a maximum because all 1,100 tons of propellant is present.

The explosive potential of LO<sub>2</sub>/LH<sub>2</sub> has been found to be approximately 60% that of tetranitromethane (TNT).<sup>19</sup> Therefore, the explosive potential of the SSV is equivalent to 660 tons of TNT, or  $W_T=660$ . This equivalent amount of TNT can now be used to determine how far the CEM must travel to escape the maximum tolerable overpressure boundary. Several of these boundaries are shown in Figure 4.3. For this paper, it is assumed that the CEM is capable of withstanding a 10 psi overpressure (pressure over and above the ambient pressure of 14.7 psi). While 10 psi is commonly used as the baseline design condition, it is possible to design a structure capable of withstanding greater pressures. No trade study was performed to determine how weight varies with the tolerable overpressure limit, however future study could identify the optimal overpressure limit which produces the lightest weight CEM.

From Reference 19, the overpressure ratio is defined as  $p/P_x$ , where  $p$  is the overpressure and  $P_x$  is the atmospheric pressure. At sea level this ratio is  $p/P_x = 10/14.7 = 0.68$ . For a one-ton explosion of TNT, this corresponds to a radial distance of  $d'=90$  ft and an arrival time of  $t'=0.0368$  seconds. Consequently, for 660 tons of TNT, the maximum tolerable overpressure of 10 psi occurs at a radial distance of 784 ft according to the following equation

$$d = d' (W_T)^{\frac{1}{3}}$$

and the arrival time of the overpressure wave occurs approximately 0.32 seconds after the explosion according to the equation

$$t = t' (W_T)^{\frac{1}{3}}$$

These empirical equations were developed from the analysis of a spherical charge of one ton of TNT at sea level coupled with the fact that for other weights of TNT "two explosions will give identical blast wave intensities at distances which are proportional to the cube root of the respective energy release."<sup>19</sup>

Also of importance to this analysis is the fact that propellant explosions behave differently than TNT explosions. This difference is thought to be due to the nonhomogeneous nature of the propellant mixing process. When the LH<sub>2</sub> and LO<sub>2</sub> come into contact, they produce a series of small explosions as they mix. On the other hand, a TNT explosion produces a single detonation and therefore a single pressure wave. The initial LO<sub>2</sub>/LH<sub>2</sub> explosion sends out a leading shock which heats the air it passes through. As subsequent

shock waves are produced by the continuous mixing of propellant, they travel through the preheated air of the first shock. Because the shock wave speed is higher in the preheated air, these waves will catch up to the initial wave and serve to reinforce it.<sup>20</sup>

As a result of the empirical nature of the preceding equations and the complex dynamics which characterize a propellant explosion, it should be noted that the numbers obtained in the separation distance analysis detailed in this section are the best figures available at the conceptual design stage. Further analysis, perhaps in the form of a scaled down explosion of the SSV configuration, is essential to determine more accurately the required separation distance and time of arrival.

According to these numbers, an abort initiated simultaneously with the explosion would require the CEM to travel 784 ft in 0.32 seconds, inducing an acceleration of 475 g's. This is well beyond the recommended maximum human tolerance limit shown in Figure 4.4. A more acceptable and commonly used acceleration of 8 g's was chosen for the thrust of the escape rockets. This thrust level along with the 784 ft radial distance to the overpressure boundary set the burn time of the rockets at approximately 2.7 seconds. Using POST, it was determined that the CEM crosses the 784 ft boundary 2.64 seconds after the solid rockets ignite. Since the overpressure wave will reach the 784 ft distance 0.32 seconds after the explosion, the imminent explosion must be detected 2.32 seconds prior to the time the explosion actually takes place. This study assumed that the time required to detonate the pyrotechnics (approximately 0.0035 seconds) was negligible.

The solid rocket ejection motors will use TP-H1148 for fuel, which has a specific impulse,  $I_{sp}$ , of 256.7 seconds for this type of application. In order to

determine the mass of fuel needed, a summation of forces must be performed on the CEM. From Reference 21, a sum of the forces yields the following equations:

$$\begin{aligned}\Sigma F &= m \frac{dv}{dt} \\ T - D - mg \cdot \sin \gamma &= m \frac{dv}{dt} \\ -u \frac{dm}{dt} - D - mg \cdot \sin \gamma &= m \frac{dv}{dt}\end{aligned}$$

The exhaust velocity,  $u$ , can be rewritten in terms of the specific impulse as  $u = g_0 I_{sp}$ . Making this substitution, multiplying both sides by  $dt/m$  and integrating from  $t_1$  to  $t_2$  (duration of the burn) gives

$$\int_{v_1}^{v_2} dv \equiv \Delta V = g_0 I_{sp} \ln \frac{m_i}{m_f} - \int_{t_1}^{t_2} \frac{D}{m} dt - \int_{t_1}^{t_2} (g \cdot \sin \gamma) dt$$

For a first order approximation, the drag term in this equation will be neglected and a burn time of 2.7 seconds will be assumed. Ignoring the drag term, the equation above becomes

$$\Delta V = g_0 I_{sp} \ln \frac{m_i}{m_f} - \int_{t_1}^{t_2} (g \cdot \sin \gamma) dt$$

It can be seen that  $\Delta V$  is equivalent to the product of the escape rocket acceleration and the burn time, or 696 ft/s. Taking into account that the flight path angle,  $\gamma$ , is  $45^\circ$ , and the initial mass is 17,051 lb, the final mass is found to be 15,559 lb. Therefore, the mass of propellant required is 1,492 lb. Solid rockets for comparable uses are typically 82% propellant and 18% structure.

Using these figures, the solid rockets (without propellant) weigh 328 lb, for a total propulsion subsystem weight of 1,820 lb.

### Pyrotechnic Separation Subsystem

In the event of a catastrophic failure, the crew module will need to be separated from the single stage vehicle in a quick and reliable manner. This function will be performed by the pyrotechnic separation system. Once an escape is initiated, a sequencer will ignite the various pyrotechnic devices, all of which have a reliability of over 99.9%, in order to separate the structure and cabling which link the CEM to the SSV. This separation is estimated to take less than 0.0035 seconds.

Through personal communication with Larry Bement of NASA LaRC, a pyrotechnic separation system for the CEM was developed. This system is made up of various pyrotechnic devices which perform different tasks during the separation sequence. First, an explosive cord (or linear charge) is placed around the skin of the CEM along the border between the CEM and SSV. This will require approximately 65 ft of cord which weighs approximately 2 lb/ft. When detonated, the cord will tear open the skin of the SSV (see Figure 4.5). Once detonated, the explosion propagates along the cord at the rate of 22,000 ft/s in vacuum (25,000 ft/s under ambient conditions). Therefore, the cord will have completely severed the skin in less than 0.003 seconds from the initial detonation. The linear charge will be detonated by redundant explosive transfer lines to insure separation. These lines are 10 ft in length each, and have propagation rates equivalent to the linear charge, which corresponds to a propagation time of less than 0.0005 seconds. Thus, the total time required for skin severance is less than 0.0035 seconds.

Second, an explosive nut and bolt combination (see Figure 4.6) will be used at each of an estimated 8 hardpoint connections to separate the CEM structure from the SSV structure. These nut/bolt combinations are approximately 1.5 lb each and provide for their own redundancy because the probability of both devices failing is 0.000001.

Third, the cables which connect the crew module to the rest of the vehicle must be severed. These cables will pass through disconnection plates which will be lined with linear charge as shown in Figure 4.7. After the charge is ignited, the plates will be pushed apart by the expanding gas and will pull the cable connection apart. It is estimated that 6 cable disconnection plates will be needed to sever the cables connecting the CEM and SSV. Each plate assembly weighs about 2 lb.

Lastly, a shape charge (see Figure 4.8) will be placed around the airlock to sever the mechanical connection of the CEM to the airlock. Two shape charges will be used for redundancy, each weighing 10 lb. A new pyrotechnic technology called Augmented Shock Wave Severance has been developed by Mr. Bement which may replace both the airlock shape charge and the explosive cord used for skin severance. This new technology is used to sever the structural link between two objects by detonating two linear charges which are embedded in the structure which is to be severed. When detonated, the shock waves from the two cords augment one another and cause the structure to fail in tension. This technology provides a lighter weight system and produces less debris when detonated.

The entire separation will be controlled by a sequencer and command controller. For safety, a redundant controller is added. Each of the controllers weighs 20 lb. They will ignite the pyrotechnics in the proper sequence via

explosive transfer lines. These lines, shown in Figure 4.9, will run to each device to initiate detonation. An estimated 110 ft of line will be needed, however 220 ft will be used in order to have a totally redundant system. The transfer line weighs approximately 0.25 lb/ft. Altogether, the pyrotechnic separation system weighs 269 lb.

#### Reaction Control Subsystem

The reaction control subsystem (RCS) will be used to stabilize the CEM in low dynamic pressure conditions (i.e. high altitudes and Mach numbers). It may also be used to stabilize the CEM during the solid rocket burn. From References 22 and 23, an RCS weight of 300 lb was derived.

#### Recovery Subsystem

Two major components comprise the recovery subsystem of the CEM. The parachute recovery subsystem and floatation subsystem are both vitally important if the CEM is to return the crew safely to Earth. The parachutes must decelerate the module to a survivable velocity at ocean impact. When the CEM lands in the ocean, a floatation subsystem is required to keep the module afloat until a retrieval team arrives.

Parachutes have been utilized for the final descent phase of all U.S. and Russian manned space flights prior to the Space Shuttle due to their high degree of reliability, ease of packaging, and relatively small volume when compared to other descent systems.<sup>24</sup> The parachutes provide a means of decelerating the vehicle to velocities which will be survivable by the crew upon impact. A descent rate of 30 ft/s (20.5 mph) is commonly accepted as a

tolerable descent velocity, however, this is excessive for a manned vehicle without some means of attenuating the g's at impact.

The CEM will utilize a parachute system similar to the Apollo parachute system which was used to decelerate the 13,000 lb Apollo capsule to 28.8 ft/s for an ocean landing. The CEM, which will weigh 15,231 lb after burn-out, will require somewhat larger chutes than those of the Apollo capsule. However, with the advent of new materials like Kevlar and Specktra along with improved design techniques, the CEM parachutes will actually be lighter than the nylon Apollo parachutes.

Many factors must be considered in developing a parachute subsystem to be used on a manned space vehicle. Inflation times, line lengths, canopy and line material, canopy type, oscillation angle, along with scores of other variables, can be manipulated to produce an optimized parachute design. This, however, is not in the scope of this study and therefore only a preliminary design will be performed. This preliminary design is described in the following paragraphs and consists of determining the main parachutes' size, weight, and stored volume.

Sizing the main parachute (see Reference 24) involves studying the parachute in stable, unaccelerated descent. This condition is shown in Figure 4.10. Balancing the forces yields the following equation:

$$D_p + D_l = W_p + W_l$$

where  $D_p$  is the drag of the parachute,  $D_l$  is the drag of the load,  $W_p$  is the weight of the parachute, and  $W_l$  is the weight of the load. In most cases, the drag of the load can be neglected in comparison to the large drag of the

parachute. Therefore, the drag force created by the parachute is equal to the weight of the vehicle (including the parachute weight).

In general, drag is defined by the equation

$$D = qSC_D$$

where  $C_D$  is the drag coefficient,  $S$  is a reference area, and  $q$  is dynamic pressure. Noting that the drag is equal to the weight of the vehicle and  $q$  is  $\frac{1}{2}\rho V^2$ , the following expression is obtained:

$$S = \frac{2W}{\rho C_D V_e^2}$$

This equation relates the area of the parachute,  $S$ , to the desired descent velocity,  $V_e$ . For this analysis, the weight is 15,231 lb (the weight of the CEM with parachutes but without the solid rockets which are jettisoned after burnout), the density of air is  $2.377 \times 10^{-3}$  slugs/ft<sup>3</sup>, the drag coefficient is 0.77, and the descent velocity is 30 ft/s. This results in a canopy area of 18,493 ft<sup>2</sup> (153.4 ft diameter). However, it is not desirable to use a single parachute design because of the probability of a catastrophic system failure (i.e. the chute not opening).

A cluster of parachutes avoids the single point failure by providing one more parachute than is required to decelerate the vehicle to the proper velocity. By clustering the parachutes, they can be made smaller. The smaller the chutes, the easier they are to fabricate, store, maintain, rig, handle, and retrieve. A cluster of smaller chutes will also inflate more rapidly than a single large chute. This is important for escape at low altitudes such as escape

during the first few seconds of launch. Parachute clusters are also more stable than an individual parachute.<sup>24</sup> This corresponds to less oscillation of the CEM as it is approaching water impact, thus allowing for a more predictable impact angle.

There are disadvantages of clustering parachutes. Clustered parachutes experience a decrease in drag, as compared to an individual parachute of like size, due to the interference of one parachute in the cluster with the other parachutes. In addition to drag reduction, "it is impossible to obtain a perfectly synchronized opening of all parachutes in a cluster. Because unsynchronized opening causes a lead/lag parachute situation, with lead parachutes having shorter filling times and higher individual parachute loads, each parachute in the cluster must be designed to handle the maximum individual load. Therefore, the total strength of the parachutes in a cluster and their associated weight and volume are higher than the weight and volume of a single large parachute of equivalent drag area."<sup>24</sup>

Manipulating the equation above to account for parachute clustering, the following equation is obtained:

$$S = \frac{2\left(\frac{W}{n}\right)}{\rho C_D V_e^2}$$

where n represents the number of parachutes in the cluster. It should be noted that  $C_D$  is now the drag coefficient of the cluster, or 0.74.<sup>24</sup> Therefore, if three parachutes were used, one parachute would only be responsible for decelerating 1/3 of the weight of the vehicle. Using a value of 3 for n, the parachutes to be used on the CEM have a canopy area, S, of 6,414 ft<sup>2</sup> (90.4 ft

diameter). Again, in case of a system failure in one of the parachutes, a fourth parachute of equal size will be used as a backup. Assuming all four chutes work without error, the descent velocity will be reduced to 26 ft/s (17.7 mph).

Parachute weight is determined by using a weight effectiveness and applying it to the parachute's drag area. The weight effectiveness is the ratio of the drag area to the weight of the parachute. From Reference 24, it can be seen that the Apollo parachutes had a weight effectiveness of 40.0. Today, "the weight effectiveness of well-designed nylon parachutes reaches 65 square feet (ft<sup>2</sup>) of drag area per pound of parachute weight. Hybrid parachutes using nylon for the canopy and Kevlar for suspension lines, canopy tapes, and radials reach 85 ft<sup>2</sup> of drag area per pound of parachute weight."<sup>24</sup> For this study a nylon parachute with a weight effectiveness of 65 ft<sup>2</sup>/lb has been used.

The drag area of the individual CEM parachutes is the product of their drag coefficient and their canopy area. This drag area is therefore the product of 0.74 and 6,414 ft<sup>2</sup>, or 4,746 ft<sup>2</sup>. Dividing this number by a weight effectiveness of 65 ft<sup>2</sup>/lb, a parachute weight of 73 lb is obtained. Therefore, the cluster of three parachutes plus the one backup chute weigh 292 lb. Using a nylon/Kevlar hybrid chute could reduce this weight to 223 lb.

A total parachute recovery system includes a first-stage drogue-chute assembly which lowers the crew module to the allowable opening speed or altitude for main parachute deployment, and pilot chutes which pull the main chutes out of their containers. "As a rule, deployment bags weigh 5 to 6% of the parachute, and deployment bags plus pilot chute and pilot chute bridle add 3 to 5%. First-stage drogue-chute assemblies will weigh from 25 to 40% of the main parachute weight depending on deployment dynamic pressure and riser length."<sup>24</sup> Using these figures, the total parachute recovery

system should weigh between 133 and 151% of the main parachute weight (170% for Apollo parachute system). Using the 151% figure this corresponds to a parachute recovery subsystem weight of 441 lb.

The parachute recovery subsystem detailed above will be operated by an onboard events controller which is incorporated into the CPU. This controller will monitor the altitude and velocity as well as mission phase to determine the sequence of events.

In the event of a catastrophic failure on the pad, the CEM will be propelled to an altitude of approximately 2,800 ft by the solid rockets. Because the velocity during this phase will be subsonic, the drogue chute, pilot chutes and subsequently the main chutes can be deployed at any time. Due to the low altitude, as well as to the fact that the CEM is unstable at subsonic speeds, the controller initiates chute deployment immediately after the escape rockets have burned out. This will allow the chutes to stabilize the CEM.

The deployment sequence at low altitudes and speeds will consist of deploying the drogue chute immediately after rocket burn-out and then deploying the main chutes via the pilot chutes 3 seconds after the CEM reaches the apex of its trajectory. The chutes will serve to stabilize the CEM at Mach numbers of 1.6 and below (the drogue chute is capable of deployment at  $M=1.6$ ).

Throughout the mission, the controller will monitor the altitude and Mach number. Once the velocity exceeds Mach 0.5, it will become necessary to decelerate the vehicle to a Mach number of 0.5 or below in order to safely deploy the pilot and main chutes. The first-stage drogue-chute will be a hemisflo ribbon parachute capable of being deployed at supersonic Mach

numbers below 3 ( $M < 3$ ). This chute not only serves to decelerate the CEM, but also to stabilize the CEM for main chute deployment.

This study assumes that the preceding parachute opening sequences occur without complication. It is possible that off-nominal abort scenarios could occur which might alter the performance of the parachutes. For example, the overpressure wave could disrupt the normal operation of the chutes, particularly if the CEM is unable to clear the overpressure zone in sufficient time. A more detailed analysis of the parachute system is required to properly address these off-nominal conditions.

Impact attenuation is not required to decelerate the CEM from its terminal descent velocity of 30 ft/s to 0 ft/s, however crashworthy seats will be used to attenuate the g's experienced by the crew at impact. The crashworthy seats are able to absorb the impact loads in all three principal directions.

The decelerations experienced by the CEM during water impact are thought to be similar to those in Reference 25 for an HL-10 lifting body which is similar in size and shape to the CEM. This study found that the g's encountered by the vehicle upon impact with the water at 40 ft/s in a nearly vertical attitude, were at or below 8 g's .

#### Thermal Protection Subsystem

The single stage vehicle will perform a mission not unlike the Space Shuttle. It will take-off vertically, pitch over as it climbs, achieve an orbit around the Earth, reenter the atmosphere, and glide back to an unpowered horizontal landing. Most of the mission, therefore, takes place at altitudes and speeds which contribute to a severe heating environment. This

environment is not survivable with conventional escape systems such as parachutes and ejection seats (open or encapsulated). It is under these conditions that a crew escape module is required for crew recovery.

Trajectories calculated using POST (see Appendix D) show that for a nominal ascent profile, the worst heating case occurs 320 seconds after take-off when the SSV is at an altitude of 297,900 ft and Mach 22.5. This heating case was analyzed by MINIVER (see Appendix C) to determine the highest heating rate and thermal equilibrium temperature experienced by the CEM.

A trade study was performed, using MINIVER, to determine the best suited thermal protection subsystem for the CEM. Three reference materials were used in this study. First, SLA-561 ablator was analyzed. This is the ablative material which was used on the Apollo capsule for thermal protection during reentry. Second, an HTP-12-22 tile was analyzed. And finally, the LI-900 tile, which is used on the Space Shuttle Orbiter was analyzed. This study found the ablator or tile thickness required to keep the stagnation point backface temperature below an acceptable level. The backface temperature is the temperature of the back of the TPS, or the interface between the Al-Li skin and the TPS. The acceptable level for this study was 250°F, the temperature (with some margin) at which the strength properties of Al-Li begin to degrade. The results are tabulated below:

<u>Material</u>	<u>Thickness</u>	<u>Weight/ft<sup>2</sup></u>	<u>Weight</u>
SLA-561	1.5 (inches)	2.09 (lb/ft <sup>2</sup> )	1,339 (lb)
HTP-12-22	1.1	1.61	1,030
LI-900	1.25	1.44	926

It can be seen that the LI-900 tile is the lightest weight option for a thermal protection subsystem. The lay-up of the TPS is shown in Figure 4.11. This tile was then used in a more detailed analysis using MINIVER to determine the required thickness of the tiles needed at each point along the centerline of the CEM. This gave a refined weight estimate of 650 lb for the TPS. The body flap requires 100 lb of TPS to protect it from the heating environment. The total TPS weight for the CEM is 750 lb.

## 5. Aerodynamics

In the following sections, the predicted lift, drag, and pitching moment coefficients are presented. The three longitudinal aerodynamic coefficients were estimated at thirteen Mach numbers from 0.3 to 25 and altitudes ranging from sea level to 270,000 feet using APAS (see Appendix B) assuming the CG location detailed in Chapter 3. The altitude information was used to compute a skin friction drag component which is added to the inviscid drag component to obtain the total drag component. The reference area and reference length used for this study were the base area of the CEM (92 ft<sup>2</sup>) and length of the CEM (19.5 ft), respectively.

Plots for Mach numbers of 1.6 and above demonstrate the effects of body flap settings of 0°, 5°, 10°, 15°, and 20°. A configuration with no body flap is also included as a reference. It can be seen that the 0° flap and no flap configurations exhibit different aerodynamic characteristics. This is because the addition of the body flap moves the center of pressure more aft, which has a stabilizing effect.

Only a 3-D analysis of the CEM was performed, therefore, the lateral directional coefficients were not examined. As a result, roll and yaw stability were not analyzed and it was assumed that a combination of the RCS and split body flap would provide sufficient stability and control for the CEM.

### Subsonic/Transonic

Data for Mach numbers of 0.3 and 0.6 are shown in Figures 5.1 and 5.2. In this speed regime, the lift and drag coefficients remain essentially constant as a function of Mach number. As the speed becomes transonic, see Figures

5.3 and 5.4, the zero lift drag coefficient increases dramatically. Figures 5.1 to 5.4 indicate that the lift coefficient remains linear as a function of angle-of-attack below Mach 1.2. This is due to the linear potential theory used to estimate the aerodynamic characteristics by APAS. However, at subsonic and transonic speeds, the CEM will be under the influence of the parachutes and therefore the limits imposed by the linear theory of APAS at subsonic and transonic speeds should not affect the results of this study.

### Supersonic

Figures 5.5 through 5.9 show data for Mach numbers of 1.6, 2, 4, 6, and 9. Over this range of speeds, both lift and drag coefficients decrease as the Mach number increases. Stability and trimability over this speed regime is attained by using the body flap. For example, at a Mach number of 6.0 (see Figure 5.8) and a body flap setting of  $10^\circ$ , the CEM is trimmed at an angle of attack of approximately  $34^\circ$ . As the Mach number decreases over this range, and holding the body flap setting fixed, the trim angle of attack decreases from  $34^\circ$  at Mach 9 to  $13^\circ$  at Mach 1.6. These trimmed conditions were used by POST to define the angle-of-attack history during the supersonic segment of the simulated abort trajectory.

### Hypersonic

Figures 5.10 through 5.13 show data for Mach numbers of 12, 15, 20, and 25. In this flight regime, lift and drag coefficients continue to decrease, but not as quickly as they do subsonically. Both the pitching moment coefficient and the trim angle-of-attack for a  $10^\circ$  body flap setting are virtually unchanged as a function of Mach number in this speed regime.

## 6. Trajectory Analysis

Profiles from the nominal ascent trajectory for the single stage vehicle are shown in Figures 6.1 to 6.8. For each abort simulation, the initial conditions of the CEM were taken from the nominal ascent trajectory of the SSV. These initial conditions included the altitude, latitude, longitude, relative flight path angle, relative velocity, and the initial azimuth angle of the relative velocity vector.

### Abort On-the-Pad

Typically, an abort initiated on the launch pad is the most demanding escape scenario to impact the design of the CEM. Not only is the explosive potential at a maximum, but the CEM must also achieve sufficient altitude to deploy the chutes as well as sufficient range to land in the ocean. These factors dictate the design of the solid escape rockets which were detailed in Chapter 4. This design was then verified using POST (see Appendix D) to confirm that sufficient altitude and range are achieved.

The results of the trajectory simulation of an abort initiated on-the-pad are shown in Figures 6.9 to 6.15. These results show that for an abort at  $T=0$  seconds, the CEM achieves a maximum altitude of approximately 2,800 ft and a range of nearly 0.69 nautical miles (~ 4,200 ft). At this range, according to oceanographic charts of the Florida coast, the CEM would land in water 30 ft deep. During this abort the CEM experiences a maximum speed of 570 ft/s (Mach 0.51) which occurs at burnout. The speed diminishes to 30 ft/s at ocean impact. Ocean impact occurs 94 seconds after solid rocket ignition.

At the time of abort, the crew experiences an 8g burn. Immediately after burnout, a drogue chute is deployed. The CEM is slowed and stabilized via the drogue chute until the apex of the trajectory is reached. Three seconds after the CEM passes through the apex, the main chutes are deployed. These chutes are reefed into three stages to decrease the opening forces. Figure 6.15 shows the forces associated with the three reefed stages of the main parachute deployment. The forces imposed on the CEM due to parachute deployment are below 5 g's.

#### Abort at Maximum Dynamic Pressure

The CEM experiences its maximum dynamic pressure of approximately 720 psf when an abort is initiated 55 seconds into the flight of the SSV. At this point, the SSV is at an altitude of 14,200 ft and is traveling 664 ft/s (Mach 0.63). The results of the trajectory simulation initiated at this time are shown in Figures 6.16 to 6.22. These results show that the CEM reaches a maximum altitude after ejection of approximately 17,500 ft. Nearly 540 seconds (9 minutes) later, the CEM lands in the ocean approximately 2.3 nmi (~ 14,000 ft) from the launch pad. During this abort, the CEM experiences a top speed of just over 1,000 ft/s (Mach 0.96) which occurs at burnout. The parachutes decelerate the CEM to 30 ft/s at ocean impact.

For an abort at maximum dynamic pressure, the crew would experience an 8g burn followed by a 3g force as the drogue chute fully deploys. The drogue chute is deployed immediately after burnout to slow and stabilize the CEM. Three seconds after the CEM passes through the apex of its trajectory, the main chutes are deployed. The three reefed stages of the main chutes limit the opening forces to 5g's and below.

### Abort at Maximum Heat Rate

Another demanding design condition for the CEM is the maximum heat rate case. The CEM experiences its maximum heat rate of 91 Btu/ft<sup>2</sup>-s when an abort is initiated 320 seconds into the flight of the SSV. At this time, the SSV is at an altitude of 297,900 ft and is traveling at 20,120 ft/s (Mach 22.5). The results of the trajectory simulation initiated at this time are shown in Figures 6.23 to 6.29. These results show that the CEM's maximum altitude is approximately 305,000 ft, while it achieves a range of nearly 2,050 nmi. During the abort, a maximum speed of 20,800 ft/s (Mach 23.3) is reached. The parachutes reduce this speed to 30 ft/s at ocean impact, which occurs 1,244 seconds (20.7 minutes) after abort.

The crew will experience an 8g burn at the time of abort. The body flap will stabilize the CEM until it decelerates to a safe speed for drogue chute deployment. Approximately 900 seconds (15 minutes) after abort initiation, the CEM will have decelerated to a Mach number of 1.6 at which time the drogue chute will be deployed. The drogue chute deployment will induce a 7.2g opening force. Once the CEM slows to a Mach number of 0.5, the main chutes will be deployed in a three reef sequence. The maximum opening force of the main chutes is calculated to be 5.3g's.

## 7. Conclusions

While the concept of a crew escape module is not new, its specific design is unique for each vehicle to which the concept is applied. The purpose of this study, was to design a crew escape module, for a single stage vehicle, capable of providing a means of abort for the crew from launch to orbital insertion. By providing this capability over the entire ascent phase, the CEM offers greater safety to the crew than would the baseline ejection seat configuration, which does not provide abort capability to the crew at high Mach numbers. The design of the module was analyzed to calculate its mass, CG, longitudinal aerodynamic characteristics, simulated trajectories, and aeroheating environment.

Because the CEM designed in this paper is for a specific single stage vehicle, the design of the SSV will have implications on the design of the CEM. For example, the amount and type of propellant used in the SSV will affect the overpressure boundary and in turn the CEM solid rocket design. The SSV configuration may also change to accommodate a CEM which could be located at the nose of the SSV rather than in the middle. This change alone would necessitate the complete redesign of the CEM. In addition, the design of the CEM hull has implications on the layout of the CEM. Increasing or decreasing the length, width, or height of the CEM opens new possibilities for the location of major subsystems and therefore the location of the CG. By changing the hull shape and the CG, an entirely new set of aerodynamics can be created for the CEM. These aerodynamics can then be optimized to produce the best combination of altitude, range, stability, and control.

This paper has summarized the weights of the required subsystems which would be carried aboard the crew module, as well as the structural

weight of the module itself. The CEM weight was calculated to be 17,051 lb, while a weight penalty of 6,106 lb was calculated for the crew escape module as compared to a non-jettisonable crew cabin. This penalty was due to the additional structural weight of the module compared to the cabin, as well as to the propulsion, pyrotechnic, RCS, recovery, and TPS subsystems which are unique to a jettisonable crew module. The CEM weight penalty translated into an increase in the dry weight of the SSV of nearly 24,500 lb (10.5%) and an increase in the gross lift-off weight of 216,300 lb (9%).

The aerodynamic analysis showed that the module was unstable over much of its operational range. A body flap and RCS system were added to stabilize the module in supersonic and hypersonic flight, while the parachutes are used for stabilization in subsonic flight.

The trajectory simulation demonstrated that the crew escape module achieved sufficient altitude to deploy the parachutes and sufficient range to land in the ocean if an abort was initiated on-the-pad. This analysis also determined the time of maximum dynamic pressure was for an abort initiated at T+55 seconds, and the time of maximum heating was at T+320 seconds. The maximum heating case was analyzed to determine the proper type and thickness for a thermal protection subsystem.

## 8. Recommendations for Future Work

The CEM design outlined in this paper is only preliminary, and as such lacks detail in many areas. Primarily, further work needs to be done in order to quantify the amount of safety the CEM provides and compare the safety to that of other vehicle configuration options. In addition, an analysis needs to be performed to identify various failure modes, the dynamics involved during the CEM separation from the SSV need to be determined, and a detailed structural analysis needs to be performed on the CEM in order to accurately determine the structural weight of the module.

Each of the subsystems required for abort should also have more detail incorporated into their design. For instance, this paper determined the parachute subsystem weight by estimating the main parachute weight and then multiplying this weight by some factor determined via regression analysis. Future work should focus on detailing the entire parachute subsystem, including the drogue chute, pilot chutes, main chutes, deployment bags, lines, reefing sequence, optimal deployment sequence, etc. Similar detail should be given to the pyrotechnic separation subsystem, propulsion subsystem, reaction control subsystem, and thermal protection subsystem, each of which is required only for the abort capability.

The shape of the CEM should also be refined to produce the best self-stabilizing, aerodynamic design for the given space available within the SSV. Further analysis should also be performed to identify the best means of controlling the CEM after it jettisons from the SSV. A split body flap, reaction control subsystem, thrusters, and gimbaled nozzles are all potentially viable options for the control of the CEM. Each needs to be analyzed and a trade study performed to select the best combination.

## 9. References

1. Lewis, Richard S.: *Challenger: the final voyage*. New York, NY: Columbia University Press. 1988.
2. Mavriplis, Fotis: Emergency Escape From Multicrew Earth Orbital Vehicles. Paper presented at the Symposium of the Astronautics Section, CASI on Satellites and Spacecraft (Montreal, Canada), Feb. 28 - March 1, 1963.
3. Bolger, Philip H.: Evolution of Escape Systems for Manned Space Flight. Paper presented at the 3rd International Symposium on Space Rescue (Constance, Germany), Oct. 5-10, 1970.
4. Presidential Commission on the Space Shuttle Challenger Accident. Report to the President: Actions to Implement the Recommendations of The Presidential Commission on the Space Shuttle Challenger Accident, July 14, 1986.
5. Whitehurst, Troy N. Jr.: Space Shuttle Orbiter Ejection Seat Survey. *SAFE Journal*, vol. 17, no. 1,
6. O'Connor, Bryan: Safety and Rescue During STS Operations. Proceedings of the Workshop on Crew Safety and Rescue in Space - An International Approach (LeBourget, France), June 7, 1989.
7. Peterson, Wayne L.: ACRV-Derived Transportation System. AIAA-92-1414, March 1992.
8. Mayer, R.T.: MOSES (Manned Orbital Space Escape System) - A Hypothetical Application. AIAA-81-0438, Feb. 1981.
9. Davis, H.P. and Teixeira, C.: A Next Generation Space Shuttle Concept. AIAA-89-0089, Jan. 1989.
10. Nguyen, H.P. and Frank, F.: Hermes Crew Escape Module. IAF-80-060, Oct. 1988.
11. Nguyen, H.P., Rolfo, A., and Charles, J.: Hermes Crew Escape Module Configuration Studies. IAF-89-616, Oct. 1989
12. Nguyen, H.P., Colrat, J., and Hirsch, H.: Hermes Escape System. Proceedings of the International Symposium on Europe in Space — The Manned Space System (Strasbourg, France), ESA SP-277, April 25-29, 1988.

13. Advanced Manned Launch System (AMLS) Study Final Report - Task 4. Contract No. NAS1-18975, June, 1992.
14. Thomas, R. E.: Orbiter Detail Weight Statement. Contract No. NAS9-14000, Dec. 1985.
15. Advanced Manned Launch System (AMLS) Study Final Report - Task 3. NASA Contractor Report 189673, Contract No. NAS1-18975, Sept. 1992.
16. Personnel Launch System (PLS) Study Final Report (DRD 12). NASA Contractor Report 187620, Contract No. NAS1-18975, Oct. 1991.
17. Personnel Launch System Advanced Manned Launch System (PLS/AMLS) -- Hardware/Software Design Description. Contract No. NAS1-18975, Dec. 1990.
18. Griffin, Michael D. and French, James R.: *Space Vehicle Design*. Washington, D.C.: AIAA Education Series. 1991.
19. Greensite, Arthur L.: Analysis and Design of Space Vehicle Flight Control Systems, vol. XVI. NASA CR-835, May 1969.
20. High, Richard W.: Some Liquid Oxygen/Liquid Hydrogen Explosive Effects in Controlled Failure-Mode Tests. NASA TN D-5382, Sept. 1969.
21. Chobotov, Vladimir A.: *Orbital Mechanics*, Washington, D.C.: AIAA Education Series. 1991.
22. Glatt, C. R.: WAATS - A Computer Program for Weights Analysis of Advanced Transportaion Systems. NASA CR-2420, Sept. 1974.
23. Bentz, M. D. and Kotker, D. J.: Conceptual Design and Analysis of Hypervelocity Aerospace Vehicles, vol. 3 - Propulsion. AFWAL-TR-87-3056, Feb. 1988.
24. Knacke, T. W.: *Parachute Recovery Systems Design Manual*, Santa Barbara, CA: Para Publishing. 1992.
25. Stubbs, Sandy M.: Landing Characteristics of a Dynamic Model of the HL-10 Manned Lifting Entry Vehicle. NASA TN D-3570, Nov. 1966.
26. Bonner, E.; Clever, W.; and Dunn, K.: Aerodynamic Preliminary Analysis System II. Part I—Theory. NASA CR-165627, 1989.

27. Engle, C.D., and Prahara, S.C., "MINIVER Upgrade for the AVID System, Vol. I: LANMIN Users Manual", NASA CR-172212, Aug. 1983
28. Brauer, G. L.; Cornick, D. E.; Habeger; and Stevenson, R.: *Program To Optimize Simulated Trajectories (POST)*. NASA CR-2770, Feb. 1977.

10. Tables

<u>Description</u>	<u>CEM</u>	<u>Cabin</u>	<u>Δ</u>
Wing	13,016	11,911	1,105
Tail	1,728	1,622	106
LH2 Tank	33,860	31,120	2,740
LO2 Tank	14,652	13,469	1,183
Basic Structure	15,902	14,877	1,025
Crew Area	8,239	2,133	6,106
Base Heat Shield	1,598	1,508	90
Body Flap	1,089	1,028	61
TPS	27,966	26,397	1,569
Helium Purge System	5,719	5,245	474
Nose Gear	1,290	1,178	112
Main Gear	7,311	6,674	637
Main Propulsion	71,115	65,216	5,899
RCS Propulsion	3,800	3,677	123
OMS Propulsion	2,521	2,349	172
Elec. Conversion & Dist.	7,187	6,893	294
Control Surface Actuation	1,760	1,607	153
Heat Transport Loop of ECLS	1,636	1,590	46
Margin (15% of SSV dry weight without engines)	27,148	24,494	2,654
		=====	
Total Dry Weight Increase			24,549 lb

Table 3.1: Summary of SSV Dry Weight Increase

<u>Description</u>	<u>CEM</u>	<u>Cabin</u>	<u>Δ</u>
Residual Fluids	2,580	2,355	225
Reserves	8,220	7,505	715
Main LH2	324,861	297,916	26,945
Main LO2	1,948,486	1,786,868	161,618
RCS Propellant	3,207	2,928	279
OMS Propellant	22,055	20,136	1,919
		=====	
Total Propellant Increase			191,701 lb

Table 3.2: Summary of SSV Propellant Increase

Description	Qty	Unit Watts (W)	Total Watts (W)	Duty Cycle (hr)	Energy (kWh)
<b>Avionics</b>					
IMU	2	33.0	66.0	0.5	0.033
GPS Receiver	2	12.0	24.0	0.5	0.012
GPS Antenna	2	20.0	40.0	0.5	0.02
Altimeter	2	30.0	60.0	0.5	0.03
Main Computers	2	126.0	252.0	0.5	0.126
Battery Controllers	2	111.0	222.0	0.5	0.111
Aerosurface Controller	1	132.0	132.0	0.5	0.066
GPS Antenna Switch	1	5.0	5.0	0.5	0.0025
Headset & Mike	2	5.0	10.0	12.0	0.12
Panel Display	2	15.0	30.0	0.5	0.015
SARSAT Transmitter	1	40.0	40.0	12.0	0.48
UHF Transceiver	2	15.0	30.0	12.0	0.36
Clock	1	5.0	5.0	12.0	0.06
Display Controller	2	25.0	50.0	0.5	0.025
Lights, low	10	5.0	50.0	12.0	0.6
Signal Conditioner	2	8.0	16.0	0.5	0.008
Voice Recorder	1	5.0	5.0	12.0	0.06
<b>ECLS</b>					
Cabin Pressure Sensor	1	1.0	1.0	12.0	0.012
Ducting	10	5.0	50.0	12.0	0.6
Cabin Fan Assembly	2	50.0	100.0	12	1.2
<b>Body Flap</b>					
Actuator	2	200.0	400.0	0.25	0.1
					=====
<b>Total Energy Required</b>					~ 4.04

Table 4.1: Power Requirements for CEM After Abort

11. Figures

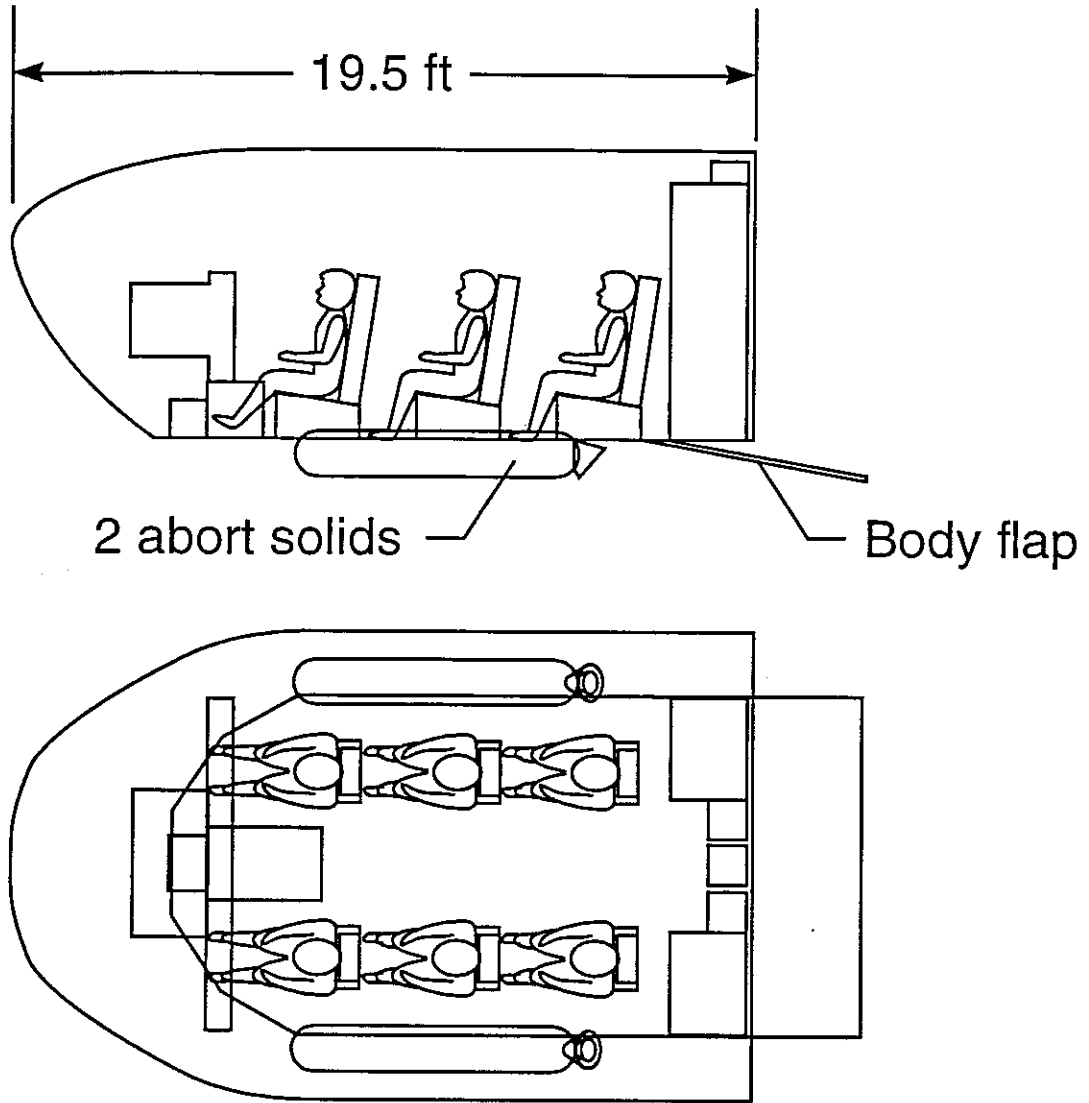


Figure 4.1: Two View of Crew Escape Module

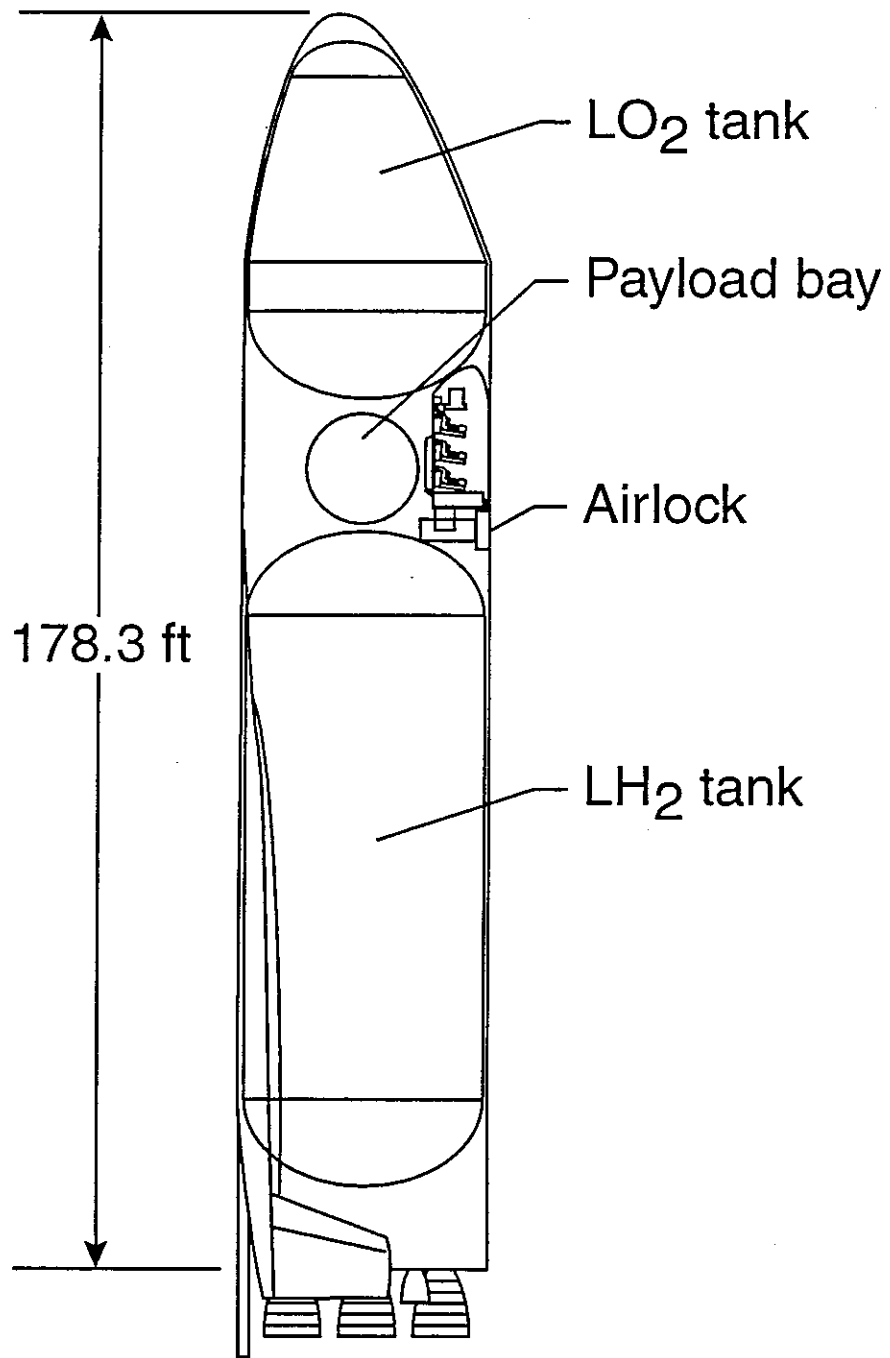


Figure 4.2: Crew Escape Module Mated with the SSV

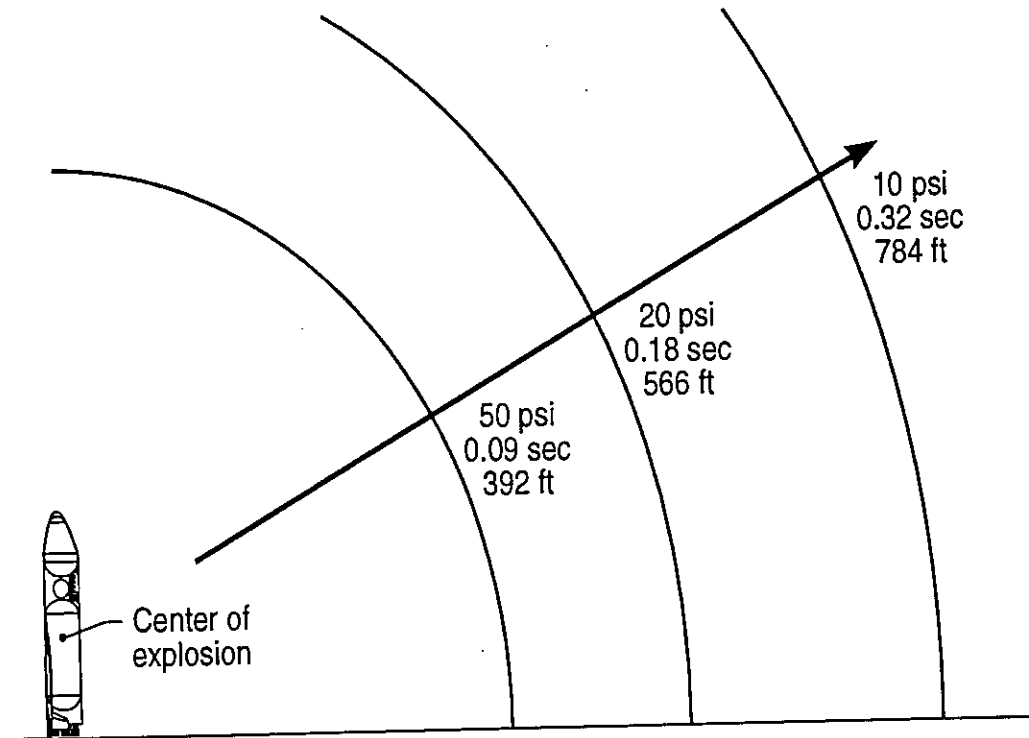


Figure 4.3: Overpressure Boundaries

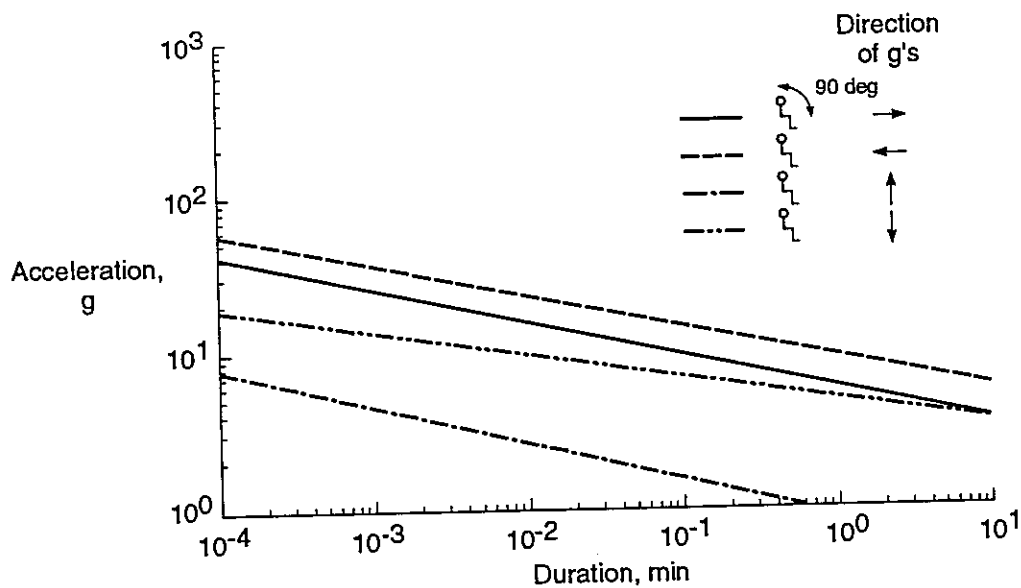


Figure 4.4: Human Tolerance Limits to Acceleration

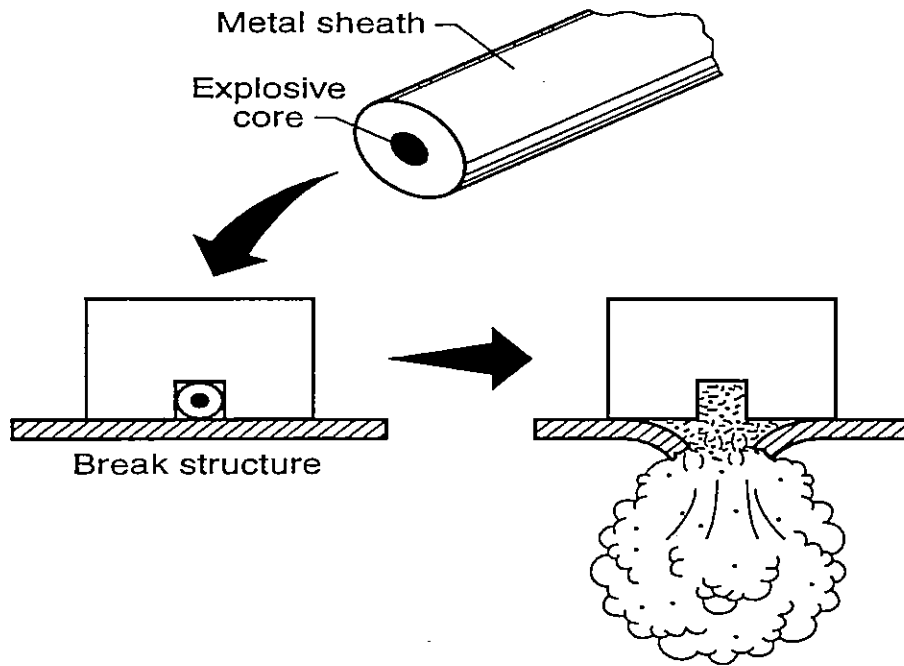


Figure 4.5: Explosive Cord Schematic

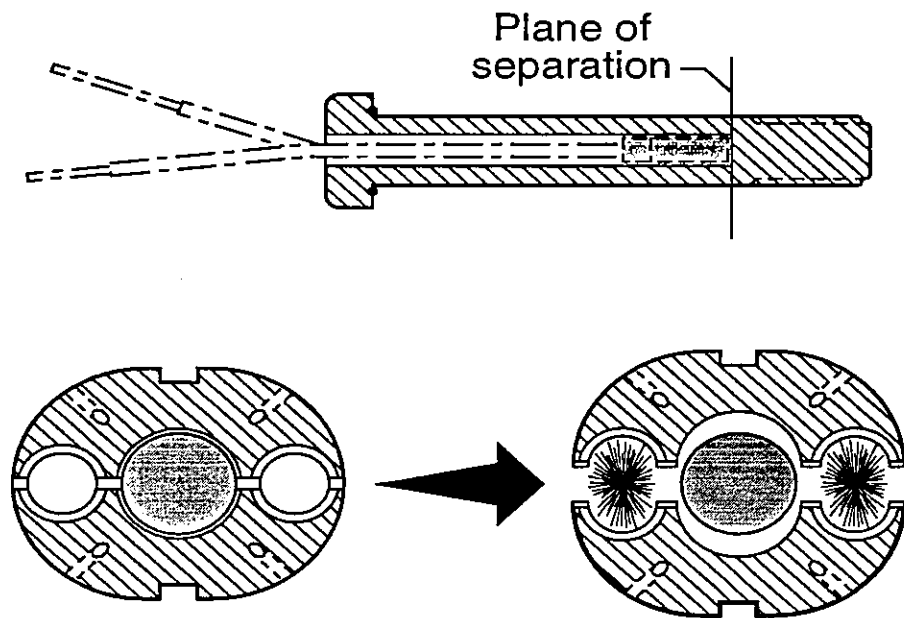


Figure 4.6: Explosive Nut/Bolt Schematic

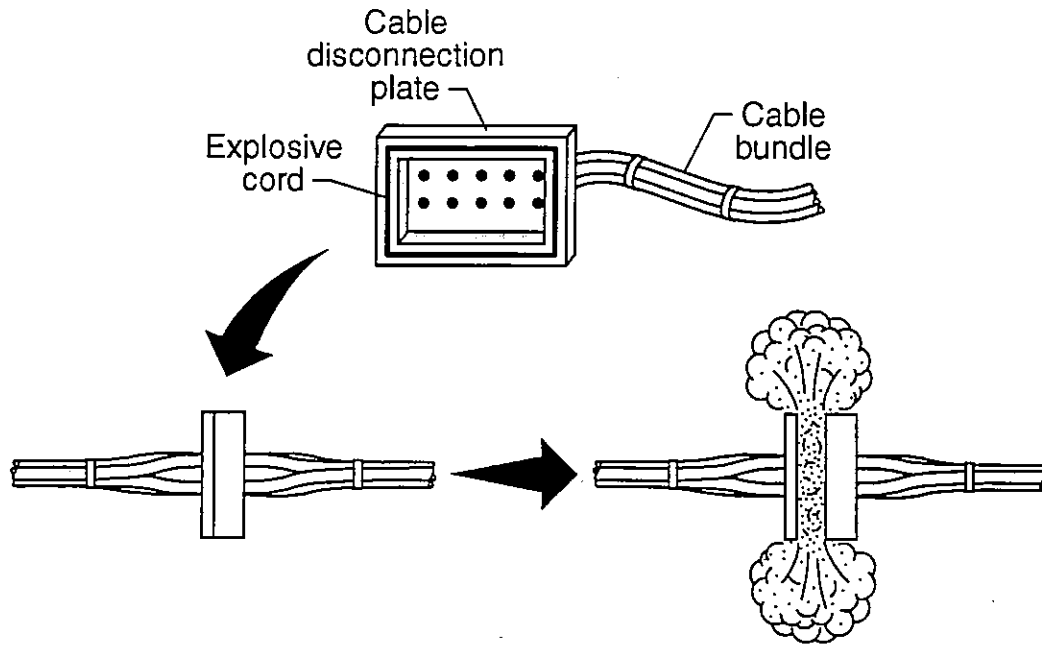


Figure 4.7: Cable Disconnection Plate Schematic

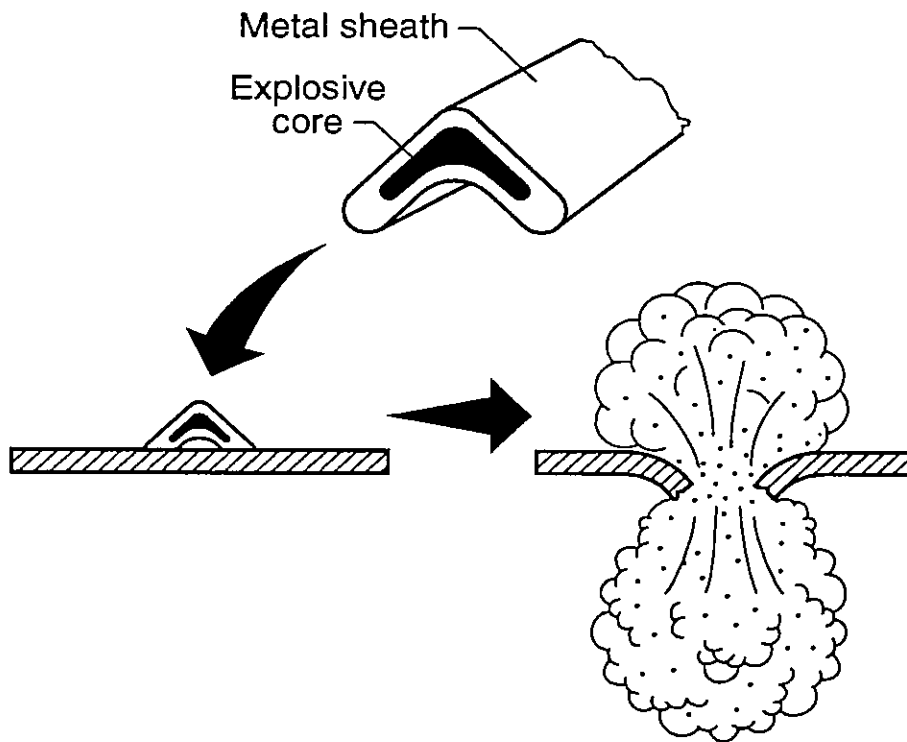


Figure 4.8: Airlock Shape Charge Schematic

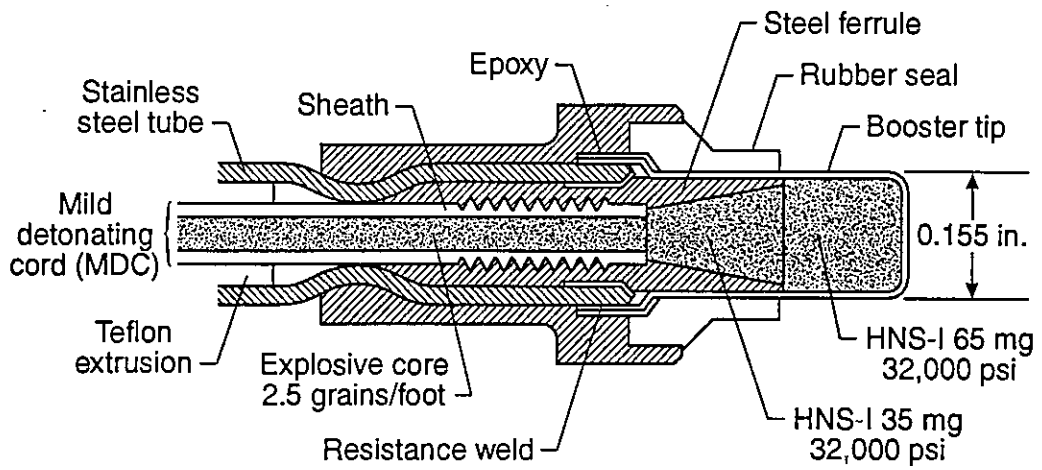


Figure 4.9: Explosive Transfer Line Schematic

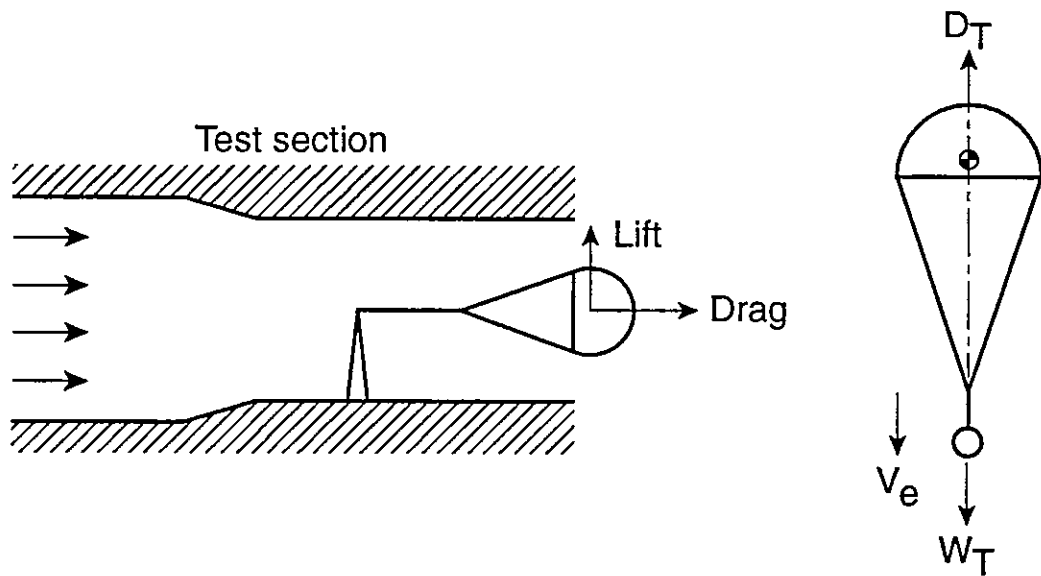


Figure 4.10: Stable, Unaccelerated Parachute Descent

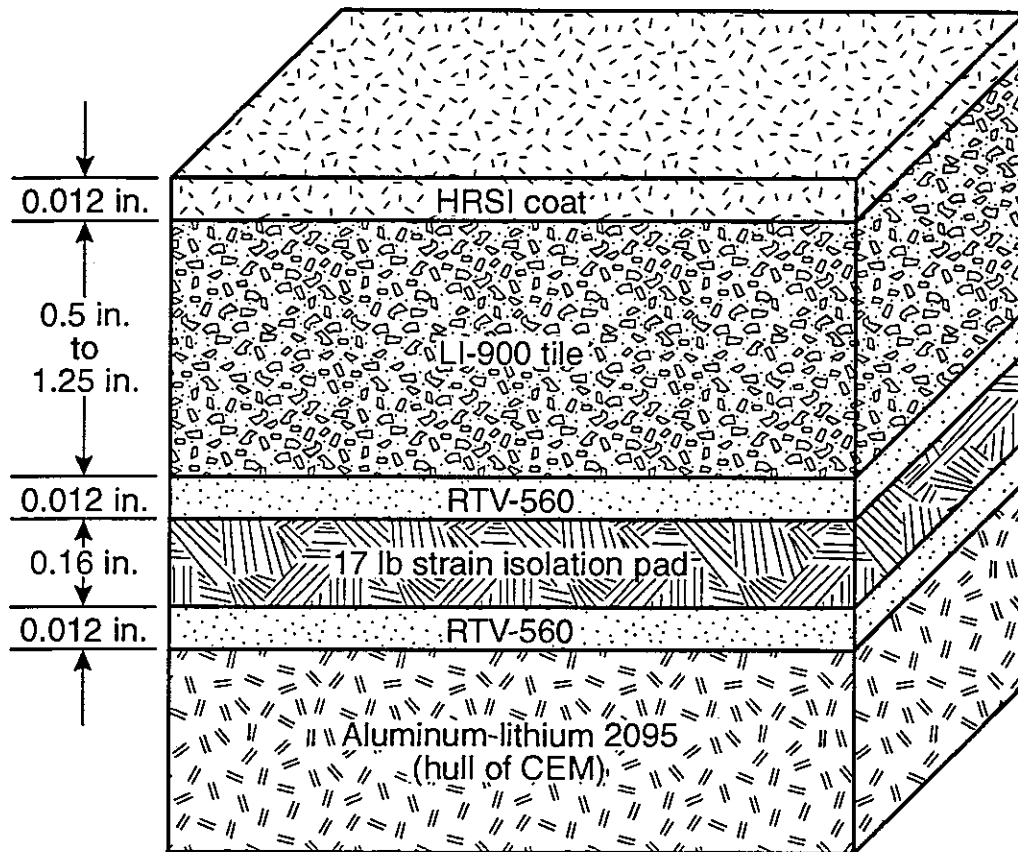


Figure 4.11: Thermal Protection System Lay-up

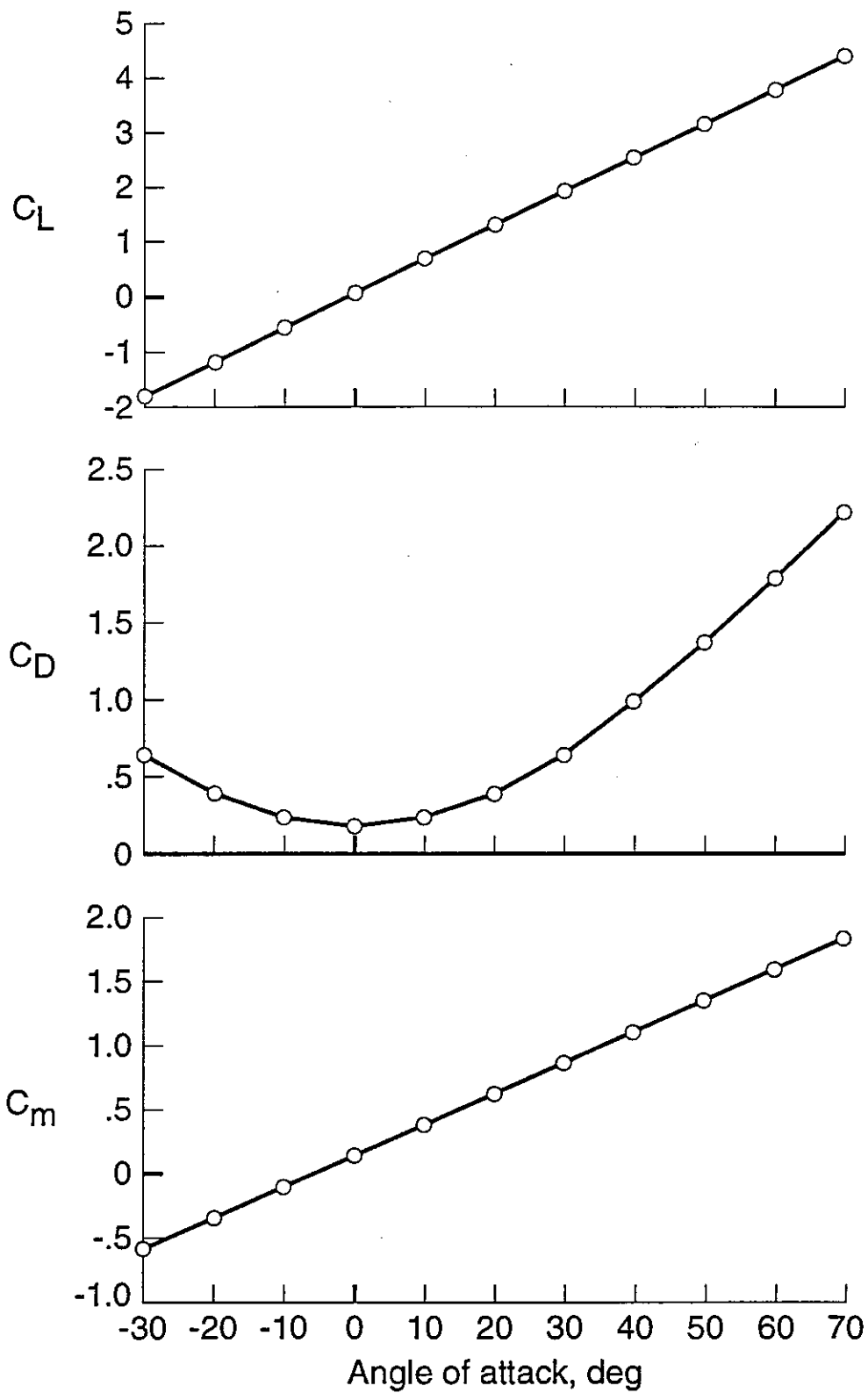


Figure 5.1: Longitudinal Aerodynamic Coefficients at Mach 0.3

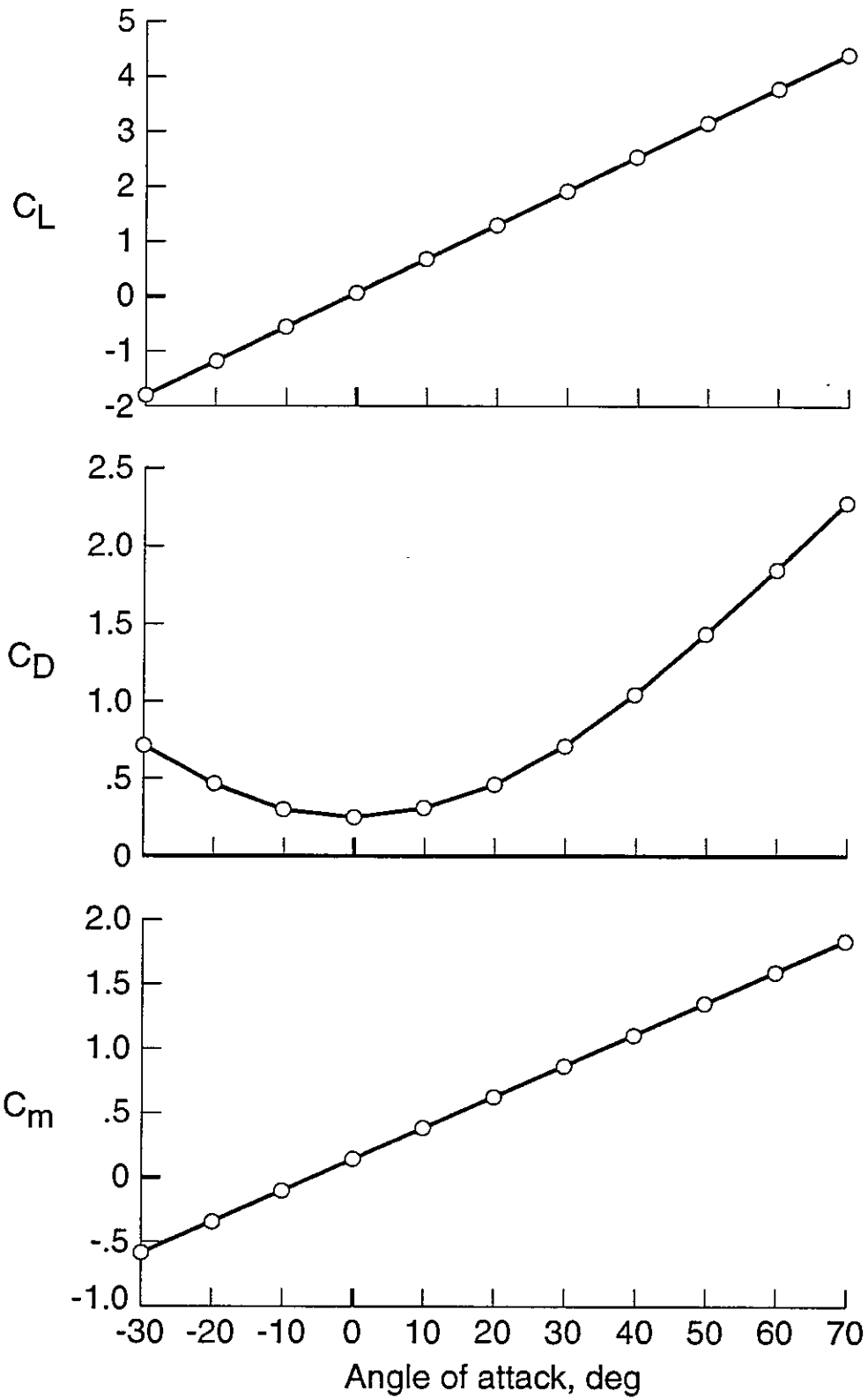


Figure 5.2: Longitudinal Aerodynamic Coefficients at Mach 0.6

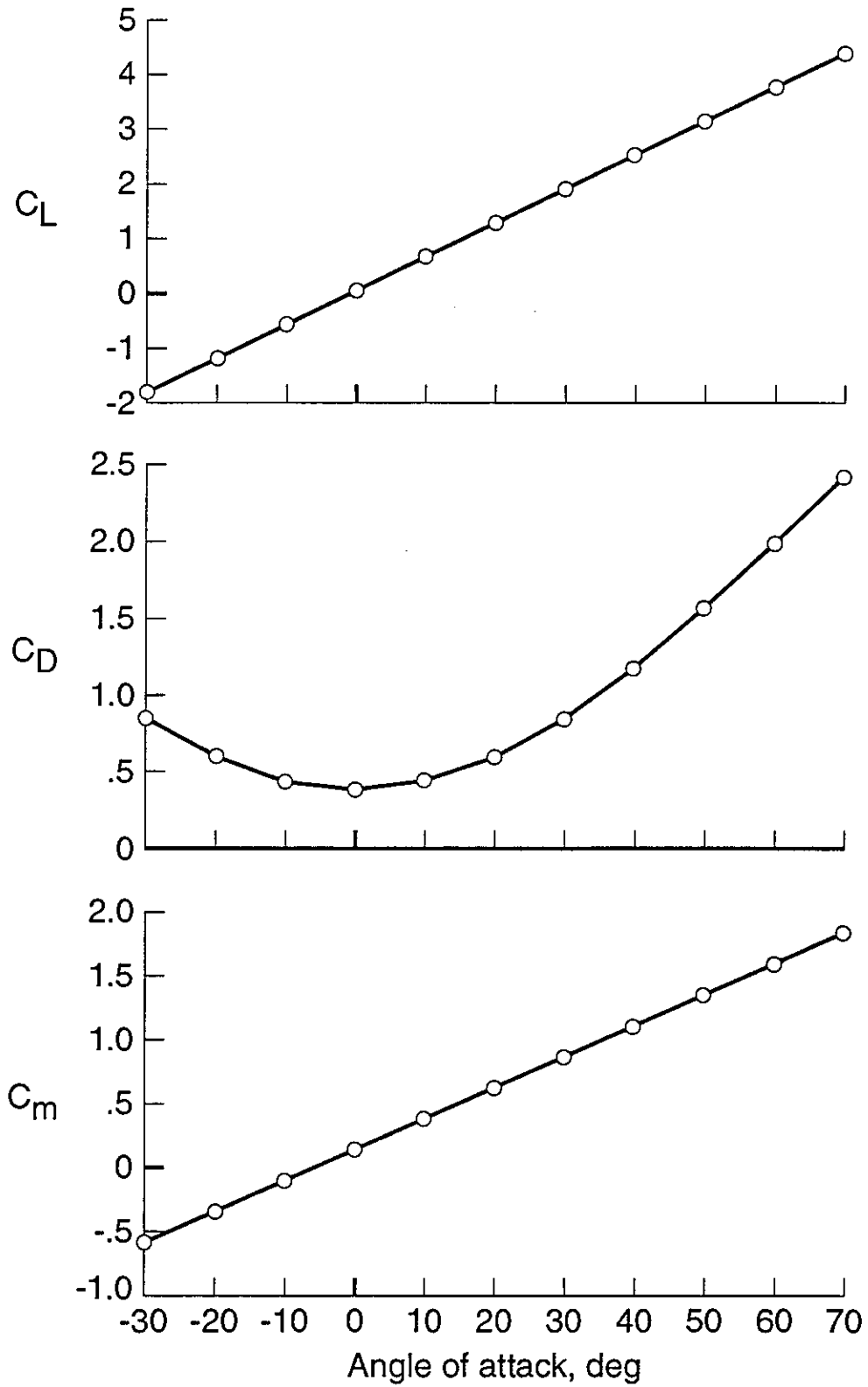


Figure 5.3: Longitudinal Aerodynamic Coefficients at Mach 0.9

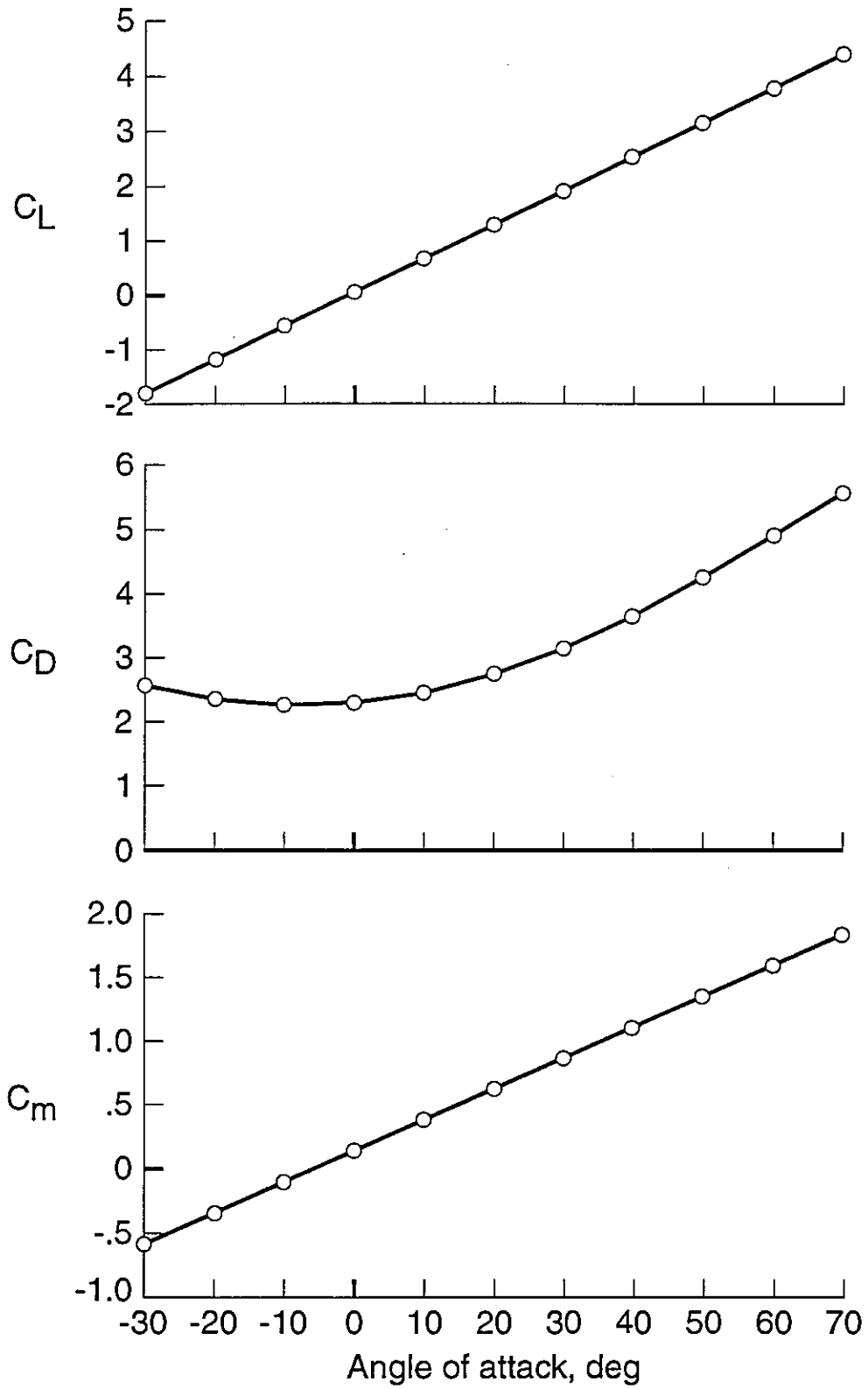


Figure 5.4: Longitudinal Aerodynamic Coefficients at Mach 1.2

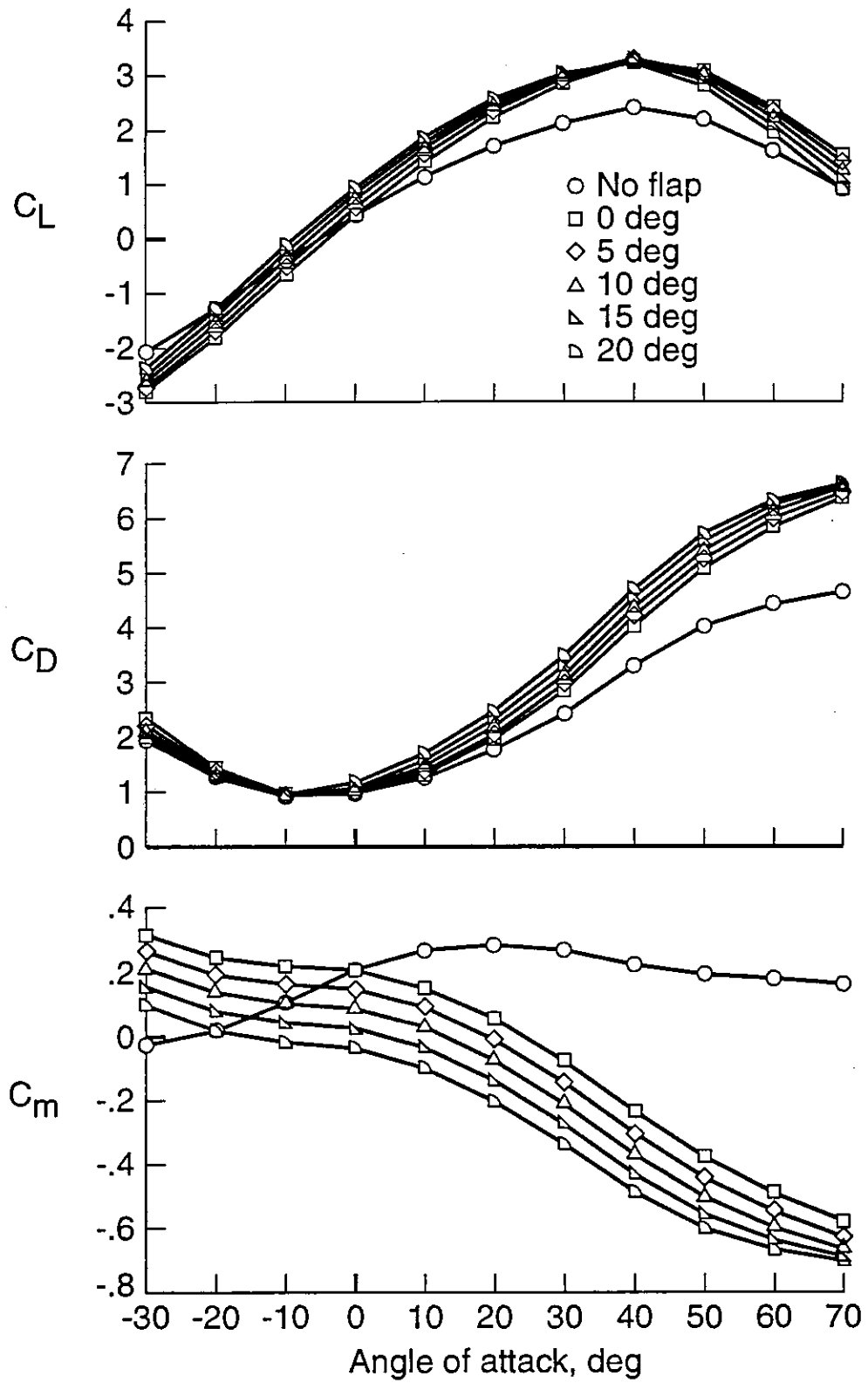


Figure 5.5: Longitudinal Aerodynamic Coefficients at Mach 1.6

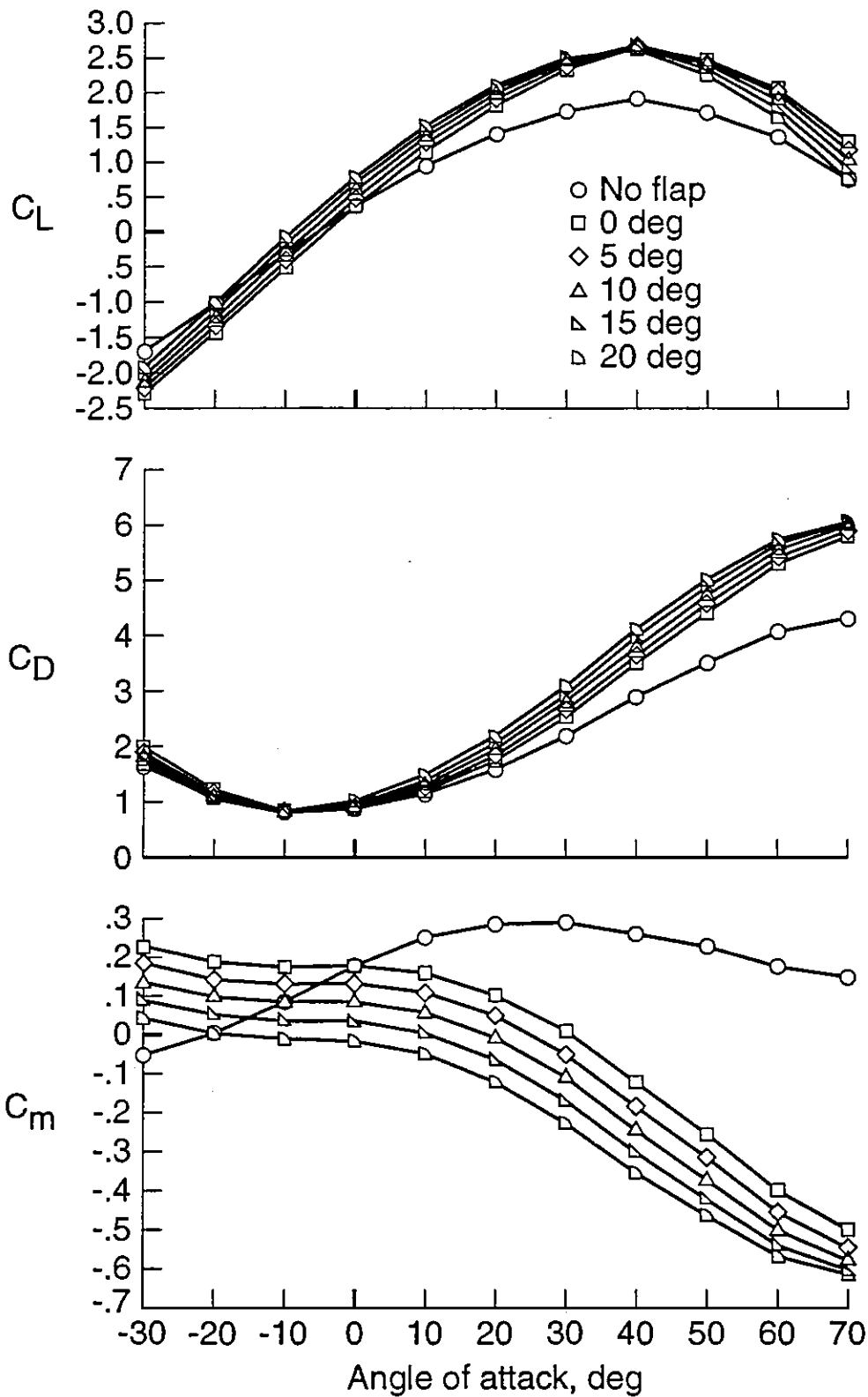


Figure 5.6: Longitudinal Aerodynamic Coefficients at Mach 2.0

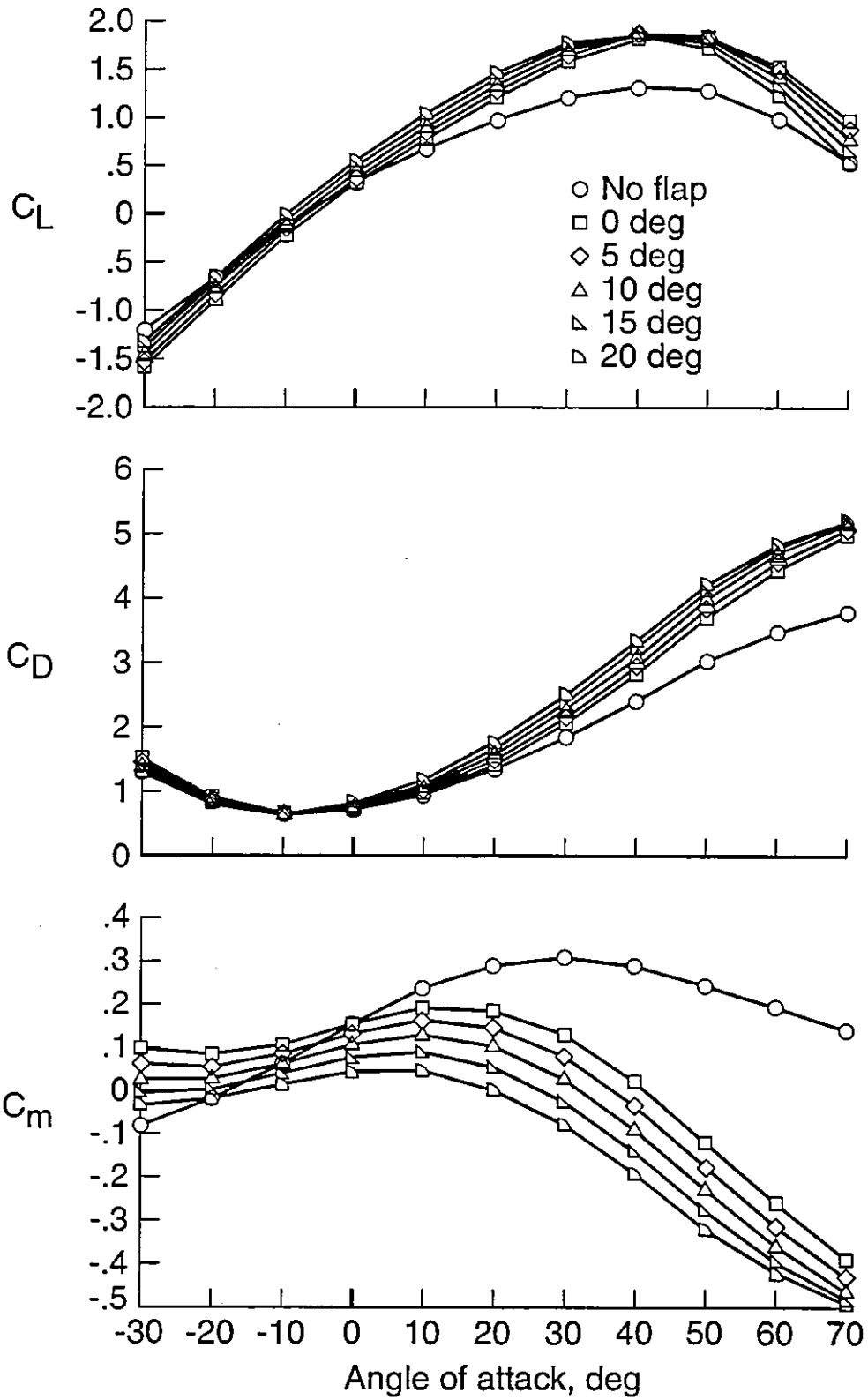


Figure 5.7: Longitudinal Aerodynamic Coefficients at Mach 4.0

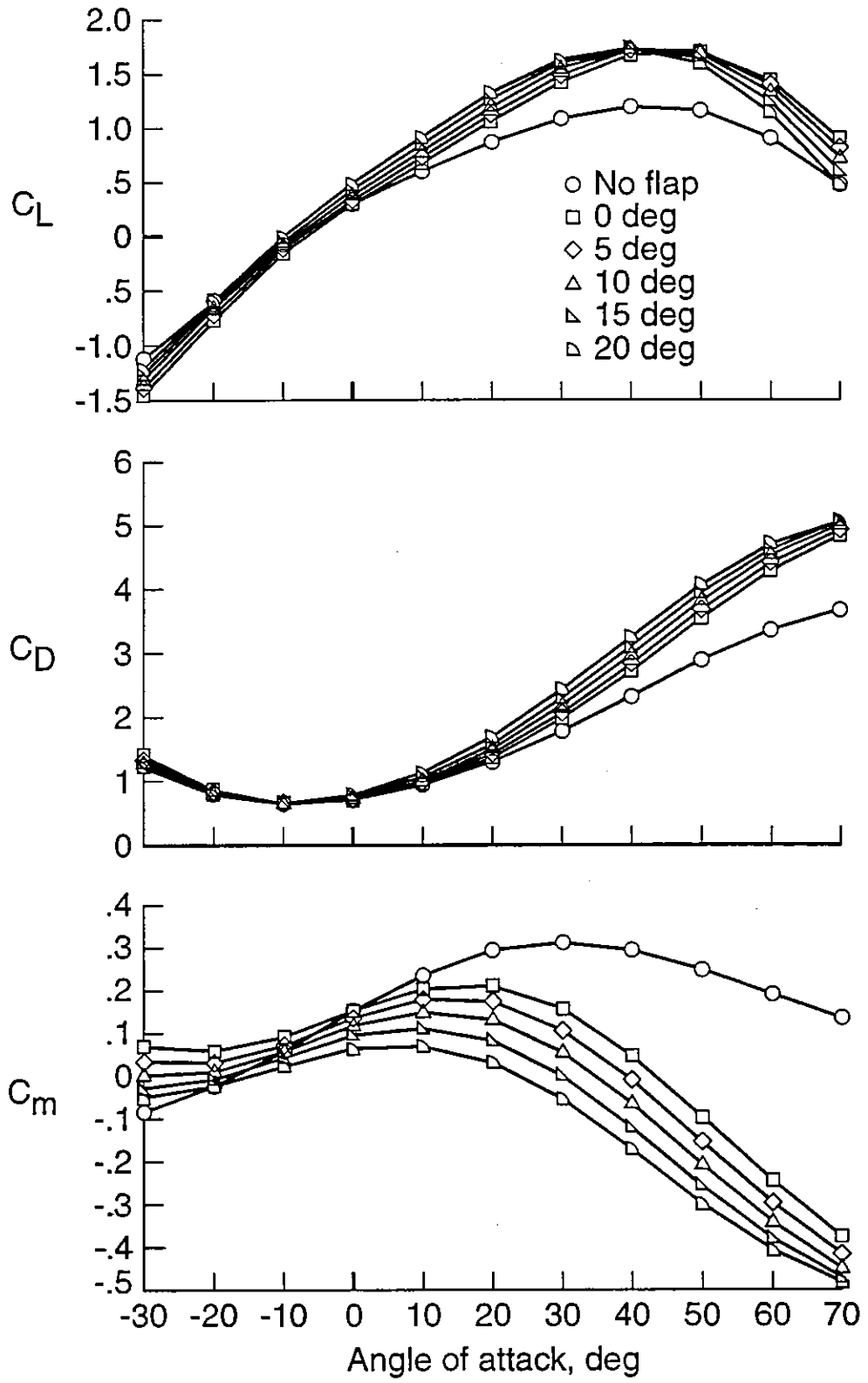


Figure 5.8: Longitudinal Aerodynamic Coefficients at Mach 6.0

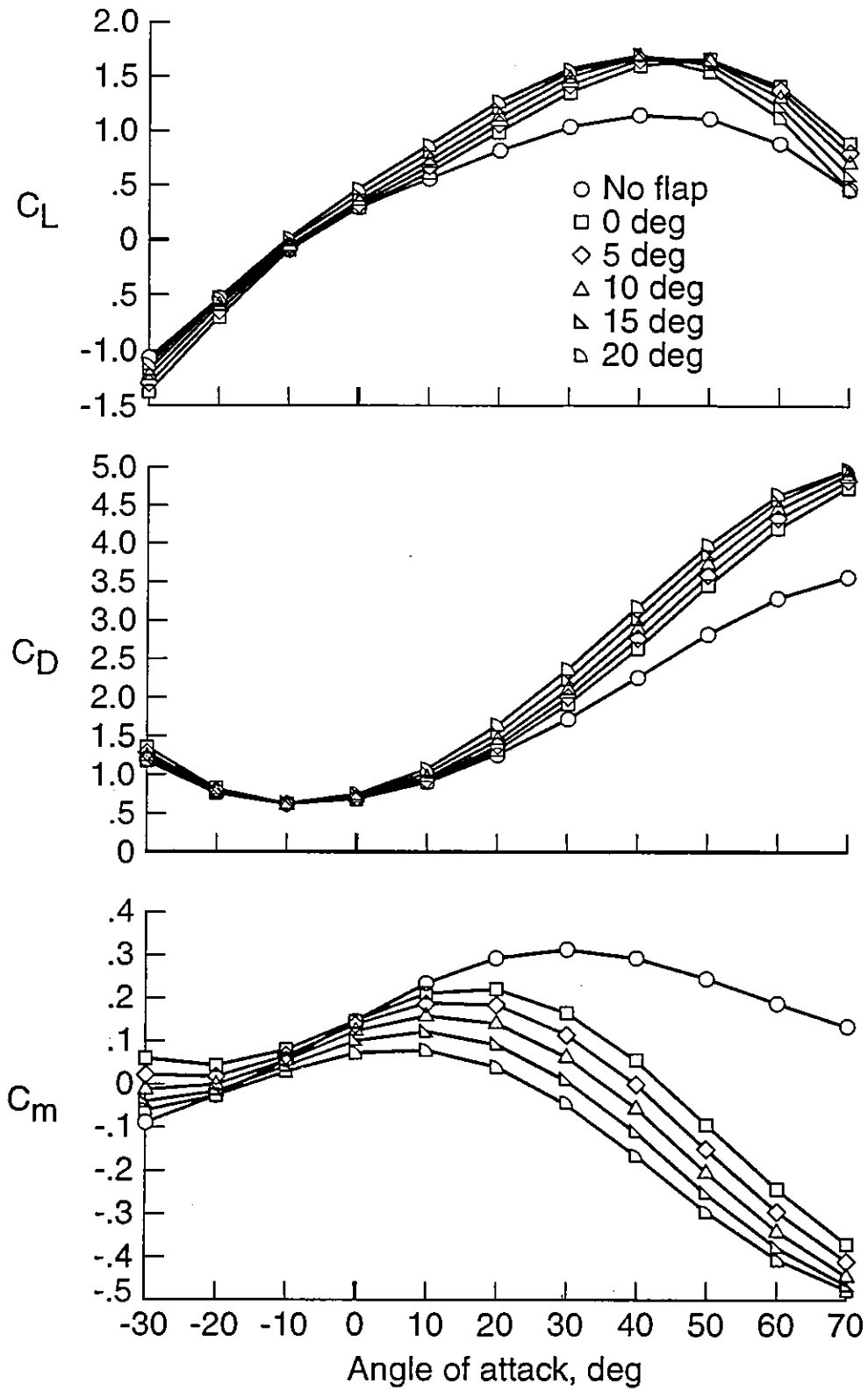


Figure 5.9: Longitudinal Aerodynamic Coefficients at Mach 9.0

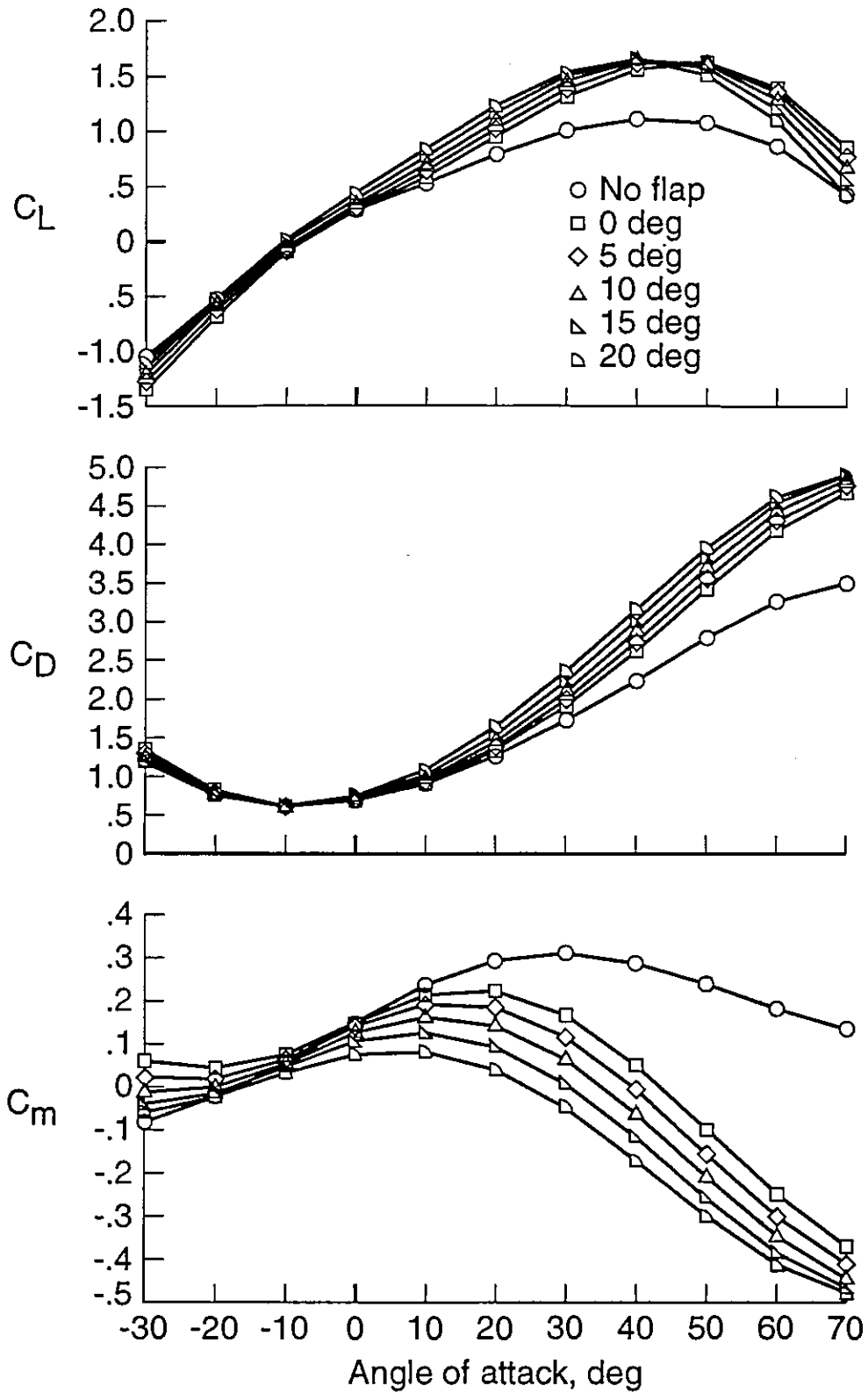


Figure 5.10: Longitudinal Aerodynamic Coefficients at Mach 12.0

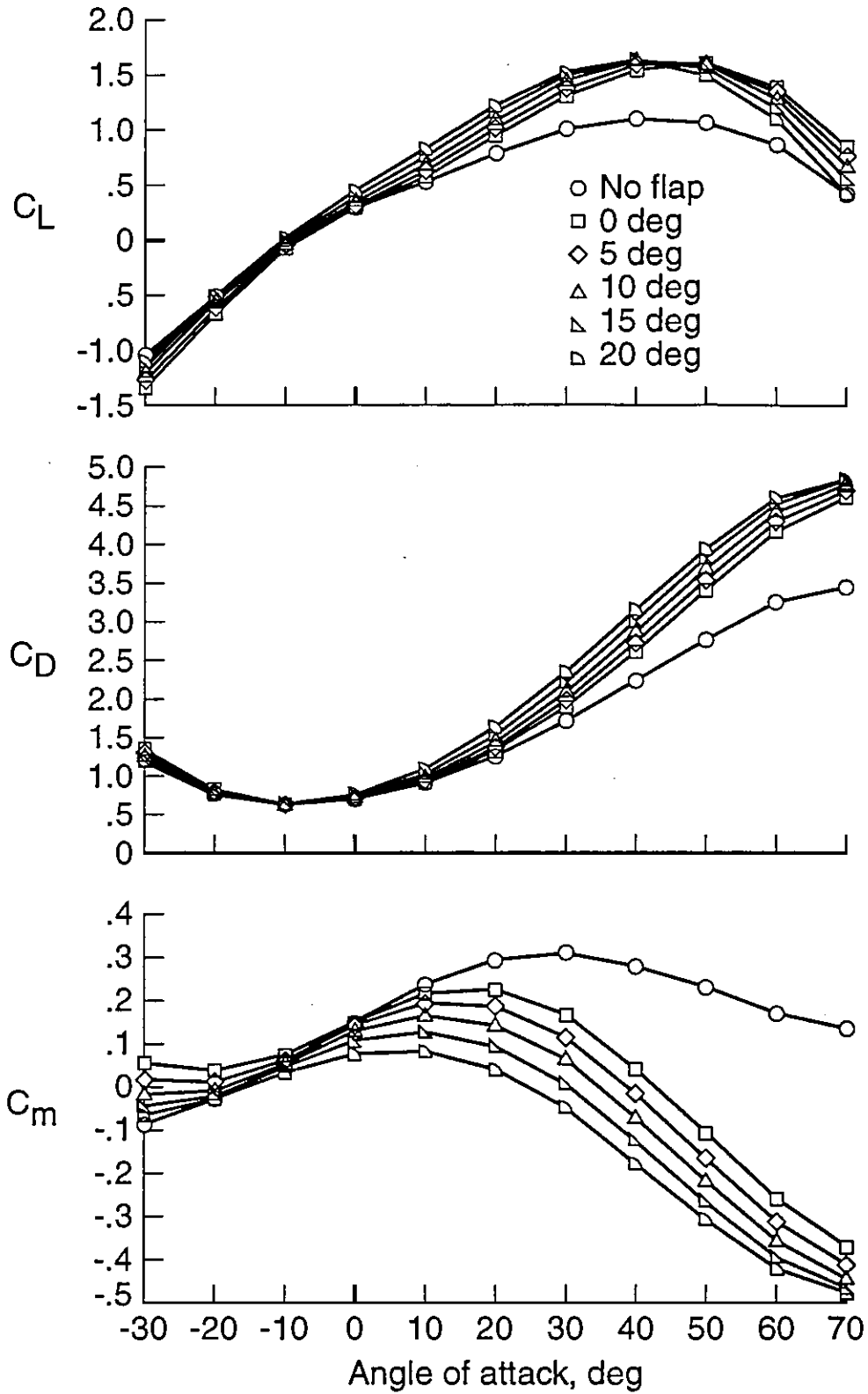


Figure 5.11: Longitudinal Aerodynamic Coefficients at Mach 15.0

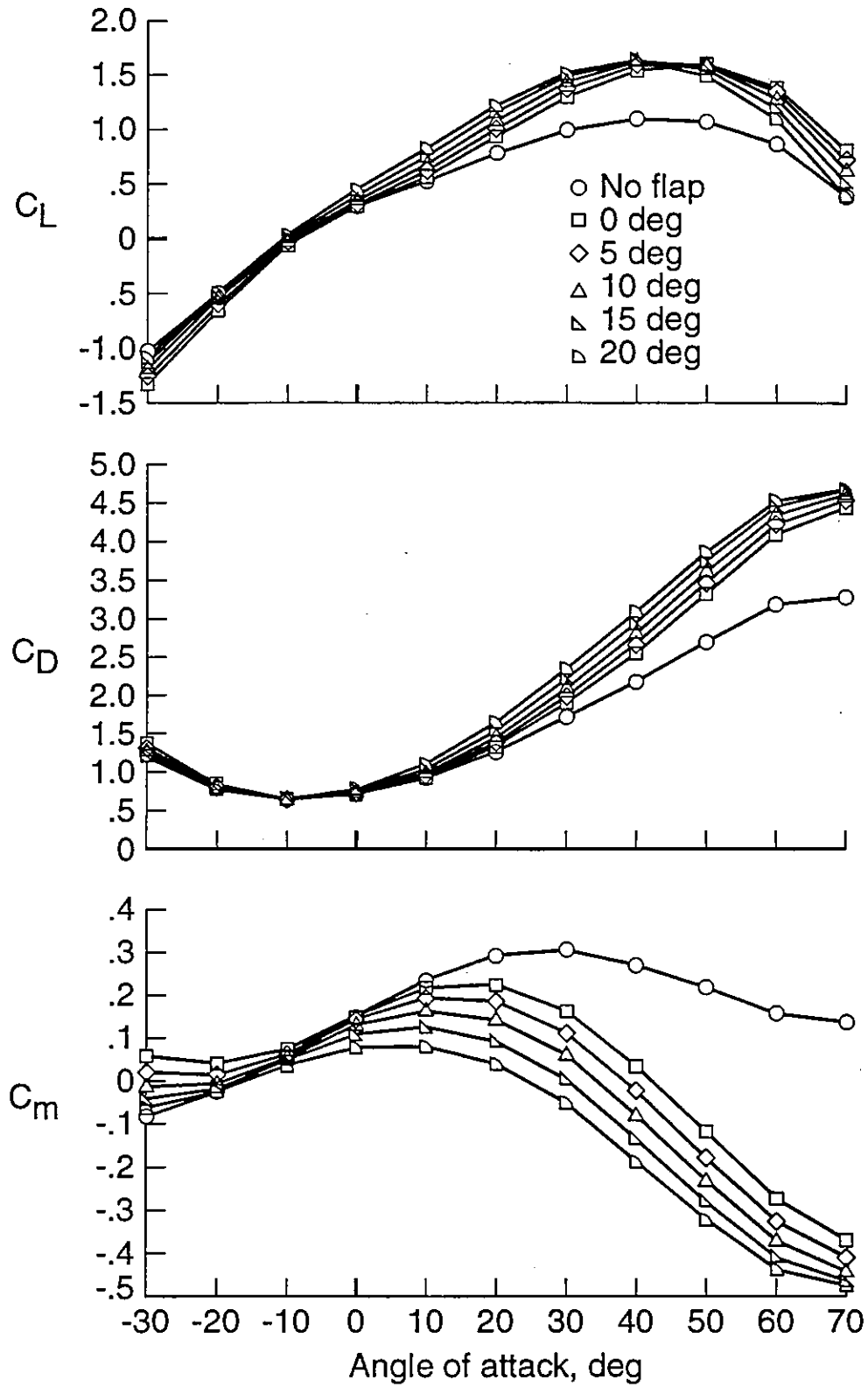


Figure 5.12: Longitudinal Aerodynamic Coefficients at Mach 20.0

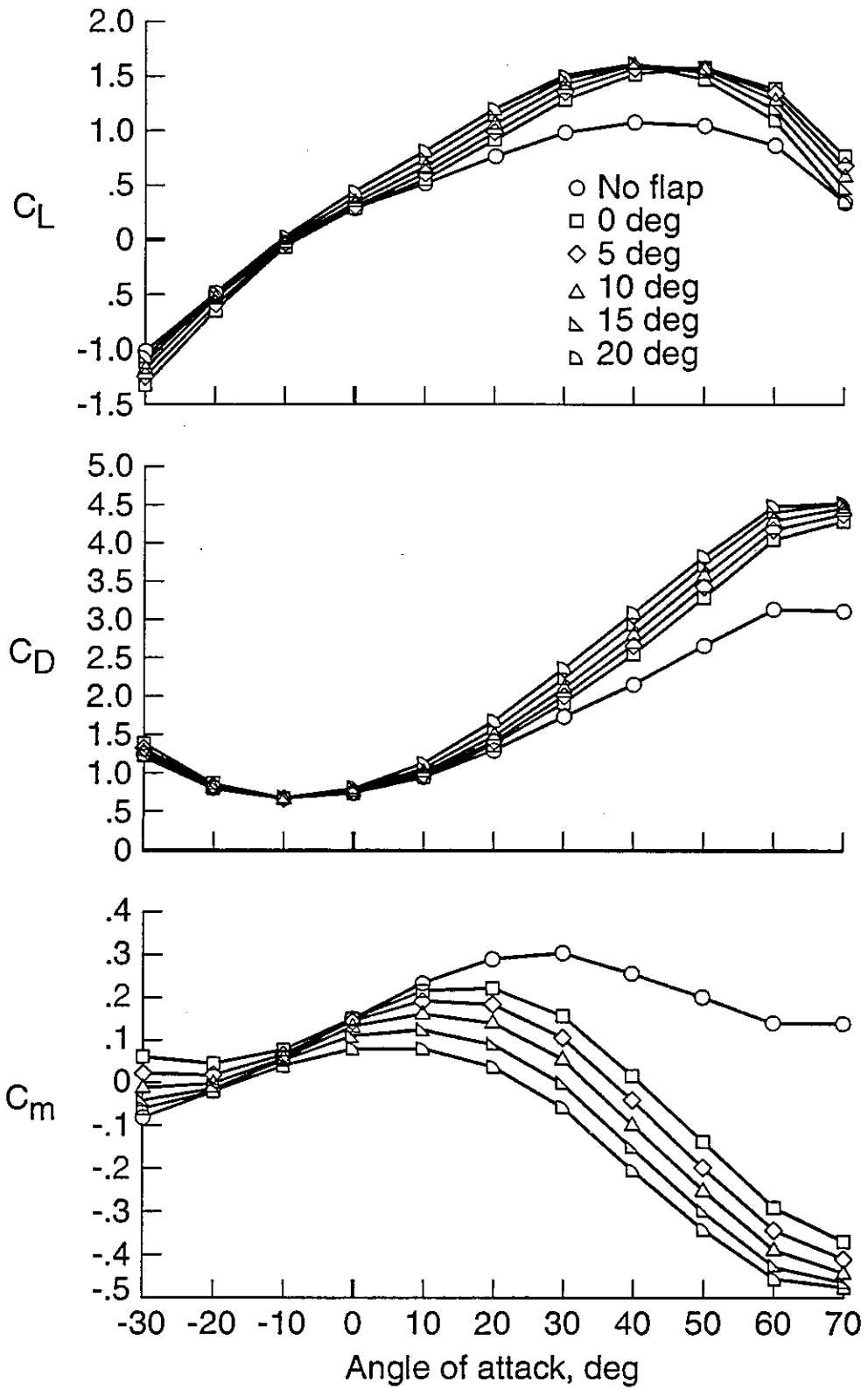


Figure 5.13: Longitudinal Aerodynamic Coefficients at Mach 25.0

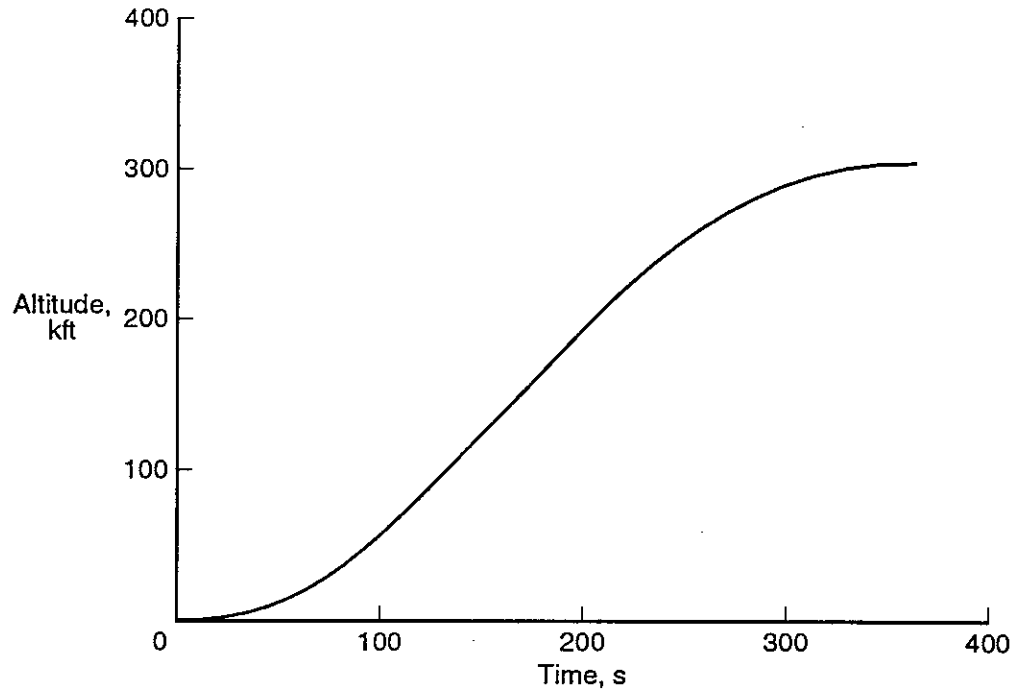


Figure 6.1: SSV Nominal Ascent — Altitude vs. Time

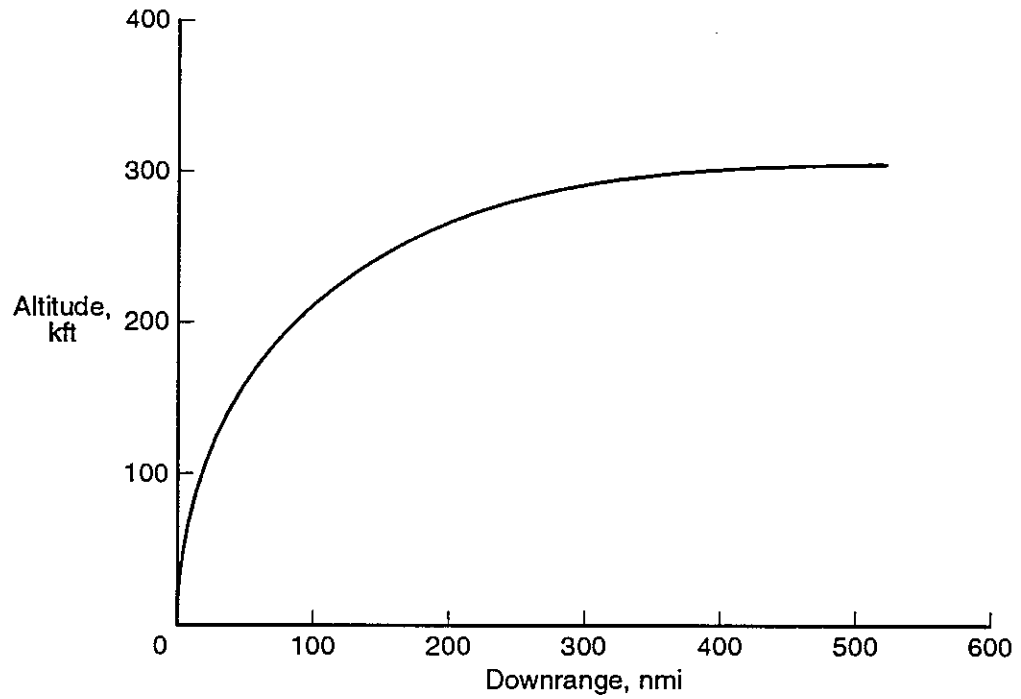


Figure 6.2: SSV Nominal Ascent — Altitude vs. Downrange

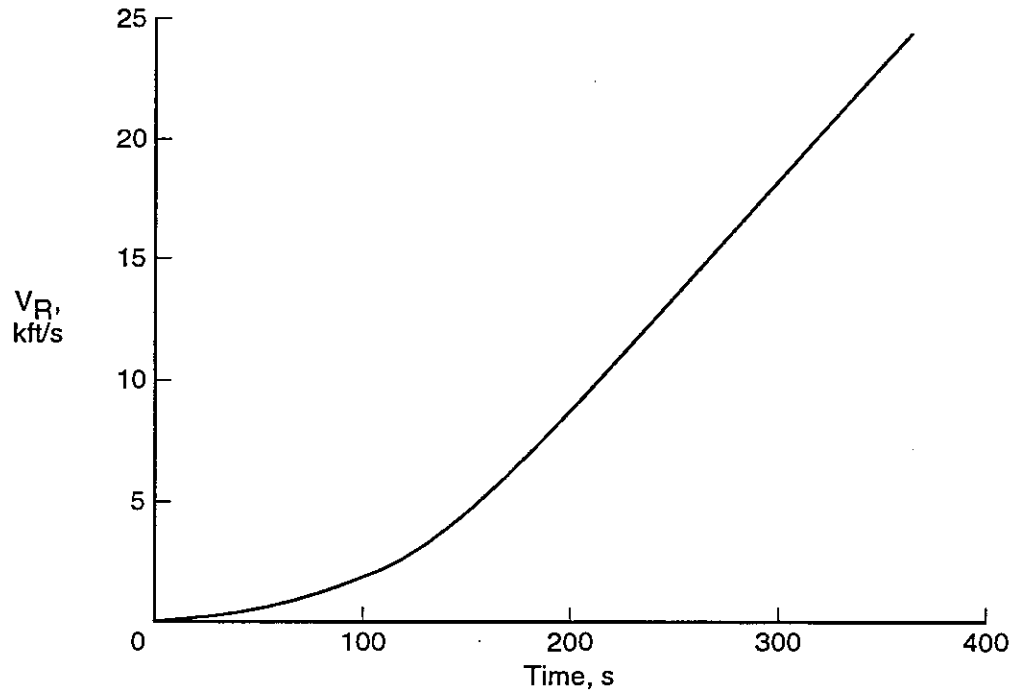


Figure 6.3: SSV Nominal Ascent — Velocity vs. Time

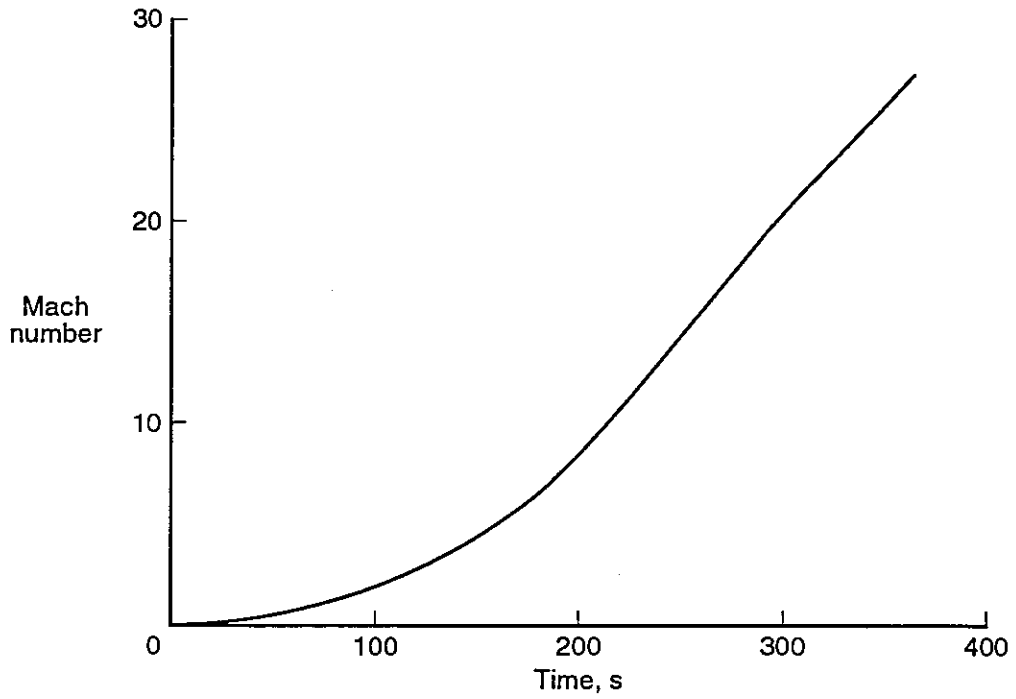


Figure 6.4: SSV Nominal Ascent — Mach Number vs. Time

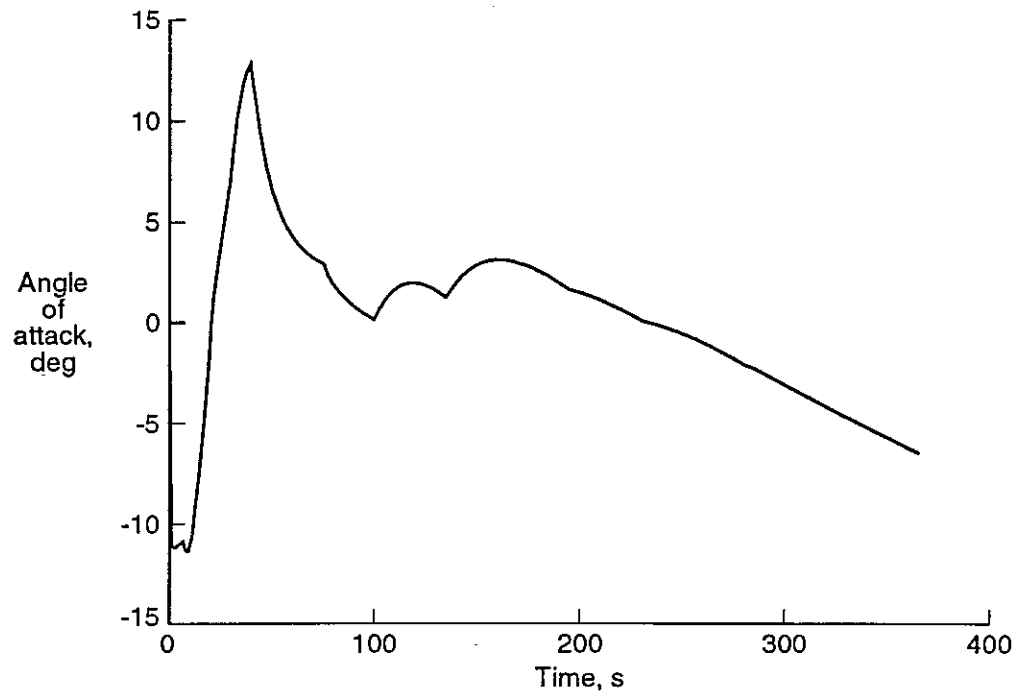


Figure 6.5: SSV Nominal Ascent — Angle of Attack vs. Time

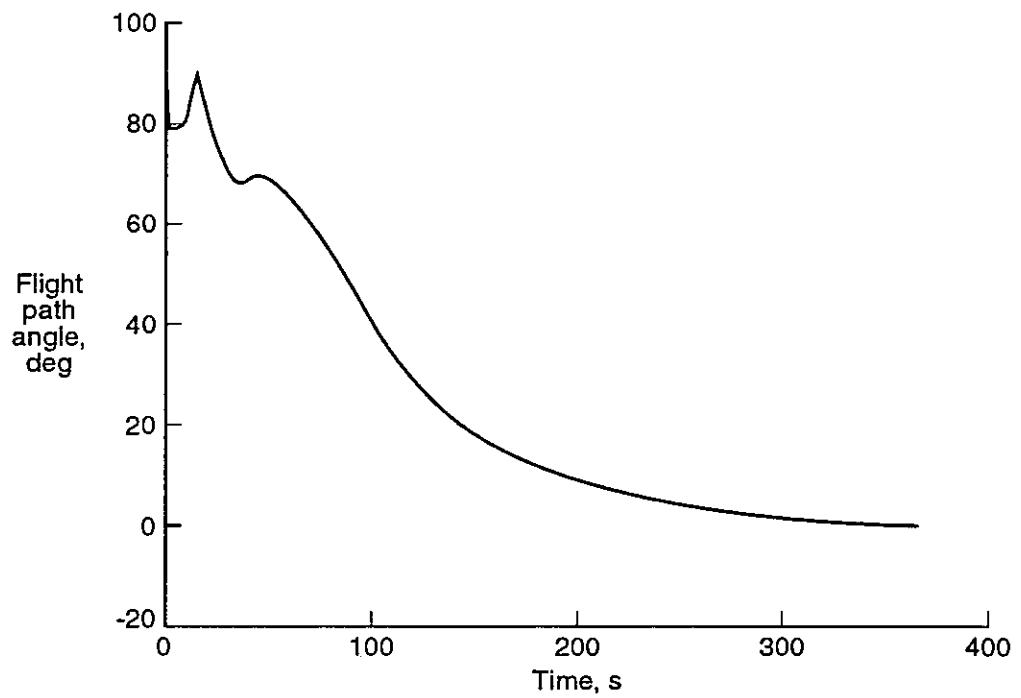


Figure 6.6: SSV Nominal Ascent — Flight Path Angle vs. Time

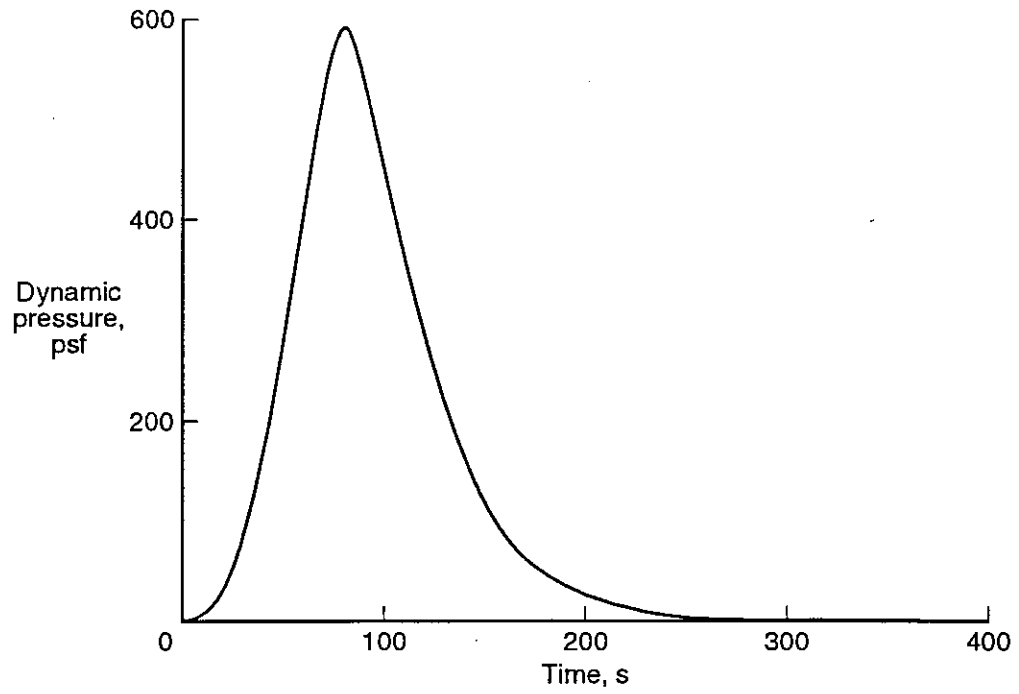


Figure 6.7: SSV Nominal Ascent — Dynamic Pressure vs. Time

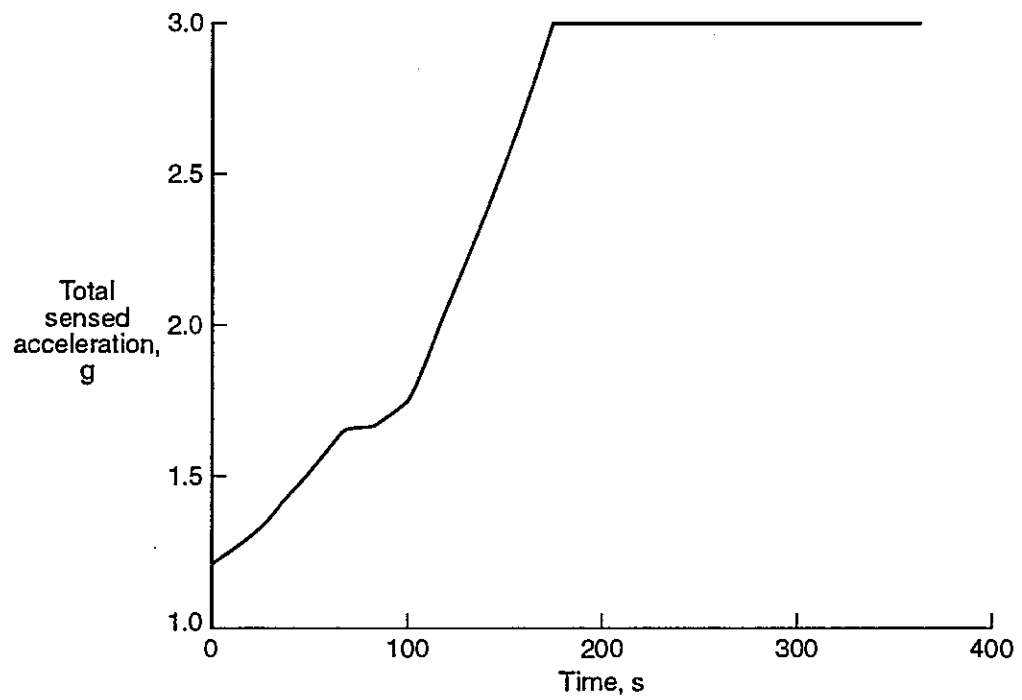


Figure 6.8: SSV Nominal Ascent — Total Acceleration vs. Time

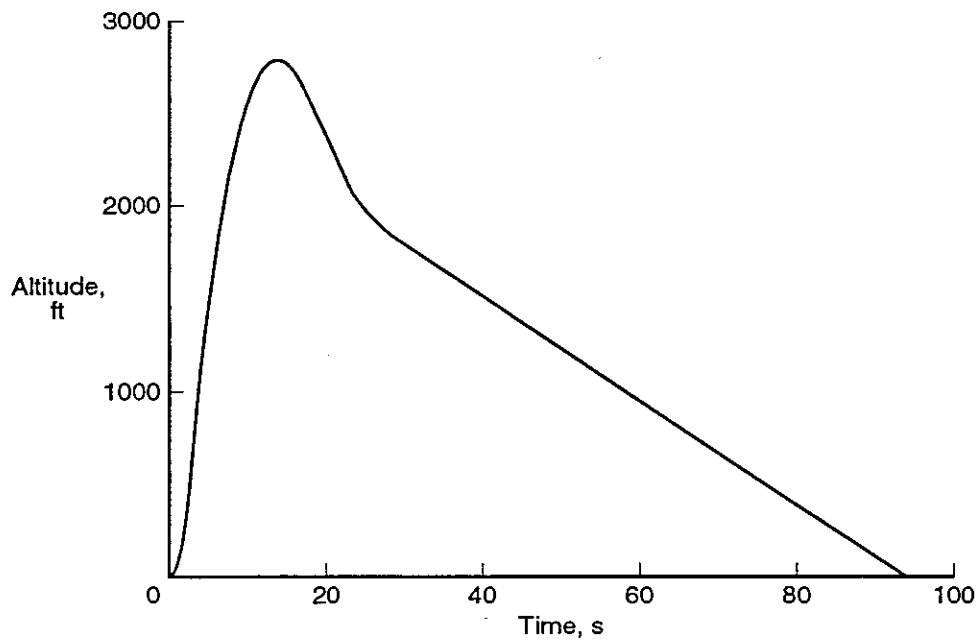


Figure 6.9: CEM Abort at T=0s — Altitude vs. Time

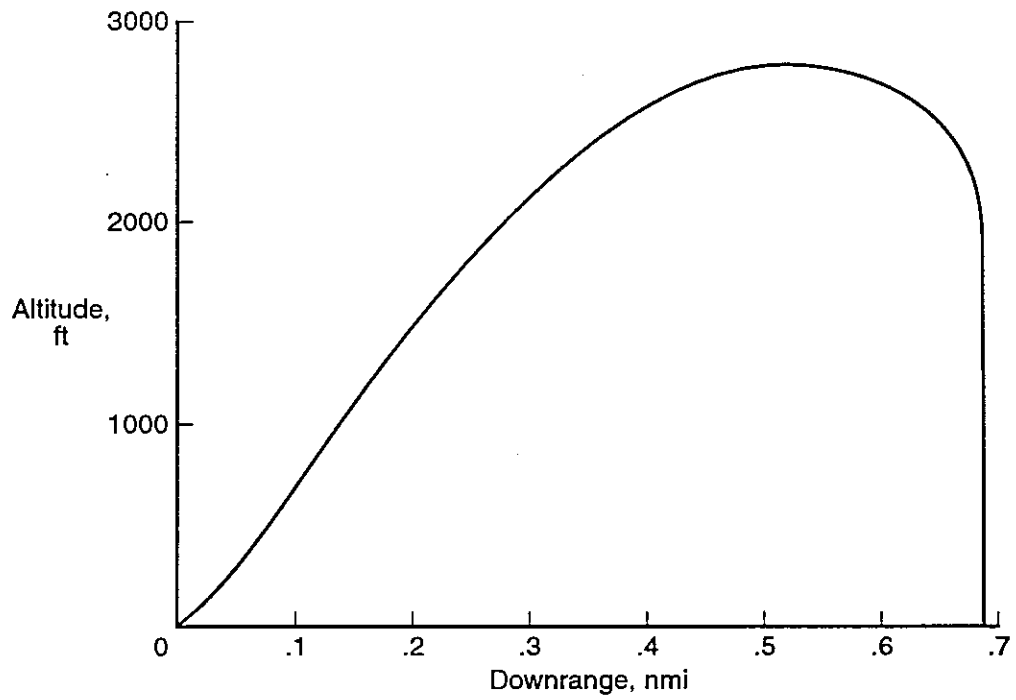


Figure 6.10: CEM Abort at T=0s — Altitude vs. Downrange

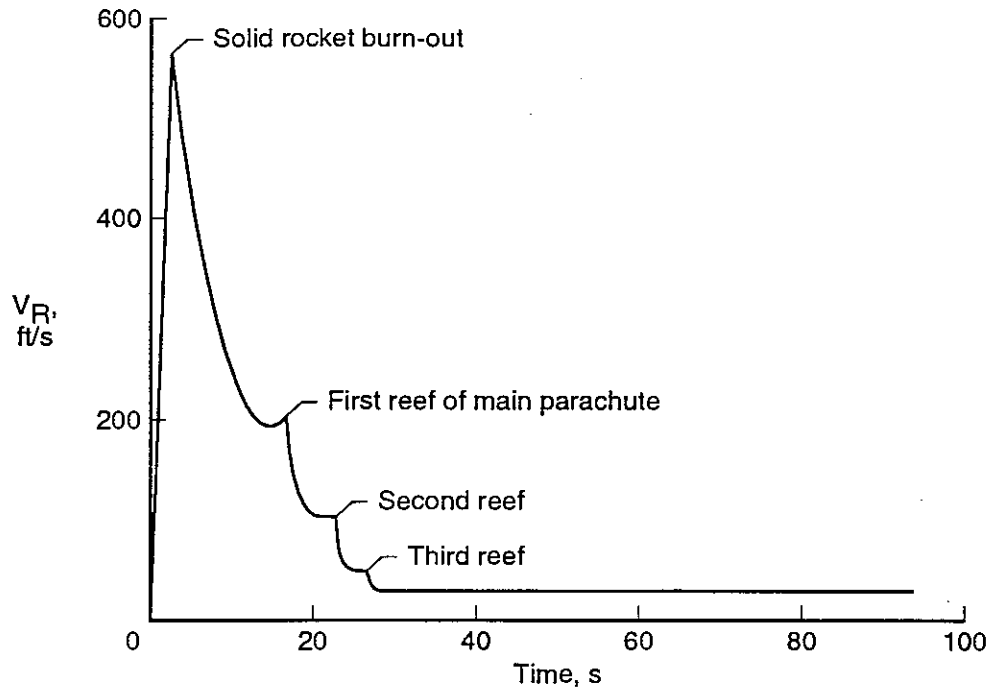


Figure 6.11: CEM Abort at T=0s — Velocity vs. Time

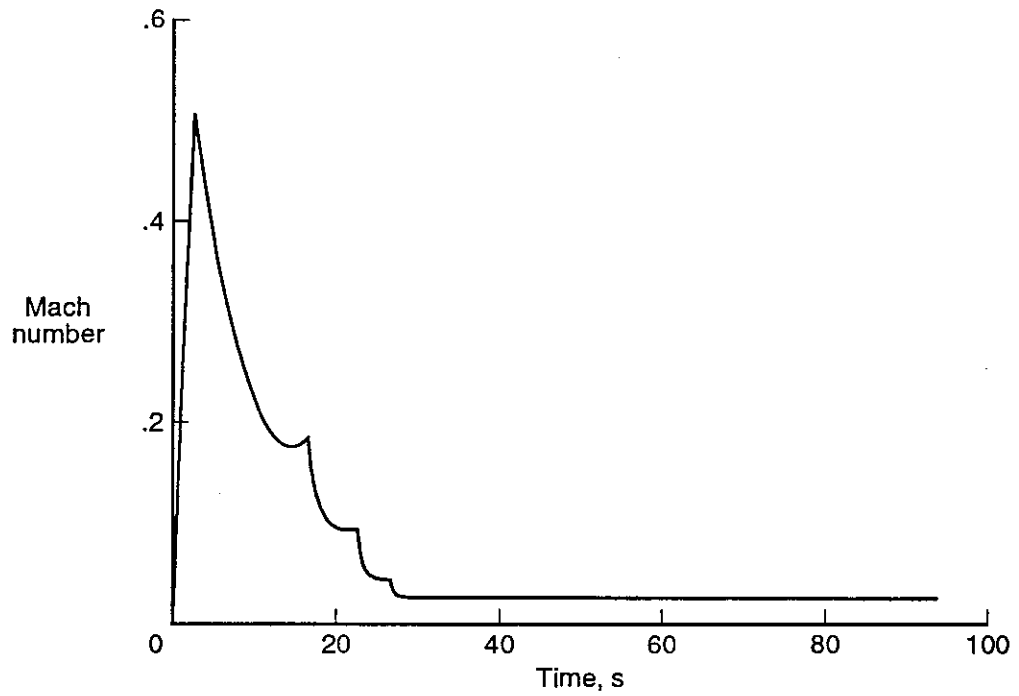


Figure 6.12: CEM Abort at T=0s — Mach Number vs. Time

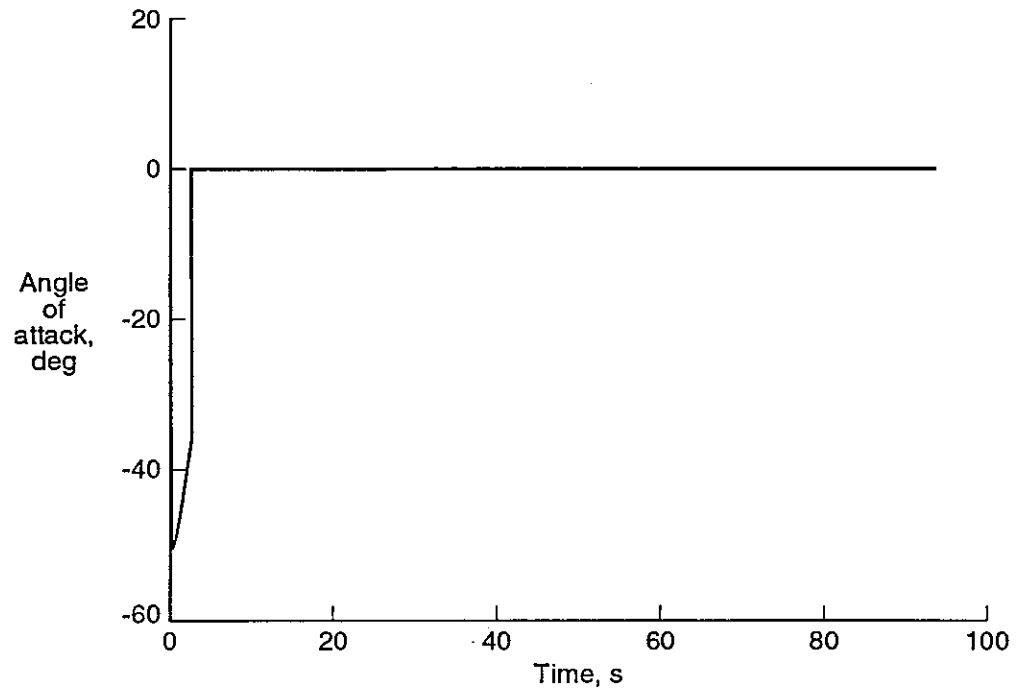


Figure 6.13: CEM Abort at T=0s — Angle of Attack vs. Time

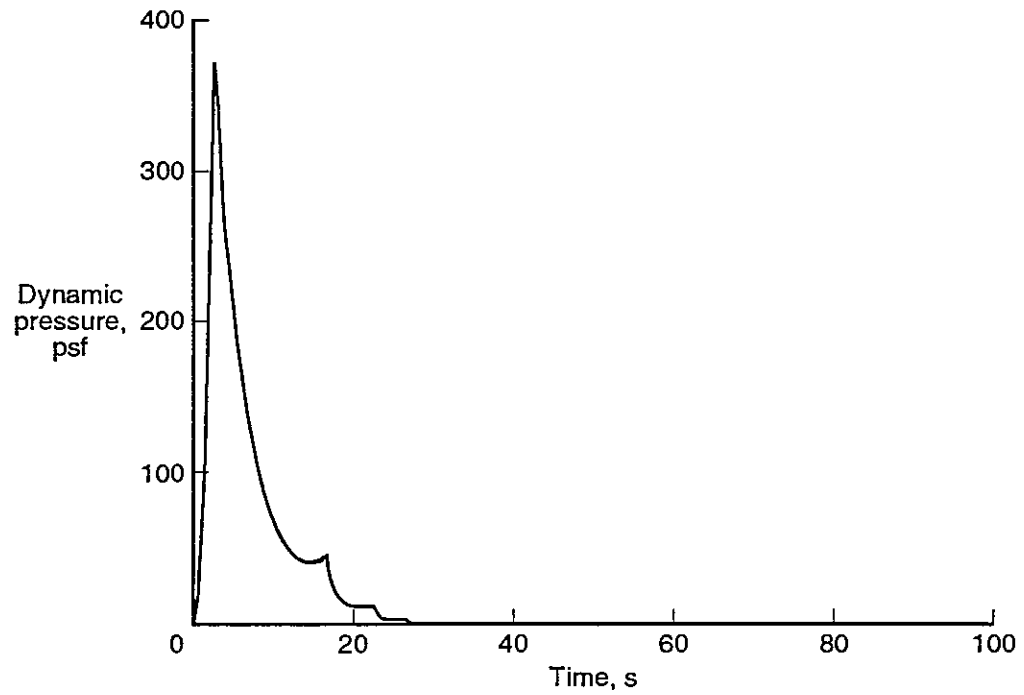


Figure 6.14: CEM Abort at T=0s — Dynamic Pressure vs. Time

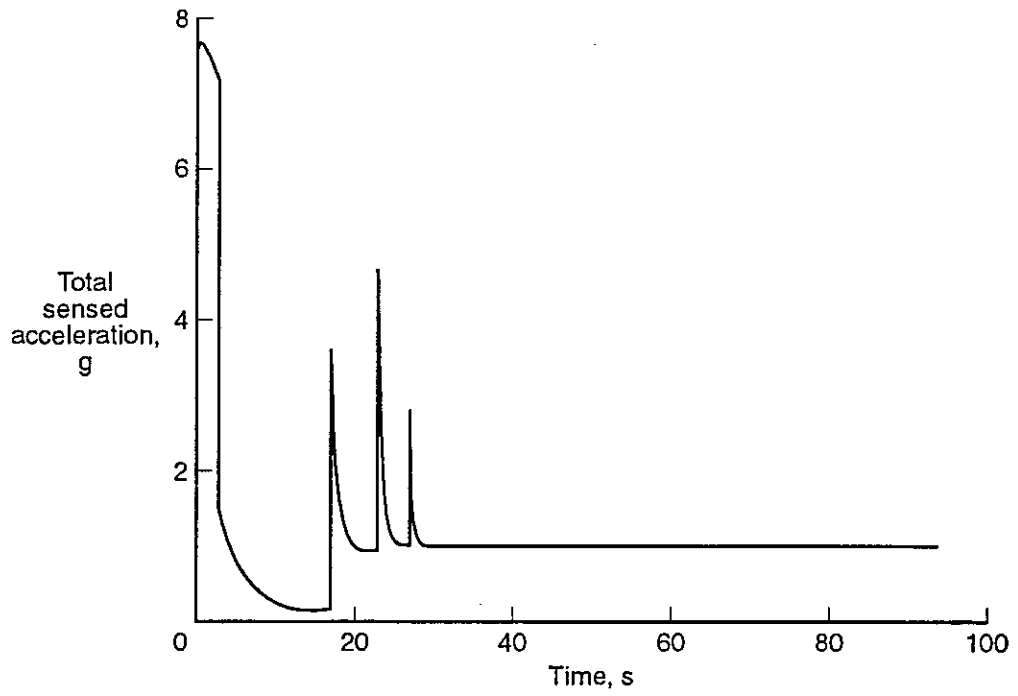


Figure 6.15: CEM Abort at T=0s — Total Acceleration vs. Time

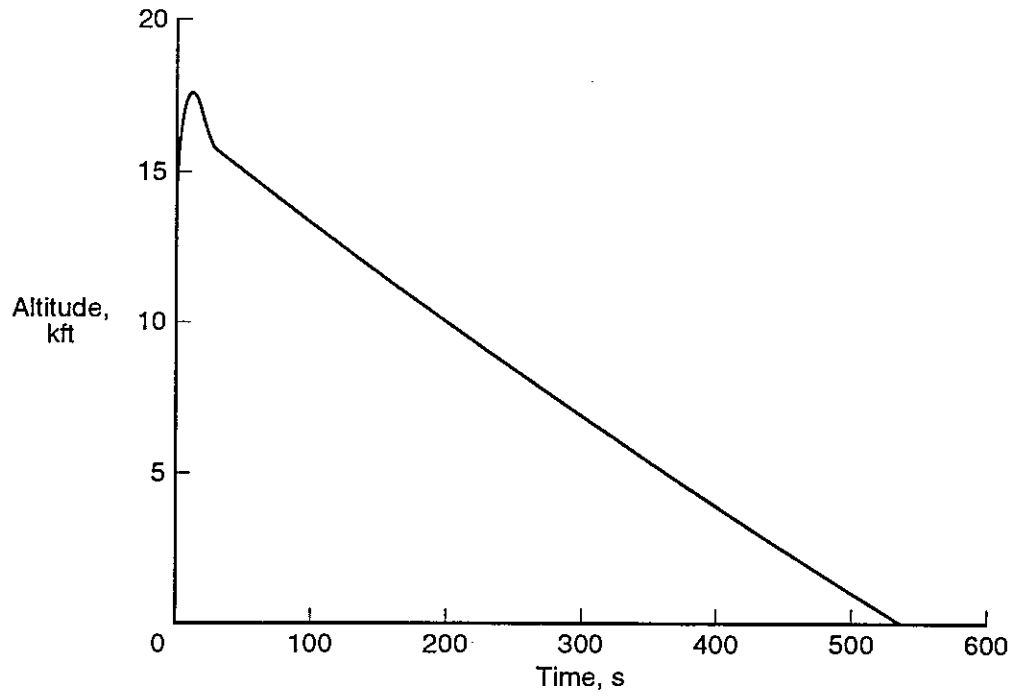


Figure 6.16: CEM Abort at T+55s — Altitude vs. Time

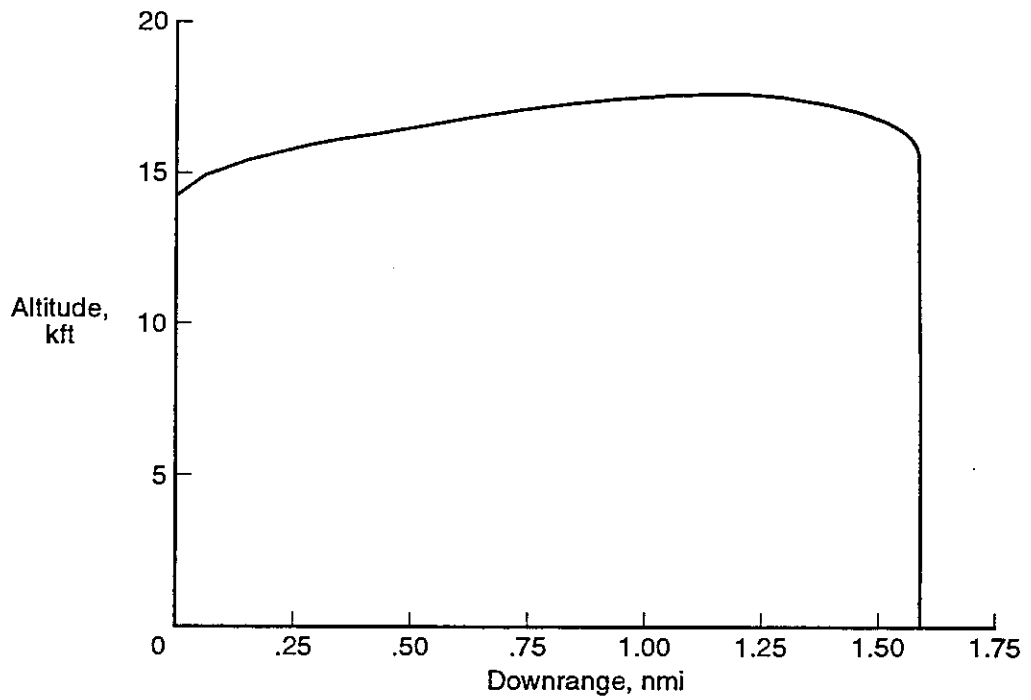


Figure 6.17: CEM Abort at T+55s — Altitude vs. Downrange

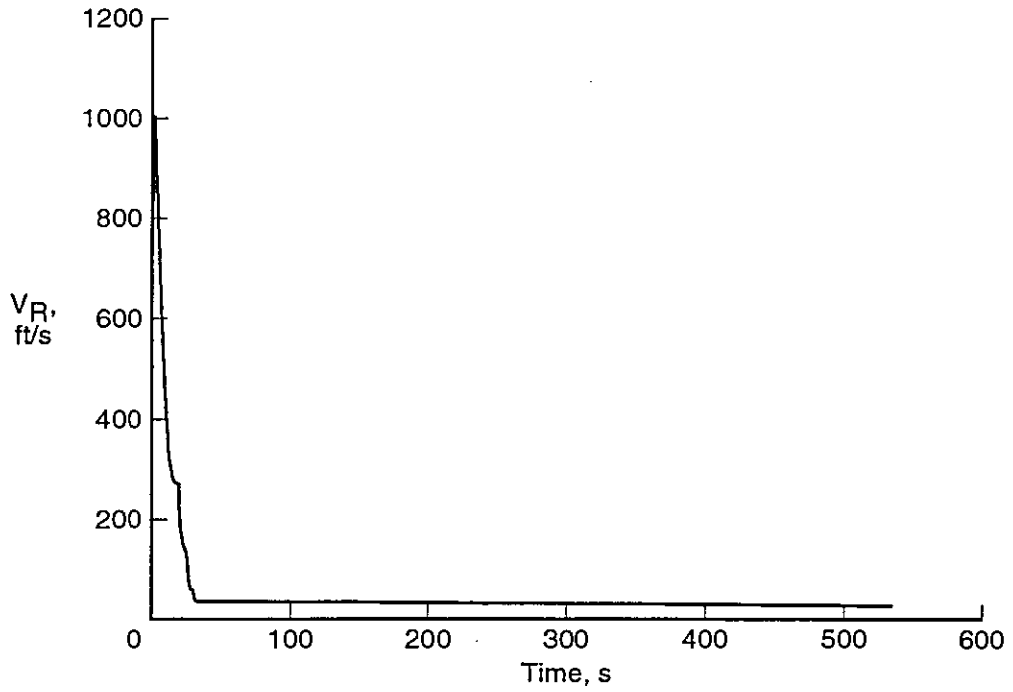


Figure 6.18: CEM Abort at T+55s — Velocity vs. Time

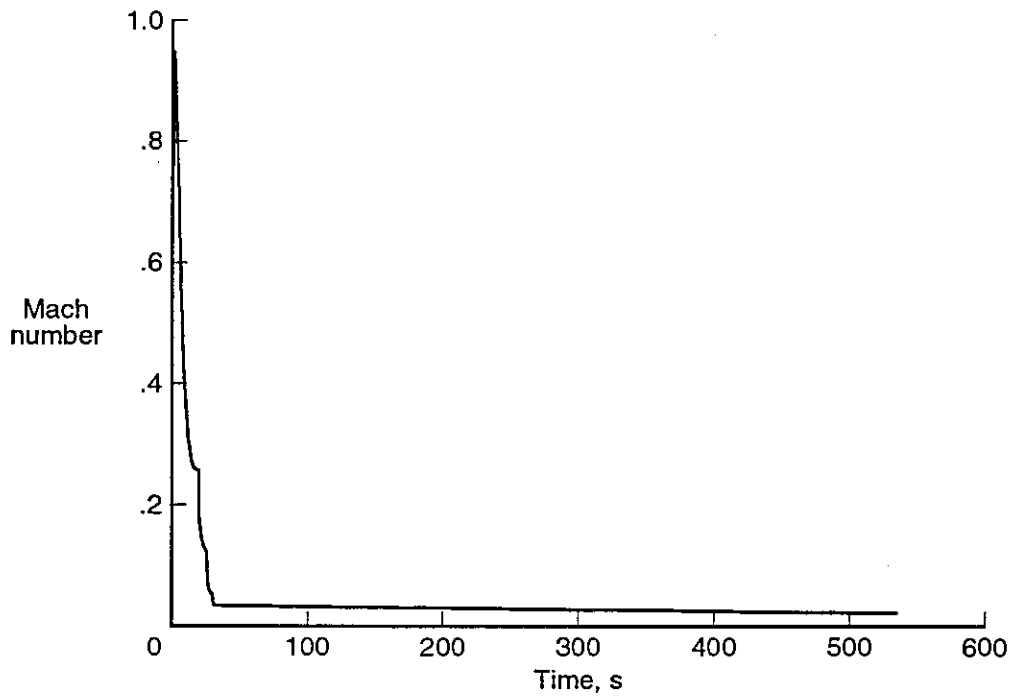


Figure 6.19: CEM Abort at T+55s — Mach Number vs. Time

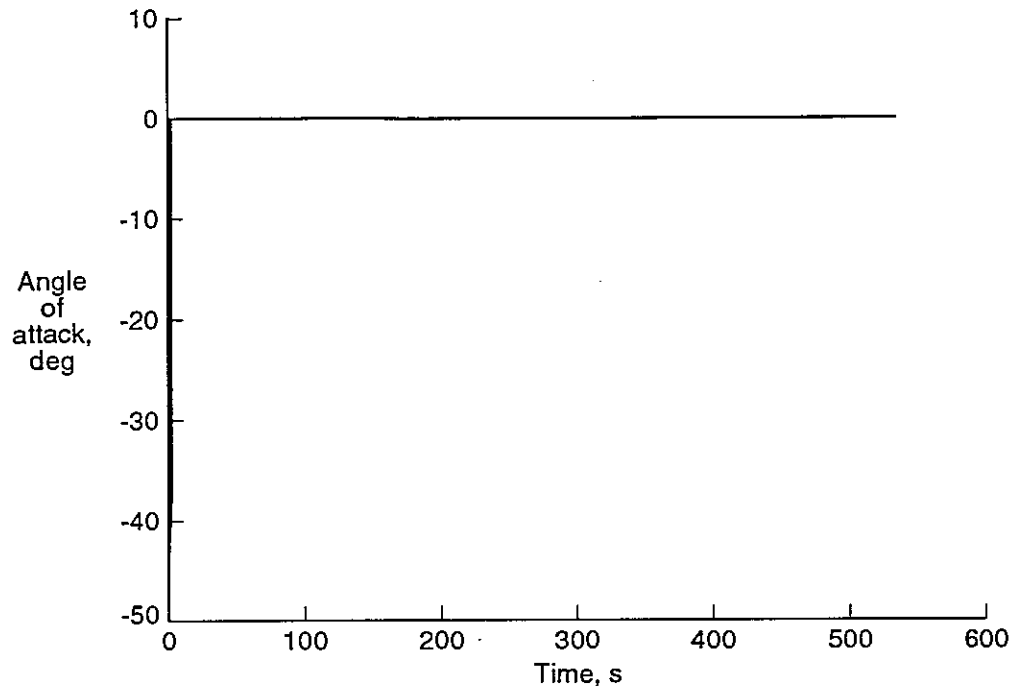


Figure 6.20: CEM Abort at T+55s — Angle of Attack vs. Time

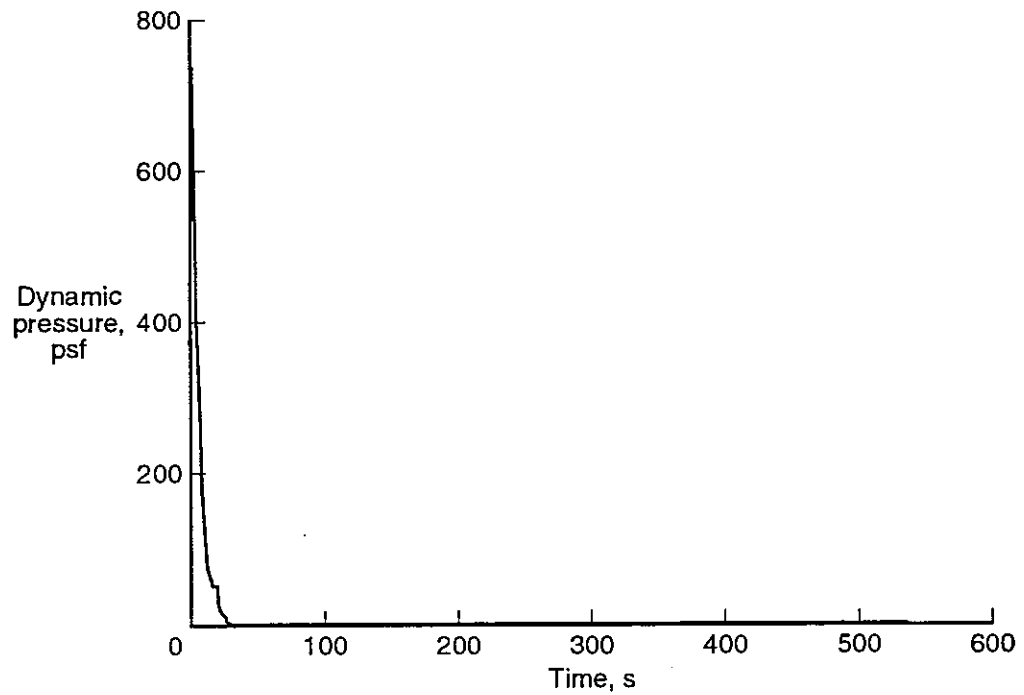


Figure 6.21: CEM Abort at T+55s — Dynamic Pressure vs. Time

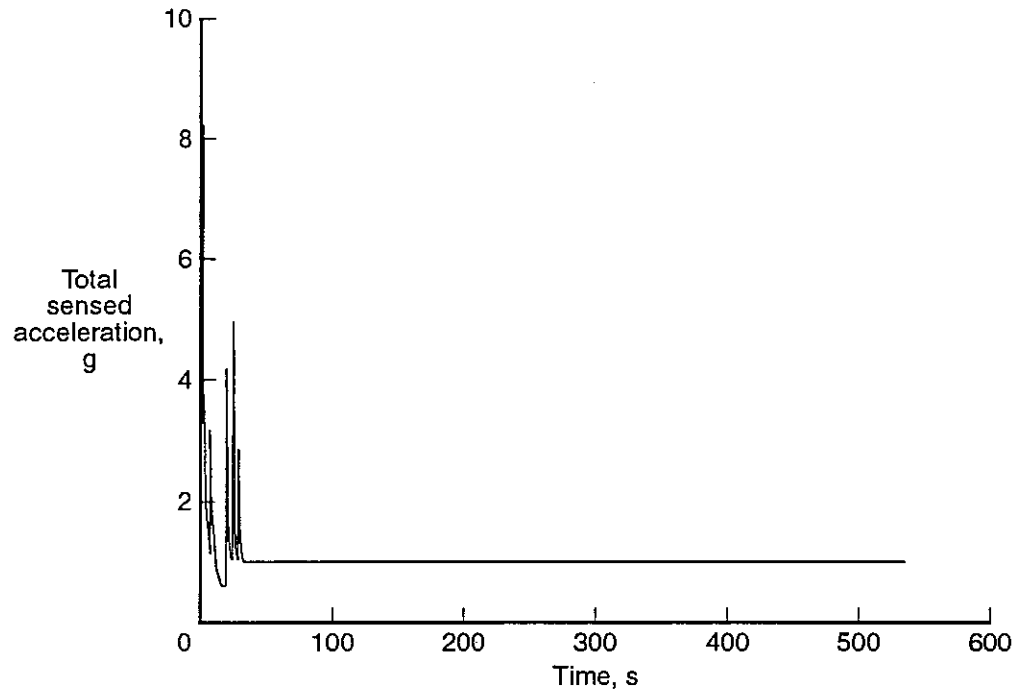


Figure 6.22: CEM Abort at T+55s — Total Acceleration vs. Time

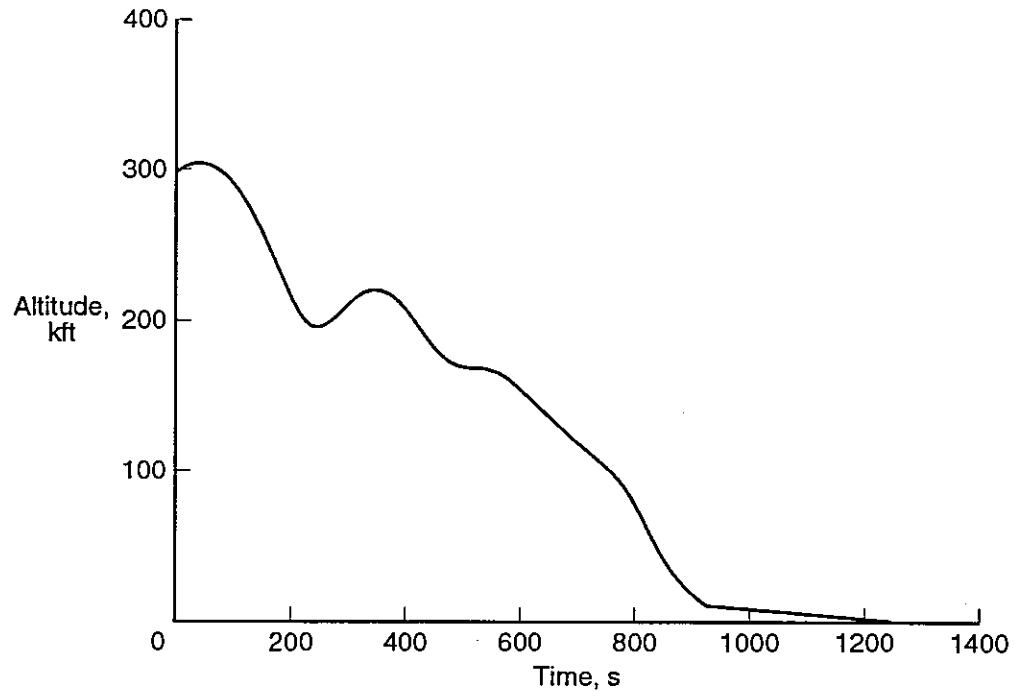


Figure 6.23: CEM Abort at T+320s — Altitude vs. Time

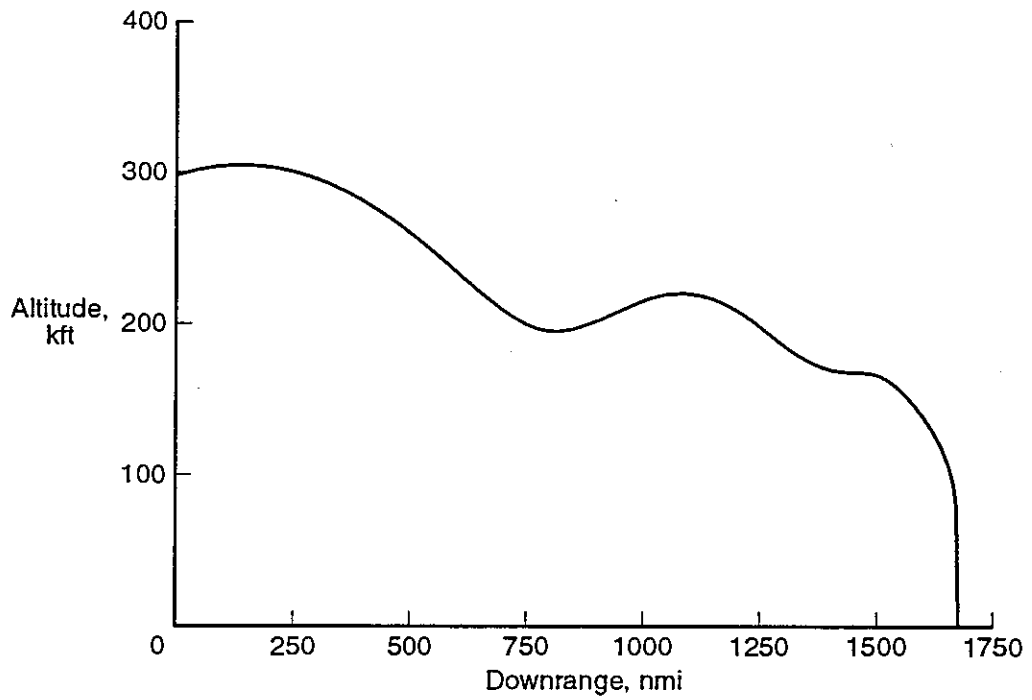


Figure 6.24: CEM Abort at T+320s — Altitude vs. Downrange

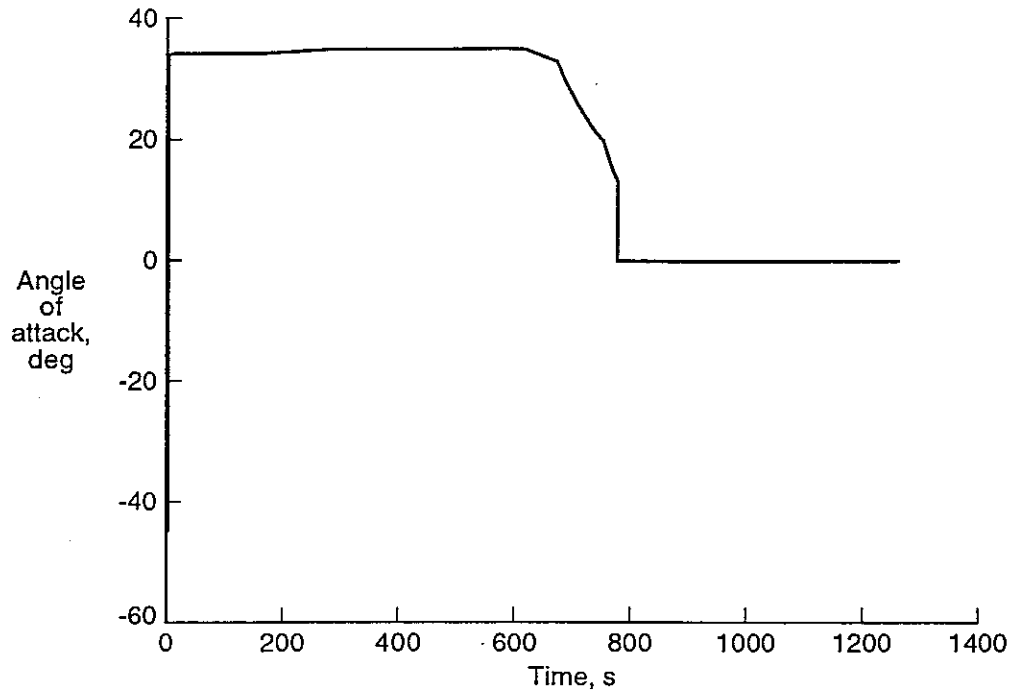


Figure 6.27: CEM Abort at T+320s — Angle of Attack vs. Time

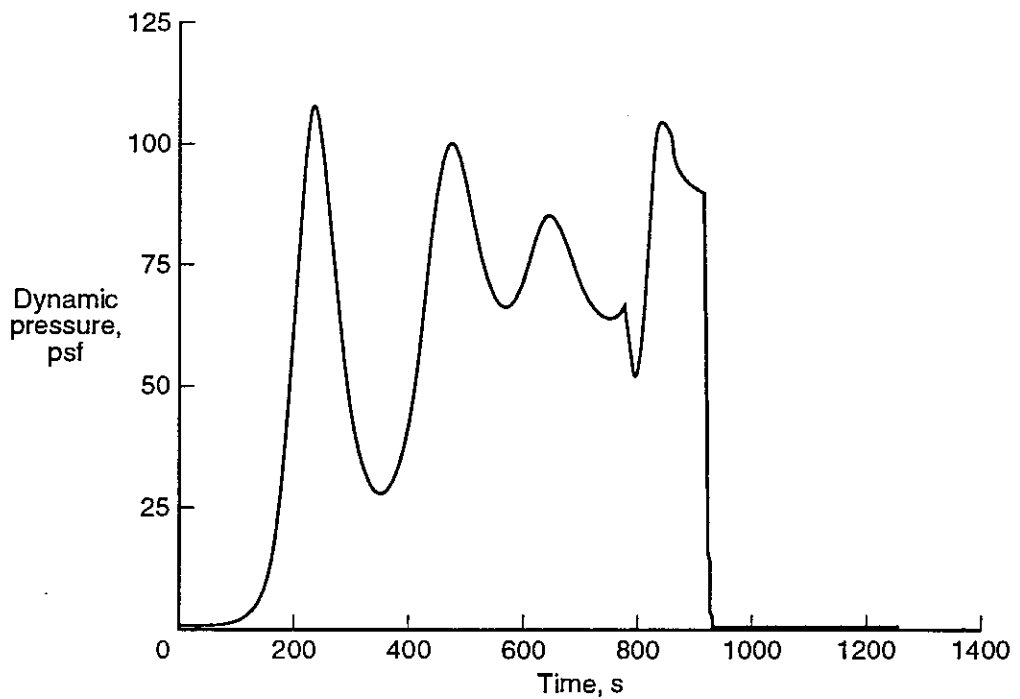


Figure 6.28: CEM Abort at T+320s — Dynamic Pressure vs. Time

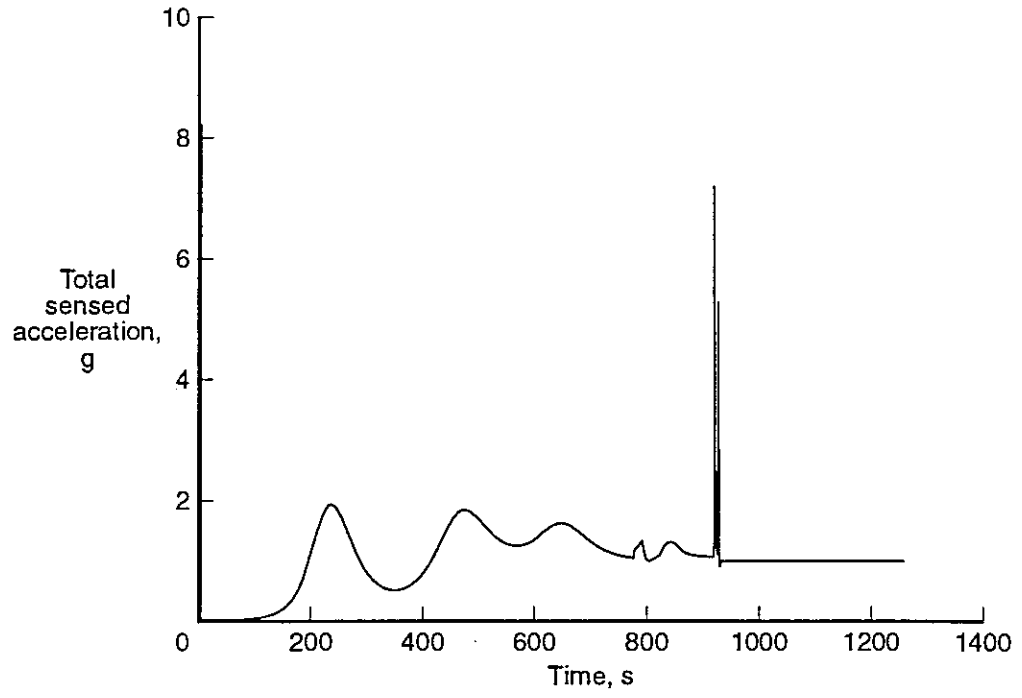


Figure 6.29: CEM Abort at T+320s — Total Acceleration vs. Time

## 12. Appendix

### A. Subsystem Weight Breakdown for Previously Defined Systems

<u>Description</u>	<u>Weight (lb)</u>
Crew (6)	990.0
Clothing	139.2
Hygiene Equipment	31.4
Survival/Rescue Gear	333.6
Ancillary Crew Equipment	109.9
Stowage Provisions	165.0
Flight Data File	30.0
Food System	189.7
Biomedical Equipment	60.0
Communications Equipment	13.4
Photographic Equipment	44.1
Ancillary Hardware	21.5
Flight Kit and Personal Preference Kit	63.0
Storage Containers/ Close-outs	340.5
Wet Trash Stowage Container	35.0
Sleep Station	128.0
Fire Extinguishers (4)	27.6
Tool Kits (IVA and EVA)	28.4
Crew Optical Alignment Set Assembly	6.9
Hygiene Stowage Container	15.5
Communications Equipment	9.1
	-----
Crew and Gear Weight	2,782

<u>Description</u>	<u>Weight (lb)</u>
Guidance, Navigation, and Control	248
Communication and Tracking	377
Displays and Controls	331
Instrumentation System	361
Data Processing	328
	— —
Avionics Subsystem Weight	1,645

<u>Description</u>	<u>Weight (lb)</u>
Personnel System	600
Equipment Cooling	708
Heat Transport Loop	1,381
Heat Rejection System	752
	— — — —
Environmental Control and Life Support Weight	3,441

<u>Description</u>	<u>Weight (lb)</u>
Seats	480
Food Management System	168.2
Waste Management System	261.0
Water Management System	242.3
Fire Detection System	46.3
	— — — —
Personnel Provisions Weight	1,198

## B. Aerodynamic Preliminary Analysis System (APAS)<sup>26</sup>

APAS is an interactive engineering code capable of estimating aerodynamic characteristics of aerospace vehicles. Developed jointly by NASA LaRC and Rockwell International, the program is a preliminary evaluation tool which is easily learned, simple and inexpensive to operate, and yields useful information. However, it is not intended to replace the results of more rigorous, analytical methods or wind tunnel results.

The APAS code is comprised of several engineering analysis algorithms. At subsonic and low supersonic velocities, APAS uses a combination of linear potential theory, slender body assumptions, empirical viscous and base drag methods, theoretical wave drag calculations, and source and vortex panel distributions. This low-speed portion of APAS is called the Unified Distributed Panels (UDP) program and is valid up to about Mach 3.

At high supersonic and hypersonic velocities, a non-interference finite surface element model of the vehicle is analyzed using a combination of theoretical and empirical surface pressure and skin friction methods. This high-speed portion of APAS is called the Hypersonic Arbitrary Body Program (HABP) and is valid down to Mach 1.

Once a geometry is developed, either within APAS using the geometry editor or from an external CAD source, a subsonic, supersonic, and hypersonic analysis can be performed. However, two additional geometry components are required for the low-speed analysis performed by UDP. Both the slender body and interference shell components are created interactively via APAS. The slender body is used to approximate the contribution of the fuselage to the total aerodynamic forces and moments of the vehicle. The interference shell component is used by UDP to determine the approximate

interference effects of the fuselage on the wing (assuming the configuration has a wing).

After geometry definition, the next step in the APAS procedure consists of interactively defining the run conditions required for the study. For this study, aerodynamic characteristics were estimated for thirteen Mach numbers ranging from  $M=0.3$  to  $M=25$ , angles of attack ranging from  $\alpha=-30$  degrees to  $\alpha=+70$  degrees, and altitudes ranging from 0 to 270,000 ft (altitude data is necessary to compute skin friction drag).

Because the UDP and HABP programs are both valid from Mach 1 to Mach 3, it becomes necessary to determine at which point to switch from one method to the other. This is done by finding the Mach number at which data from both programs shows the best agreement. This Mach number was found to be Mach 1.6. Therefore, at Mach numbers below 1.6, the UDP program was used to estimate the aerodynamic coefficients, and at Mach numbers of 1.6 and above, the HABP program was used.

### C. Mini-Version of JA70 Aerodynamic Heating Program (MINIVER)<sup>27</sup>

MINIVER is a simple, yet versatile engineering tool which can be used to predict the aerothermal environments to which vehicles operating in the hypersonic speed regime will be exposed. It can also be used to design and size the thermal protection systems (TPS) for such vehicles. The current version utilizes three separate modules; PREMIN (the preprocessor used to set up the input), LANMIN (Langley MINIVER, used to compute the aerothermal environments) and EXITS (used to predict the thermal response of the TPS and structure).

The vehicle is modeled using simple geometric shapes including; spheres, cones, swept cylinders, and wedges. Time-dependent freestream conditions are computed using an input trajectory coupled with any of several atmospheric options. Local flow properties are computed by processing the flow through the appropriate shock option followed either by compression to the local pressure Newtonian, tangent cone, or wedge flow, or expansion using Prandtl Meyer. Pertinent heating parameters are then calculated for critical regions of the vehicle based on any of a number of approximate engineering techniques including; Fay-Riddell stagnation point, Eckert reference enthalpy flat plate, and Beckwith and Gallagher swept-cylinder stagnation-line methods. Both laminar and turbulent heating calculations are performed and the transition location determined based on a variety of options available in the code. MINIVER includes a data base of more than one hundred TPS and structural materials. These materials can be laid up into layers to create a 1-D conduction model of the TPS and structure. Available configurations include combinations of thin skins, slabs, radiation gaps, standoffs, and ablators. Heat transfer coefficient and recovery enthalpy

time histories provide the aerothermal environments which are then applied to these models to determine the thermal response of the skin and structure.

In terms of the aerothermal environments and TPS design for the CEM, the stagnation area and windward surface were assumed to be the critical regions. In this study, the calculations were based on equilibrium-air chemistry. Angle-of-attack effects were simulated via an equivalent tangent cone. The stagnation area heating was calculated by the Fay-Riddell stagnation point method which requires a nose radius as input. An effective nose radius of 2.979 ft was used in the determination of stagnation point heating rates. This radius was computed by SMART for the CEM at its hypersonic trim angle-of-attack of 34°.

For body points other than the stagnation point, Eckert's Reference Enthalpy Flat Plate Method was used to predict the heating environment. This method utilizes the Blasius solution for laminar flow and the Shultz-Grunow skin friction for turbulent flow. The flow was computed for the three-dimensional surface of the CEM through use of the Mangler transformation for flat-plate to sharp-cone conditions. A blunt body solution was used assuming normal shock entropy and Newtonian pressures. Running lengths were based on the wetted distance from the stagnation point as calculated by SMART for the hypersonic trim angle-of-attack of 34°. Transition from laminar to turbulent flow was estimated to take place at  $Re_{\theta}/M_e=240$  with fully turbulent flow occurring at twice the distance at which onset occurs. This value is similar to that used in the original Shuttle Orbiter design. Heating rates were based upon the wall temperature from the previous time step as computed assuming radiation equilibrium values for an emissivity of  $\epsilon=0.85$  (typical of current RCG coating on Shuttle tiles).

Using this approach, time histories of the heating rates along the windward centerline were calculated. These time histories were then used in conjunction with a 1-D conduction model of the TPS to determine the applicability of the various TPS options available as well as the insulation requirements (i.e. type and thickness). The TPS was sized for each point such that the backface temperature of the structure would not exceed the aluminum-lithium limit of 250°F. The final TPS lay-up is shown in Figure 4.11.

#### D. Program to Optimize Simulated Trajectories (POST)<sup>28</sup>

POST is a generalized point mass, trajectory optimization program capable of simulating trajectories for a vehicle operating near a single planetary body. The overall trajectory is broken into events, such as launch, solid rocket burnout, and ocean landing. During each event, both physical (e.g. vehicle weight, engine type, thrust) and non-physical (e.g. burn time, parachute reefing sequence) aspects of the simulation can be modeled or modified. Any variable calculated in POST can be constrained or optimized. POST has been used to simulate and optimize launch, ascent to orbit, entry, and landing of aerospace vehicles.

For this study, POST was used to simulate the CEM abort trajectories in order to determine the highest heating and dynamic pressure cases, as well as to verify that sufficient altitude and range can be achieved during an abort on-the-pad to land in the ocean after parachute deployment. POST was also used to verify that the g's experienced by the crew during each abort are within human tolerances.

The inputs to POST include the aerodynamic characteristics of the CEM generated by APAS, the weight of the CEM and abort system, and the thrust and specific impulse of the abort solid rocket motors. The initial position and velocity of the CEM was taken from points along the nominal ascent of the SSV. Trajectories were calculated at various points along the SSV's ascent.

The CEM abort solid rockets burn 2.7 seconds with an Isp of 256.7 seconds. Immediately after burnout, a 10 ft diameter drogue chute is deployed to stabilize the CEM. Three seconds after the CEM reaches the apex of its trajectory, the main chute deployment sequence is initiated. These main chutes have been modeled to incorporate reefing in order to keep the opening

forces under 8 g's. The trajectory simulation is then terminated when the altitude of the CEM reaches 0 ft at ocean impact. For other abort initiation times, the chute opening sequence was varied in POST.